Characterization of Bioeffects on Endothelial Cells Under Acoustic Droplet Vaporization

by

Robinson Seda

A dissertation submitted in partial fulfillment
of the requirements for the degree of
Doctor of Philosophy
(Biomedical Engineering)
in the University of Michigan
2014

Doctoral Committee:

Professor Joseph L. Bull
Professor Steven L. Ceccio
Professor J. Brian Fowlkes
Professor Shuichi Takayama

To my mom, Awilda
And my sister, Awilmarie

Acknowledgements

This has been an extremely long and rough ride, but I can finally say I am done. I never thought I could have accomplished half of what I have accomplished in my life, but the truth of the matter is that these things just happen, and that there are people that help make it happen. There was never a moment during this journey when I can say I acted all by myself. This page is dedicated to those people who have been part of my life either academically, socially and personally, making this a more enjoyable experience.

First and foremost, I would like to thank my family, especially my mother and sister whom I love dearly, for all of their kind words of support during my entire career as a graduate student. I know they are really proud of what I have accomplished; without them I would have not been the man I am today.

I would like to thank my immediate advisors, Dr. Bull and Dr. Fowlkes for multiple things: for their guidance and understanding, but also for their patience. I know I was probably not the average graduate student and maybe I was stubborn and difficult at times, but I always appreciated all the words of feedback. Thank you for

guiding me and teaching me the ways of becoming a successful graduate student as well as for all the scientific exchange of words in every Friday meeting; I am going to definitely miss those. I also thank the other members of my committee, Dr. Takayama and Dr. Ceccio for helping shape this big project from the very beginning. Although our interaction has been limited in the past couple of years, your feedback was still important for the execution and conclusion of this work.

I would also like to thank my previous and current labmates, especially David Li, Stan Samuel and John Pitre for their help with experiments, long discussions and camaraderie. This journey has definitely been a lot more enjoyable because of the people I had the pleasure to have worked with and they are probably in the top of the list. Doing science and finding ways to relax our minds is what we do best.

I am immensely thankful for being able to interact not only with the people from my lab, but also other labs with which I have being directly involved running experiments, using equipment or having long conversations of just about anything. I would like to thank Dr. Mario Fabiilli from the Radiology department for all of his help, supply of droplets and feedback; Paras Patel from the Kipke Lab for sharing materials and being helpful; Marian Vigen from the Putnam Lab for sharing equipment and teaching me how to use it and Dr. Yohan Kim from the Ultrasound Lab for taking time to do calibrations for our lab during the weekends.

I am also thankful for the excellent caliber of people we have running our

department. The BME staff is perhaps the coolest, most responsible set of people I know. Special thanks go to Maria Steele, for all of her hard work and for being our mom away from home.

Finally, I would like to thank all my friends for being part of my life and making me look forward to every single day. I have learned as much outside of the lab as I have inside. Thank you all for being who you are, for loving me, respecting me and believing in me. You have all made a contribution to this dream and have made my life just perfect. Thank you!

Robinson

Contents

List of Figures

List of Appendices

List of Acronyms

ADV	acoustic droplet vaporization
BCA	bubble cloud area
BSA	bovine serum albumin
BW/HW	beam width/half width
DCF	dead cell fraction
DDFP	dodecafluoropentane
DNA	deoxyribonucleic acid
EC	endothelial cell
EGM	endothelial cell growth medium
EthD-1	ethidium homodimer-1
FDA	Food and Drug Administration
GE	gas embolotherapy
HCC	hepatocellular carcinoma
HIFU	high intensity focused ultrasound
HUVEC	human umbilical vein endothelial cell
IC	inertial cavitation

KZK	Khokhlov-Zabolotskaya-Kuznetsov
MI	mechanical index
NO	nitric oxide
PBS	phosphate buffer saline
PFC	perfluorocarbon
PNP	peak-negative pressure
SPPA	spatial peak-pulse average
TCF	total cell fraction
US	ultrasound
VEGF	vascular endothelial growth factor

Abstract

Characterization of Bioeffects on Endothelial Cells Under Acoustic Droplet Vaporization

By Robinson Seda-Padilla

An ultrasound-mediated cancer treatment called gas embolotherapy has the potential for providing selective occlusion of blood vessels for therapy. Vessel occlusion is achieved by locally vaporizing micron-sized droplets through acoustic droplet vaporization (ADV), which results in bubbles that are large enough to occlude blood flow directed to tumors. Endothelial cells, lining of our blood vessels, will be directly affected by these vaporization events and as such are the subject of this study. Damage to the endothelium could lead to a number of pathological states that, if left untreated could be harmful. However, if under control, these bioeffects could provide benefits that would be synergistic with bubble occlusion like increased endothelial permeability or occlusion by thrombosis. We investigate bioeffects caused by ADV under *worst-case scenario* cases by using a static endothelial culture model.

Two insonation frequencies (3.5 MHz and 7.5 MHz) were chosen to characterize the effects of ADV and aid in the exploration of frequency dependent effects. Damage was observed through changes in peak-negative (rarefactional) pressure and pulse length, and described by the absence of cells after treatment. Damage was dependent in bubble cloud area and highly localized. Additional data was obtained to elucidate the role of ADV in open or confined environments, which simulate relatively large and small vessels, respectively. Through these experiments we try to provide the reader with some of the tools necessary to make an assessment on the repercussions of performing ADV in situations that allow the droplets and ultimately the bubbles, to be in direct contact with the endothelium. Knowing when significant damage is expected in gas embolotherapy could help in the development of preventive measures as well as additional therapeutic aids during treatment.

Chapter 1

Introduction

1.1 Motivation

Embolotherapy is the intentional injection of a blocking agent (embolus) to slow or stop the blood flow for therapeutic purposes. It has been shown that permanent damage to tissue is possible if enough solid emboli are delivered or sufficient occlusion can be achieved during the therapy [1, 2]. Embolotherapy can also be implemented in conjunction with drug-releasing emboli for localized drug delivery. Some potential applications of embolotherapy include hemorrhage, and some types of cancers, such as hepatocellular carcinoma (HCC), and hypervascular tumors such as renal cell carcinoma [3]. HCC for example, has been treated more effectively using embolotherapy than using chemotherapy or resection [4]. However, embolotherapy is only used as a last resort after conventional treatments have failed.

The success of embolotherapy greatly depends on several factors, such as the

selection of the embolic agent, the application and the ability to direct and confine the emboli to the targeted area [3]. Unfortunately, all of these factors present unique challenges that need to be taken into consideration. For example, the selection of the embolus can be quite difficult. They can be extremely toxic and painful (e.g. ethanol), permanent (e.g. n-butyl cyanoacrylate), thrombogenic (e.g. coils and balloons) or non-target specific (e.g. microspheres). In addition to the selection and confinement of the emboli, some embolotherapy procedures may involve more complicated and invasive work, exposing the patient to other health risks. Future embolic agents need to be non-toxic, easily transported and target-specific in order to provide a more robust, localized and less invasive therapy. Consequently, there is a need for improving current embolotherapy techniques.

Gas embolotherapy (GE) is a minimally invasive procedure that provides means for selective occlusion of blood vessels and offers relief to most of the disadvantages encountered in conventional embolotherapy techniques [5, 6, 7]. The principle behind GE is the use of albumin (or lipid)-coated microdroplets that are vaporized locally to provide gas emboli [8, 9, 10]. These droplets are small enough to pass through the microcirculation ($d < 6$ μm), thus avoiding the risk of occlusion of vessels feeding healthy tissue. These bubbles are generated using focused ultrasound (US) via acoustic droplet vaporization (ADV) [8, 10, 11]. During this process (Figure 1), microdroplets, with a dodecafuoropentane (DDFP, C_5F_{12}) core are

injected into the bloodstream and allowed to circulate the body until an area (tumor) has been targeted. DDFP (29ºC boiling point) is a perfluorocarbon (PFC) capable of undergoing vaporization at body temperature due to its level of superheat, but it is stabilized by the albumin or lipid shell. Table 1.1 summarizes the physical properties of DDFP.

Table 1.1: Physical Properties of Dodecafluoropentane (C_5F_{12})

Property	Value
Molecular weight	288 g/mol
Boiling point	29ºC
Density	1630 kg/m^3
Viscosity	0.00652 N s/m^2
Surface tension	0.7 N/m

Once the cancerous tissue has been targeted (with the aid of imaging tools) and the vaporization threshold is reached, the ADV process will take place. This process will be capable of transforming these microdroplets into bubbles that are 125 to nearly 150 times their original volume capable of occluding blood vessels feeding the tumor [8]. A focused US transducer will make possible that vaporization of these droplets and subsequent occlusion will only occur at or near the tumor reducing

the risk of collateral damage. Also, due to the low solubility of PFC gases in water, a large number of these bubbles will be able to provide prolonged occlusion to cause tumor infarction. While it was previously stated that the ADV process would be localized, there are still some important things to consider, which are subject of this dissertation. High pressures and shear stresses generated during this event (i.e. phase transition and bubble expansion processes), capable of affecting blood cells and the vessel wall, are examples of important considerations that may affect the advancement of this therapy. Therefore, we focus our efforts in investigating the impact of ADV on the vessel wall.

Some of the first studies addressing the potential impact of ADV on the anatomy of a blood vessel showed the results of two direct numerical simulations that recreated the bubble expansion process following ADV in a rigid and flexible tube [12, 13]. Pressures and shear stresses were found to be much higher in the rigid tube case compared to the flexible tube suggesting that flexibility of the vessels might have a dampening effect. A limitation of this study was the lack of an appropriate internal bubble pressure condition (due to unavailable empirical data), which yielded rather high results. However, both studies are relevant to our application because they show the role of blood vessel flexibility and its impact on bubble expansion and possible implications on the cellular response. Our blood vessels are naturally flexible, but the level of flexibility depends on their type and size. Capillaries, for

example, are stiffer because they lack smooth muscle and are embedded in surrounding tissue. Consequently, if vaporization occurred in small, rigid vessels close to the targeted area, high wall stresses could develop. These stresses in conjunction with vessel wall strength may lead to rupture, petechial hemorrhage or even cell death. On the other hand, if vaporization occurred in relatively large (flexible) vessels, stresses will be dampened out, but direction and confinement of the emboli will be lost jeopardizing the selectivity of the therapy.

Gas bodies formed as a result of ADV provide means for yet *other* important biological effects (bioeffects) when interacting with US pulses. A review article described these bioeffects considering diagnostic US and contrast agents [14]. When in contact with contrast agents, US produces microbubble pulsations that can trigger cavitation events (stable or transient) that could be harmful to surrounding tissue [15, 14]. These events may involve the expansion of the gas bubble followed by a violent collapse driven by the inertia of the inrushing fluid, which is the case in transient (or inertial) cavitation. Many bioeffects have been associated with inertial cavitation (IC), including cell death, vessel rupture, hemorrhage and platelet aggregation [14, 16]. Other effects related to microbubbles driven by US pulses, which may not be so undesirable, include angiogenesis, remodeling of vessels and increased cell permeability [17, 18, 19]. For example, studies have found that the use of US and contrast agents, such as microbubbles, may facilitate the delivery and

increase the endothelial uptake of several molecular species, such as calcium, nitric oxide and growth factors, such as VEGF (vascular endothelial growth factor) [2, 20, 21, 22, 23]. These studies demonstrated that the interaction between US and microbubbles does increase the permeability of cells through what has been referred to as sonoporation [24, 25]. However, it was found that reduced cell viability [26, 27] and other altered cellular responses have also been observed [28]. Reduced viability has been attributed to this US-microbubble interaction capable of generating high temperatures, pressures and fluid velocities [29, 30, 31].

While the aforementioned bioeffects were generated by the interaction of an acoustic field and *preexisting* bubbles, it is important to emphasize that ADV will go through different stages before a stable bubble is formed. We believe that the ADV process may generate other bioeffects that may be *unknown* in addition to those generated by an US-microbubble interaction, while providing the added advantage of vessel occlusion (Figure 1.3). In addition, it is vital to understand that although most of these vaporization events are limited to the blood vessels, these bioeffects could magnify and propagate elsewhere [17, 18]. More specifically, the endothelium, as one of the possible targets during ADV and main subject of this dissertation, could give rise to a cascade of events that could affect a number of vital bodily functions. A more detailed description of these effects is provided in section 1.2.

Knowing the degree of these effects may be important for multiple reasons. For instance, as GE is in its early investigative stages, it will be important to know what the potential pitfalls of this technique are as well as when and where these are more likely to occur. This is not only interesting, it is also necessary for subsequent improvement of this therapy. Alternatively, these bioeffects could potentially be used as new mechanisms for enhancing drug delivery to the tumor through permeabilization of the endothelial wall. It has been shown that permeabilization of the endothelial wall is possible when US is applied to thin-shelled microbubbles *in vivo*, which can aid in the delivery of drugs and genes through regions in the body where the endothelial wall is highly impermeable, such as the blood brain barrier [32, 33, 34, 35].

1.2 Significance

The endothelium is a very thin layer of cells that covers the lumen of our blood vessels (Figure 1.2). It is composed of endothelial cells (ECs), which are constantly exposed to mechanical (pressure, shear) and hormonal stimuli associated with the blood flow [36, 37]. They adapt and respond to these stimuli by signaling cascades that can lead to different events such as cytoskeleton reorganization, release of cytokines, up and down regulation of protein expression, cell division and programmed cell death (apoptosis) [17, 38]. Depending on their location ECs may

experience a level of shear stresses in the range of 5-20 dyne/cm^2 (in major vessels) average pressures of around 120 mmHg (for the systolic phase) and up to 24% of deformation [17, 37]. However, several studies have shown that ECs may respond and adapt to an increase in these normal levels of stresses and that their response is dependent on the location of ECs around the cardiovascular circuitry in the body [39]. For example, ECs experiencing laminar flow shear stresses might decrease the rate of cell proliferation, while those subjected to altered flow shear stresses, as observed in the aortic arch or stenotic vessels, will increase DNA synthesis and cell proliferation [36]. The endothelium is a also regulator of vascular homeostasis because it acts as selective barrier, reduces turbulence and play vital roles in other physiological events, such as white blood cell migration, coagulation, angiogenesis and vasoactive functions by the secretion of important signaling molecules like nitric-oxide (NO). Damage to the endothelium can lead to *endothelial dysfunction*, an important cardiovascular risk factor.

During endothelial dysfucntion, ECs reduce their ability to secrete nitric oxide (NO) [40], leading to impairment of vasodilation, which reduces the ability of the blood vessels to relax and decrease vascular resistance. There is also an increase in endothelial permeability, platelet aggregation and leukocyte adhesion; events that promote *atherosclerosis* [41], (Figure 1.4). This pathological state can be quite serious if necessary measures are not taken, yet it could be a great tool if used intelligently in

conjunction with available cancer treatments, especially GE. Local platelet aggregation, clotting and thrombosis, for example, could potentially be beneficial if vessels supplying the tumor are affected. This could provide a parallel mechanism for vessel occlusion without additional vaporization.

It is known that ECs are more stable than cancer cells and as such have been pursued as possible targets for anti-angiogenic therapies to treat tumors using the anti-VEGF monoclonal antibody [42]. This antibody blocks VEGF, which is a chemical signal that stimulates blood vessel growth. However, recent studies [43] have shown that ECs growing within a tumor might develop genetic abnormalities that could make them more resistant to these therapies. Therefore, local *mechanical* injury caused by high stresses, preferably through ADV, could potentially be more effective.

Through this set of experiments we intended to identify some of the bioeffects of GE on ECs by investigating the direct impact of ADV on a cultured monolayer. The main focus is primarily to determine the extent of the damage once ADV is triggered, its immediate effect on cell viability and differences between peak-negative pressure (PNP), pulse length and insonation frequencies. Vaporization at two levels of confinement in the presence of ECs is also investigated to provide a broader view of the significance and impact of these effects *in vivo*. We also comment on the droplet-endothelial interaction that may facilitate these effects. Currently, bioeffects

associated with ADV and the endothelium have not been reported yet, thus this dissertation is aimed to fill this void.

The dissertation is organized into five chapters. Chapter 2 presents the first findings on the effects of vaporizing droplets on a cell monolayer of ECs using a focused, single-element 3.5 MHz. In this chapter we present the bubble cloud (generated as a result of ADV) as a function of pressure and pulse length while observing and quantifying cell detachment and cell viability. Chapter 3 discusses these bioeffects when using a 7.5 MHz transducer and makes a comparison to those obtained when insonating at 3.5 MHz providing explanations to possible frequency-dependent mechanisms of cell injury. Chapter 4 investigates vaporization confinement and proximity effects. This chapter shows how the effects seen in the previous chapters are lessened or amplified by localizing vaporization away from the cell monolayer in open or confined environments. Finally, chapter 5 summarizes our findings and makes appropriate conclusions based on our evidence, while chapter 6 discusses some of the limitations of our studies and provides ideas for future experiments. It is the intention of this dissertation to build a platform for subsequent studies that are capable of filling the remaining voids in the quest for a better cancer treatment: *Gas Embolotherapy*.

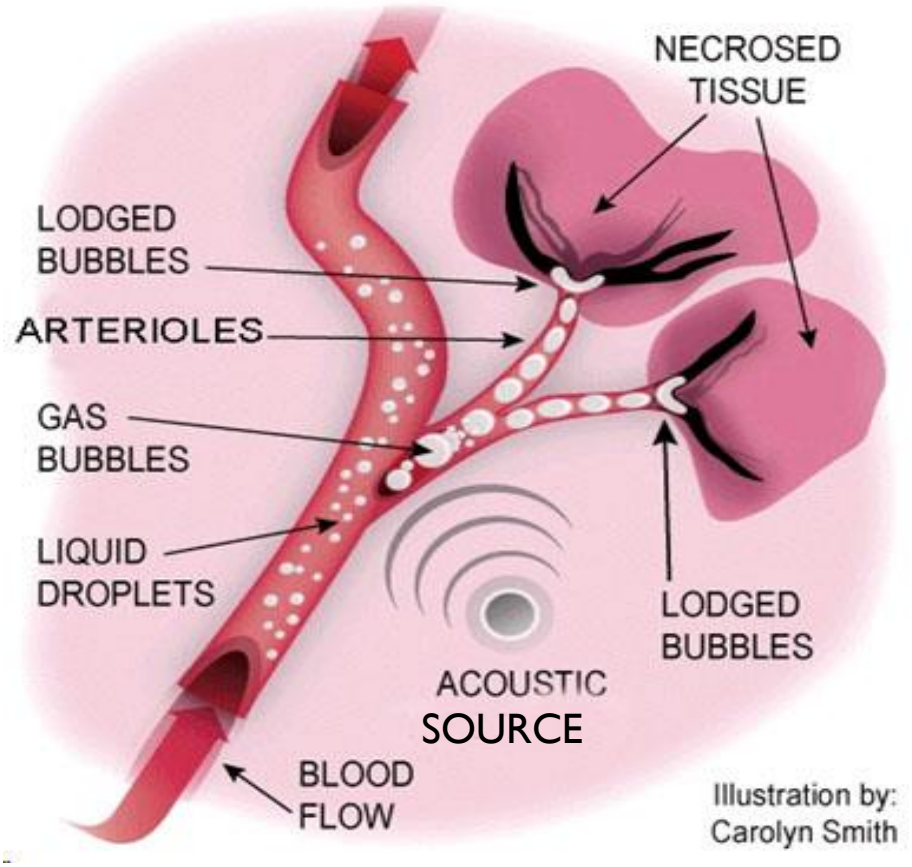

Figure 1.1: An illustration of gas embolotherapy. Droplets circulate freely through the bloodstream until the target is detected. Acoustic droplet vaporization using a highly focused ultrasound turns the microdroplets to gas bubbles that will eventually lodge in the tumor vasculature and cause tissue necrosis.

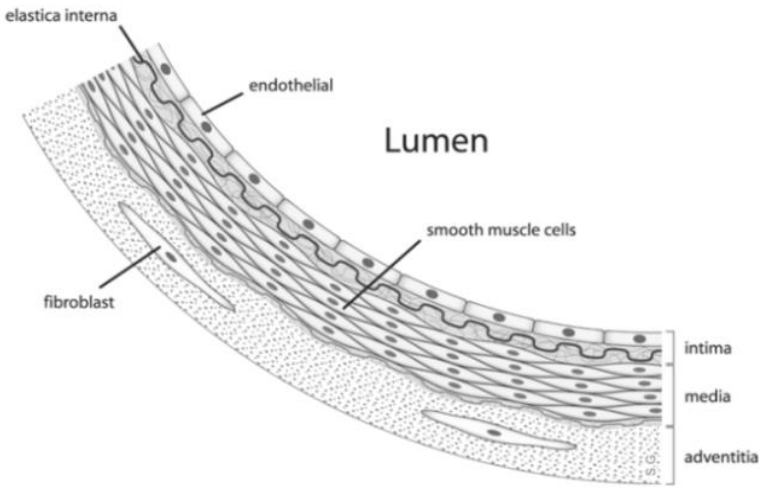

Figure 1.2: Anatomy of a blood vessel showing the location of the endothelium (innermost layer). http://en.wikipedia.org/wiki/File:Anatomy_artery.png

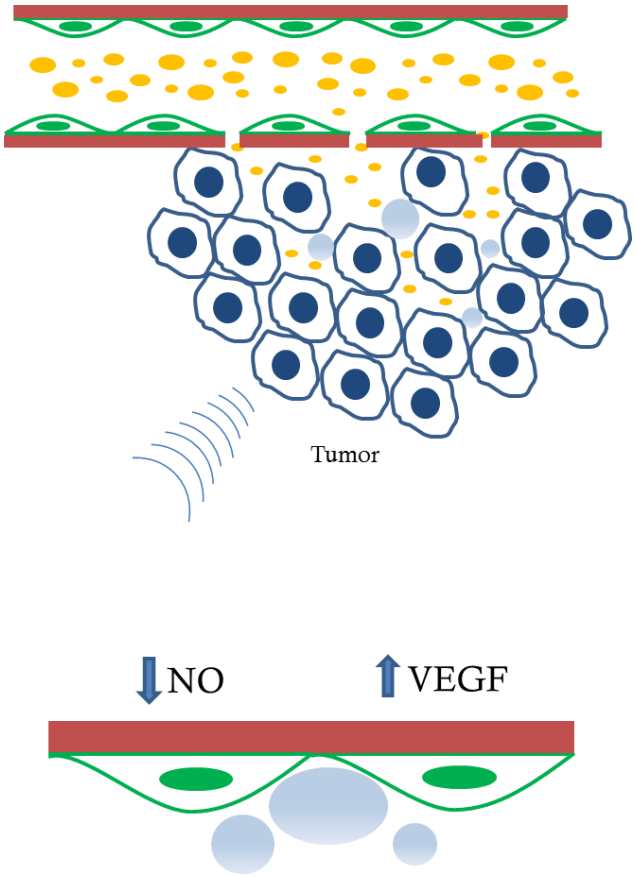

Figure 1.3: ADV applications in drug delivery and cancer therapies. In addition to occlusion of vessels, leaky endothelium in tumors may allow droplets to enter and accumulate in the intersituim allowing for highly localized drug delivery to cancerous cells.(top). Bubbles formed through ADV and subsequent interaction with US may increase endothelial wall permeabilization and induce upregulation or downregulation of certain molecular species (bottom).

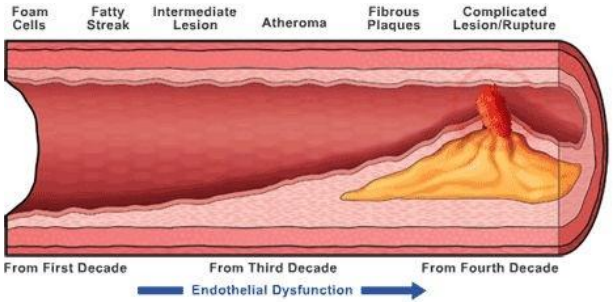

Figure 1.4: Progression of an artery with endothelial dysfunction. The first lesion occurring during the first decade will develop into a major lesion that could lead to atherosclerosis (seeing at the fourth decade).
http://www.hivandhepatitis.com/0_images2009/endothelial.jpg

Chapter 2

Characterization of ADV-induced bioeffects on endothelial cells using a 3.5 MHz transducer

2.1 Introduction

ADV is capable of transforming DDFP microdroplets into bubbles that are up to 150 times – in volume – larger than the original droplet size [8]. This dramatic change in size will provide enough volume for occlusion of small blood vessels supplying tumors, but could also lead to significant cell injury due to the generation of high pressures and shear stresses during bubble expansion [8, 10, 12, 13, 44, 45]. Bubble expansion resulting from ADV inside tubes was previously investigated by our group, but it was not until recently that effects of initial droplet size along with the liquid consumption phase and bubble evolution was further investigated in a series of studies [44, 45]. These new studies presented a theoretical [44] and computational [45] model that described the evolution of a droplet undergoing ADV inside a rigid

tube, from the liquid consumption (phase transition) to bubble expansion and whose initial conditions were empirically obtained. The results showed the existence of a critical droplet size below which the bubble evolution is highly oscillatory, whereas a damped evolution is observed otherwise. These differences in bubble evolution represent oscillations driven by viscous dampening inside a tube sufficiently large when compared to the initial droplet diameter. Three bubble growth regimes with particularly high pressures in the early stage of bubble evolution were also observed. With these new studies, shear stresses were found to be dependent on the initial droplet size, but were significantly lowered (*by five orders of magnitude*) when compared to those previously reported in earlier studies [12, 13]. Nonetheless, calculated pressures were still far above those found physiologically.

As thousands of these microdroplets of various sizes circulate the bloodstream spanning the entire cross section of a blood vessel it will be possible for multiple vaporization events to occur at or near the vessel wall (Figure 2.1). The relative size of the US beam when compared to the diameter of the blood vessel under treatment will likely determine the extent of the damage, making smaller vessels (relative to the beam width) more susceptible to events near the vessel wall. Not only will these vaporization events be important, but also the rapid oscillations of the subsequently formed bubbles if the US remains on after vaporization has been completed [46, 47, 48, 49, 50].

Droplet concentration, bubble evolution (dependent on droplet size), relative location inside the blood vessel and also the selection of acoustic parameters could determine the range of bioeffects associated with ADV and consequently their clinical relevance and potential application. The high probability of these events due to droplet concentration in conjunction with high pressures and shear stresses generated during vaporization and bubble expansion could translate to a higher risk of denuding or affecting the endothelium, for example. However, if under control these effects could aid in a number of applications, such as cellular permeability and localized thrombosis for therapy.

This chapter focuses on ADV events close to a vessel wall and using a 3.5 MHz transducer. Other parameters like peak negative pressure (PNP) and pulse length are varied, while droplet concentration is held constant. With this study we intend to provide the first insights in bioeffects of ADV on endothelial cells. It is of particular interest to characterize the direct effects of ADV while finding those acoustic parameters that would allow us to perform significant ADV with minimal damage to the endothelium as well as understanding the underlying mechanism of cellular injury.

2.2 Materials and Methods

2.2.1 Cell Culture

Primary human umbilical vein endothelial cells (HUVEC) were cultured and supplemented with EGM-2 cell media (Lonza Clonetics™; Walkersville, MD). These cells were incubated at 37°C in a humidified environment and 5% CO_2. Cells were grown in culture flasks for one passage and then transferred to OptiCell™ culture chambers (Nalgene Nunc International; Rochester, NY) previously coated with fibronectin (Ca. No. 354008, BD Biosciences; San Diego, CA) prior to US experiments. The cells were grown to ~90% confluence and only passages one through four were used in these experiments.

2.2.2 Droplets

Albumin-coated droplets with a DDFP core were obtained from the Department of Radiology at the University of Michigan, Ann Arbor. The droplet solution was made following a procedure described elsewhere [8]. Briefly, droplets were made by combining 750 μL of 4 mg/mL (BSA) bovine serum albumin (Sigma Aldrich, St Louis, MO), dissolved in normal saline (0.9% w/v, Hospira Inc., Lake Forest, IL), and 250 μL of perfluoropentane (C5F12, CAS Number 678-26-2), Strem Chemicals, Inc., Newburyport, MA). While in an ice bath the two phases were emulsified via sonication using a tapered microtip accessory (model 450, 20 kHz, 3.2 mm diameter,

Branson Ultrasonics, Danbury, CT) operating at 125 W/cm^2 for 30 seconds in continuous mode.

2.2.3 Ultrasound Setup

A schematic of the setup is provided in Figure 2.2. All experiments were conducted in a tank containing degassed, deionized water maintained at 37ºC. The tank was made from acrylic with a polystyrene window at the bottom to provide a clearer view when looking through the microscope. Six pegs located around the polystyrene window were used to slide an OptiCell™ chamber and hold it in place. The tank was placed on top of an inverted microscope (Nikon Eclipse TE2000-S, Nikon Instruments, Inc., USA) to observe and record the ADV event and for fluorescence microscopy. A single-element 3.5-MHz (A381S, 1.9 cm-diameter, 3.81 cm-focal length, Olympus Panametrics-NDT, Waltham, MA) transducer was focused at a 40º angle to the bottom membrane of an OptiCell™ chamber located at the bottom of the tank. The transducer was calibrated using an in house designed fiber-optic probe hydrophone [51]. Data on the axial and cross sectional beam profiles as well as pressure at the focus were obtained (). The transducer was placed at an angle to minimize standing waves from the bottom of the tank. A "dummy" OptiCell™ (upper membrane cut out) was used for the alignment of the transducer. The US pulses were generated using two function generators. A primary function generator

(HP-3314, Hewlett Packard) was used to produce a signal while a secondary function generator (33120A, Agilent Technologies; Palo Alto, CA) was used as a gate. The output signal was then amplified using a power amplifier (-60 dB, GA 2500A, Ritec Inc.; Warwick, RI) whose output was connected to the single-element transducer. An omnidirectional hydrophone (ITC-1089D, International Transducer Co.; Santa Barbara, CA) was also used to record acoustic noise. All the signals were monitored using an oscilloscope (WaveSurfer 44Mxs, LeCroy; Chestnut Ridge, NY).

2.2.4 Exposure Protocol

The cell media was replaced with fresh, warm (37°C) media prior to the experiments. A volume of 100 microliters of a solution containing 10^8 droplets per milliliter was added to the 10-mililiter cell culture chamber to produce a final concentration of 10^6 droplets per milliliter. This concentration yielded and approximate 10:1 droplet to cell ratio. The OptiCell™ was gently tilted side to side to evenly distribute the droplets over the cell monolayer. The OptiCell™ was then submerged inside the tank and left for 2 minutes to equilibrate and for the droplets to settle to the bottom of the chamber. One OptiCell™ chamber was divided into a grid that consisted of 13 rows and 9 columns. This accounted for 13 different experimental groups and at most, 9 different replicates. These 13 experimental groups contained all combinations of pressure and pulse length including a treatment with zero (0 MPa)

pressure. A second OptiCell™ chamber was used and divided in the same way to perform a control experiment that included the same treatments, but without droplets. Both OptiCells™ were seeded using the same cell density and kept until they reached ~90% confluence. A motorized stage (Proscan II, Prior Scientific; Rockland, MA) mounted onto the inverted microscope was used to move the tank along with the OptiCell™ to the specific area for treatment. The transducer was moved away from previously formed bubble clouds to avoid any shadowing effects. PNPs ranged from 0 to 8 MPa, while pulse length was varied by changing the number of cycles to 4, 8 or 16. The number of cycles was the input number into the system and were used as the nominal value, however due to the ring-up/ring-down artifacts, the actual number of cycles was 3, 7 and 15, respectively (see Apendix D). These corresponded to pulse durations of 0.86 μs, 2 μs and 4.29 μs, respectively. The upper limit of the pressure range selected corresponded to the saturation pressure of the transducer, while the cycles corresponded to a range that has been previously used in our lab for *in vivo* experiments [52]. The ADV events (i.e. bubble clouds) were recorded using a camera (CoolSNAP ES, Roper Scientific Photometrics; Tucson, AZ) mounted into the inverted microscope and MetaMorph Premier (Molecular Devices, Sunnyvale, CA). Upon completion of the treatments, the chambers were immediately taken out of the tank for fluorescence staining.

2.2.5 Fluorescence Microscopy

The cell media was carefully withdrawn from the culture chambers using a 10 milliliter syringe. The cell culture was rinsed 2x with phosphate buffered saline (PBS) containing 2% bovine serum albumin (BSA) to remove any excess droplet solution. One milliliter of a solution containing nucleic acid stain Hoechst 33342 (Ca. No. H3570, Molecular Probes®, Life Technologies™, Carlsbad, CA) and ethidium homodimer-1 (Ca. No. L-3224 (component B) Molecular Probes®, Life Technologies™, Carlsbad, CA**)** was added to the culture chamber and supplemented with 9 milliliters of culture media to a final concentration of 3 μM. OptiCells™ were incubated for 30 minutes at 37ºC in the dark. Following incubation the staining solution was withdrawn; the OptiCells™ were rinsed with PBS and fixed in 4% paraformaldehyde for 15 minutes. After fixation, the OptiCells™ were rinsed 2x and stored in HEPES (with sodium azide) at 8ºC.

Each area exposed to an ADV event was examined using a 4x magnification objective (Plan Fluor, Nikon; Melville, MA). A fluorescence image consisting of a Hoechst stained (total cell count) and an EthD-1 stained (dead cell count) frame was obtained for each area and recorded using MetaMorph 7.5 (Molecular Devices, Sunnyvale, CA). In a different experiment, a 2 μM solution of calcein AM (Ca. No. L-3224 (component A) Molecular Probes®, Life Technologies™, Carlsbad, CA) was used to stain the cytoplasm of the cells (green fluorescence).

2.2.6 Image Processing

The collected images were post processed using Adobe Photoshop CS5.1 (Adobe Systems Inc., San Jose, CA) to create overlays. Individual frames of cells were transferred to ImageJ (U. S. National Institutes of Health, Bethesda, Maryland) for image processing that included conversion to binary (black and white) and particle count using the "Analyze Particles" tool to determine the total number of cells and the number of dead cells per frame.

2.2.7 Statistics

Each treatment consisted of between 6 and 9 replicates. R (The R Project for Statistical Computing) and Minitab 16 (Minitab Inc., State College, PA) were used to carry out the statistical analysis. Statistical significance of effects was assessed by performing a general linear model (GLM) analysis as well as a Dunnet's test to compare experimental groups to our control. P-values below 0.05 were considered statistically significant throughout the experiments.

2.3 Results

Each spot in the culture chamber was exposed to only one pressure and pulse length combination. All treatments were randomly selected inside the chamber to minimize uncontrollable sources of error like differences in cell density. Comparisons between the control and experimental groups were used to identify the

effects caused by ADV including those caused by either US alone or droplets alone. As we mentioned in section 2.2.4, the control group consisted of all the pressure and pulse length combinations without the addition of droplets, while the experimental group consisted of all the combinations with the addition of droplets and thus provided the elements necessary for ADV. It has been previously shown that ADV is a threshold phenomenon [8] , and as such it only happened when the PNP was above said threshold (~4 MPa). This threshold was optically obtained by observing consistent vaporization (production of bubbles) as the acoustic pressure and pulse length was increased. DDFP droplets have minimal acoustic scattering compared to gas bubbles so those treatments below the threshold served to investigate the effect of droplets alone.

2.3.1 Bubble cloud and localized damage

Once above threshold, the size of the bubble cloud generated by ADV increased with pressure, but was not affected by the pulse length (Figure 2.3 and Figure 2.4). Preliminary experiments showed damaged areas as stained with fluorescent dye calcein AM and EthD-1 after ADV was performed. These areas were inspected and overlaid using the corresponding bubble clouds to evaluate the localization of the damage. Qualitative observations of these images showed that the impact of ADV was highly localized as damage zones corresponded to an area that was almost equal

in size to that of the bubble cloud (Figure 2.5). In addition, viable cells were observed inside the damage (vaporization) area.

2.3.2 Cell attachment

The total number of cells from each spot was used to determine differences in cell density within and between culture chambers. This number not only helped determine initial cell density, but also the number of cells that could have been sheared-off during ADV (Figure 2.6), and as a consequence, washed away from the chamber during rinsing steps. This was carried out for both the control and the experimental culture chambers. The total number of cells between treatments in the control group, which included all treatments without droplets, was not significantly different. Forty five untreated spots were randomly selected in the experimental chamber to account for cell density. These were not significantly different when compared to our control chamber. This result showed that the same order of cell density was found in both chambers.

According to the statistical analysis, pressure was a significant factor, but a change in pulse length (number of input cycles) was not significant. However, a two-way interaction effect was also found significant. Major and significant differences were found when the pressure-pulse length combination was greater or equal to 6 MPa and 4 cycles (Figure 2.7). These pressures were responsible for the

generation of larger bubble clouds and as a consequence, larger affected areas. Significant differences in the total number of cells when compared to our control (100%) ranged from an average of 20% to 47% cell reduction when the pressure-pulse length combination was increased from 6 MPa and 4 cycles to 8 MPa and 8 cycles, respectively. For those treated with pressures below the ADV threshold (pressures under 4 MPa) there were no significant differences when compared to the control group.

2.3.3 Cell Death

The number of dead cells was also obtained for both the control and experimental groups. No significant differences were found across treatments in the control group. Cell death was approximately 1% of the total cell count. In the experimental group pressure was found to be a significant factor, whereas cycles were not. However, an interaction effect was found to be significant as well. Cell death was no higher than 5% of the total cell count in the experimental group, but was found to be significantly different when compared to the control group at a pressure-pulse length combination of 6 MPa – 8 cycles or higher (Figure 2.8).

2.3.4 Additional Experiments

Another experiment was carried out following the procedure aforementioned having pressure as the only dependent variable with increments of 1 MPa. Pulse length

was not a significant factor in the previous experiment (Figure 2.9) and as such was kept constant at 8 cycles. Cell attachment and viability was not significantly affected in the control group. A pressure greater or equal to 6 MPa was found to be significant for the experimental group (Figure 2.10). Cell death was still kept at near 1% of the total cell count for the control group and between 2% and 5% for the experimental group (Figure 2.11). However, cell death was significantly different between the control and experimental group for all treatments.

2.5 Discussion

The present study shows the effects of ADV on an EC monolayer. To the best of our knowledge this is the first study that shows the ADV-endothelial interaction under acoustic conditions relevant to GE. The main findings of this work are the dependency of bubble cloud area (BCA) and cell attachment to PNP at a given frequency and droplet concentration. Both BCA and cell detachment increase with increasing PNP. The increase in BCA can be explained by the shape of the US beam and the area fraction above threshold and its direct relationship to pressure. A maximum area, limited by the saturation limit of the transducer, will be reached even if the transducer is driven at higher pressures. Consequently, this increase in BCA can explain the increase in cell detachment as more droplets were included (and vaporized) under the beam area as the pressure was increased. Interestingly, cell

death did not behave as such. Cell death was found to be significant only above a certain pressure-pulse length combination indicating that a threshold phenomenon may be responsible for this effect. However, a second experiment did not support this hypothesis as cell death was significantly different across all treatments containing droplets when compared to the control group. This discrepancy may be due to inherent differences between cell populations coming from different donors.

Another important finding of this work is the lack of an effect due to pulse length for bubble cloud formation. In theory, one effective cycle (from amplifier to transducer) above threshold should be sufficient to trigger vaporization, while subsequent cycles of the pulse would be responsible for driving the previously formed bubbles. Hence, the lack of dependency on this parameter was no surprise. Other studies [53, 54] have shown similar trends in which pulse length had no effect on the ADV threshold, especially for pulse lengths under 1000 μs. However, these studies did not address the size of the bubble cloud. Bubble cloud size was considered by other studies [55, 56] and found to be dependent on pulse length; however these results were based on *cavitating* bubble clouds generated by histotripsy pulses (PNP > 21 MPa). The pulses used in the present study were kept under 5 μs with PNPs not exceeding 8 MPa.

If a bubble is formed with one cycle, then cell damage may be affected by pulse length as cells will be exposed other mechanical events aside ADV, as for example,

bubble oscillations. Interestingly, cell damage (detachment and death) was not affected by pulse length. An explanation for these results may be that cell injury happens during the first cycle(s) of the US pulse when the bubble cloud is initially created or during the phase transition stage. This event may be so violent that cells are killed and sheared off almost immediately from the insonated area and as a result, subsequent bubble oscillations occurring in a depleted area will have no effect.

A two-way interaction effect was found to be significant between pulse lengths and PNP. The relevance of these interaction effects falls under the definition of non-additive effects. In other words, a change in one variable (e.g. pulse length) does not yield a proportional (additive) effect in the response (total cell fraction) when a second variable (PNP) is kept constant, but rather it may subdue or amplify such effects. For example, pulse length was doubled each time, but the total number of dead or detached cells did not respond proportionally. Notion of this interaction effect may confirm that it is in fact a portion of the US pulse responsible for the observed damage as this did not respond proportionally to an increase in the pulse length. In other words, the first couple of cycles of the US pulse (and not the whole pulse) were responsible for most of the damage. Addition to more cycles should have translated to more damage proportionally had this not shown an interaction effect.

No depletion or significant cell death was observed in any of the controls

indicating that it is indeed, an US-droplet and/or US-bubble interaction, the cause of significant bioeffects. Phase transition, bubble formation and subsequent expansion may have been responsible for injuring, killing or weakening the anchor created between the cells and the fibronectin coating the culture chamber, and as such cells were released and lost as fluid was withdrawn and replaced from the chamber during rinsing steps. In addition, droplets may have been directly attached to the cell surface breaking off the cell membrane at the time of vaporization. In the results from experiments as the ones observed in Figure 2.5 the number of dead cells is appreciable for a pressure of 4.5 MPa, while those affected by a pressure of 4 MPa in a second experiment, where significantly less. These discrepancies in dead cells are attributed to the differences in staining protocols for both experiments, in which it was necessary to perform more rinses in the second experiment when compared to the first possibly removing more "floating" or weakly attached injured cells.

Shear forces created with the syringe during fluid replacement were thought to be important, but only near the inlet or outlet ports. Special care was taken when injecting and withdrawing fluid to avoid any cell detachment. The success of this technique was evaluated by observing the cell attachment and viability in the control group chamber, where differences in cell count in a number of spots including those near the inlet ports were non-significant. Cell detachment was also reported in an earlier study [27] in which Chinese hamster ovarian (CHO) cells were exposed to

ADV for the delivery of a chemotherapy agent using dual phase microdroplets. Cell detachment was thought to be caused by high velocities generated by a rapid liquid consumption and bubble expansion process or IC during ADV, which in turn could potentially induce high pressures and shear stresses during the collapse phase.

The area depleted of cells was optically compared to the bubble cloud area generated during ADV by overlaying both images. It was observed that the affected area was less than or equal to the bubble cloud area. This matching of areas is another important finding of this work because it demonstrates that the cell damage is limited by the size of the bubble cloud as it is implied by the absence of detached or dead cells beyond the bubble cloud area emphasizing the concept of localized damage. This result hints yet another explanation of the mechanism of cell injury in which the droplet's albumin shell may play an important role. The EC surface contains a number of albumin-binding proteins that have been described previously and are believed to induce endocytosis [57, 58, 59]. Hence, it is plausible to state that the albumin shell covering the surface of the droplets may have stimulated an endocytosis pathway leading to attachment or partial transport of some droplets inside the ECs putting these at risk of direct ADV events capable of affecting vital organelles and the cell membrane.

Cell death was evaluated by the uptake of ethidium homodimer-1 (EthD-1), a cell-impermeant nucleic acid stain that produces a bright red fluorescence on

damaged or dead cells. Cell death is a naturally occurring phenomenon mediated either by a necrotic or apoptotic pathway, so the presence of dead cells in our controls was normal. Therefore, a normalized dead cell count was used to estimate the percentage of cells affected by ADV. This was achieved by obtaining the ratio of the number of dead cells for each experimental case over that of our control. Dead cell fractions were found to be significantly different from our control when the pressure-pulse length combination was 6 MPa and 8 cycles or higher, but kept below 5%. However, on a second experiment cell death was found to be significantly different from our control for all treatments going from an average dead cell percentage of 1% to 4%. Although, this dead cell percentage was still maintained at or below 5%, we believe that a phenomenon described by a rolling "sticky ball" may have been partially responsible for this increase in cell death. This mechanism involves droplets (sticky balls) rolling down the cell monolayer (mainly during the removal of these from the culture chamber), constantly sticking and detaching from the cells possibly breaking off the cell membrane.

Error in the measurement of the dead cell count, quantified as one standard deviation from our mean for each case was rather high for all treatments containing droplets. This observation led us to comment on another event capable of causing an increase in cell death. As mentioned earlier, ADV and IC are both threshold phenomena, but it was shown in an earlier study that IC is also a probabilistic event

[53]. Thus, cell injury during ADV may be attributed to permanent factors such as rapid liquid consumption and bubble expansion, but also to probabilistic events such as IC. Therefore small error bars should be found at pressures where IC is very unlikely or very likely to happen (low and high pressures respectively). Conversely, higher error should be present at mid-range pressures where IC is equally bound to occur or not. Unfortunately, our data showed no evidence of this, as there was high error for all treatments.

In the vasculature, EC sense shear stresses and other mechanical stimuli and through mechanotransduction can change their morphology as well as alter important intra or intercellular signaling cascades to meet metabolic needs and the overall body homeostasis [38]. Some examples of altered endothelial functions include the upregulation of growth factors, cytoskeletal reorganization and increased permeability. However, if these stresses are increased (or decreased) beyond physiological conditions EC functions could be impaired resulting in endothelial dysfunction or death [23]. From a physiological perspective, impairment of endothelial functions could be of great concern and even pathological if they are not identified promptly and controlled [38]. Risks of thrombus formation, fat accumulation, and atherosclerosis are major consequences of endothelial dysfunction to name a few. However, it is pertinent to point out that loss of normal endothelial functions will *not* necessarily translate to undesired effects. As a cancer treatment,

gas embolotherapy could potentially benefit from some of these effects providing yet additional mechanisms to aid in the eradication of the cancerous tissue, which is the ultimate goal of any cancer therapy. Damage to the endothelium could induce thrombosis at the site of vaporization providing additional occlusion to those affected vessels. Controlled impairment of endothelial functions like permeability could also aid in the delivery of drugs or other substances that will need to cross the endothelial barrier during treatments. Several studies [20, 22, 28] have confirmed this by showing an increase in the uptake of different molecular species when endothelial cells were exposed to US in the presence of contrast agents, but more importantly, ADV was also proved to provide similar effects in cell permeability [27]. In other words, if controlled, not only will ADV provide an embolus to a specific location in the vasculature, but will also provide a mechanism for triggering local drug delivery following occlusion given that cell viability can be sustained.

It is imperative to emphasize to the reader that the aforementioned results were obtained in a controlled *in vitro* experiment and that *in vivo* situations are difficult to mimic. An idealized monolayer of endothelial cells (HUVEC) supported by fibronectin was used when in actuality the endothelium is supported by an extracellular matrix composed of a mesh of different molecular components and other different layers of cells with different mechanical properties. HUVECs are commonly used cells in this field; however it is worth mentioning that the cellular

response endothelial cells in general may vary depending on their origin as well as their initial pathological state in the vascular tree [39]. These experiments only accounted for damage to the endothelium when ADV happened in close proximity to the cell monolayer and probably represent a worst case scenario that may occur during treatment, but how this damage changes with distance away from the monolayer is still unknown, but a work in progress. Other parameters like droplet to cell ratio and droplet size are believed to affect the degree of damage and should also be studied. Longer pulses or the inclusion of pulse repetition frequency (PRF) may be needed in clinical practice to increase the number of vaporized droplets in the vasculature and increase the probability of occlusion.

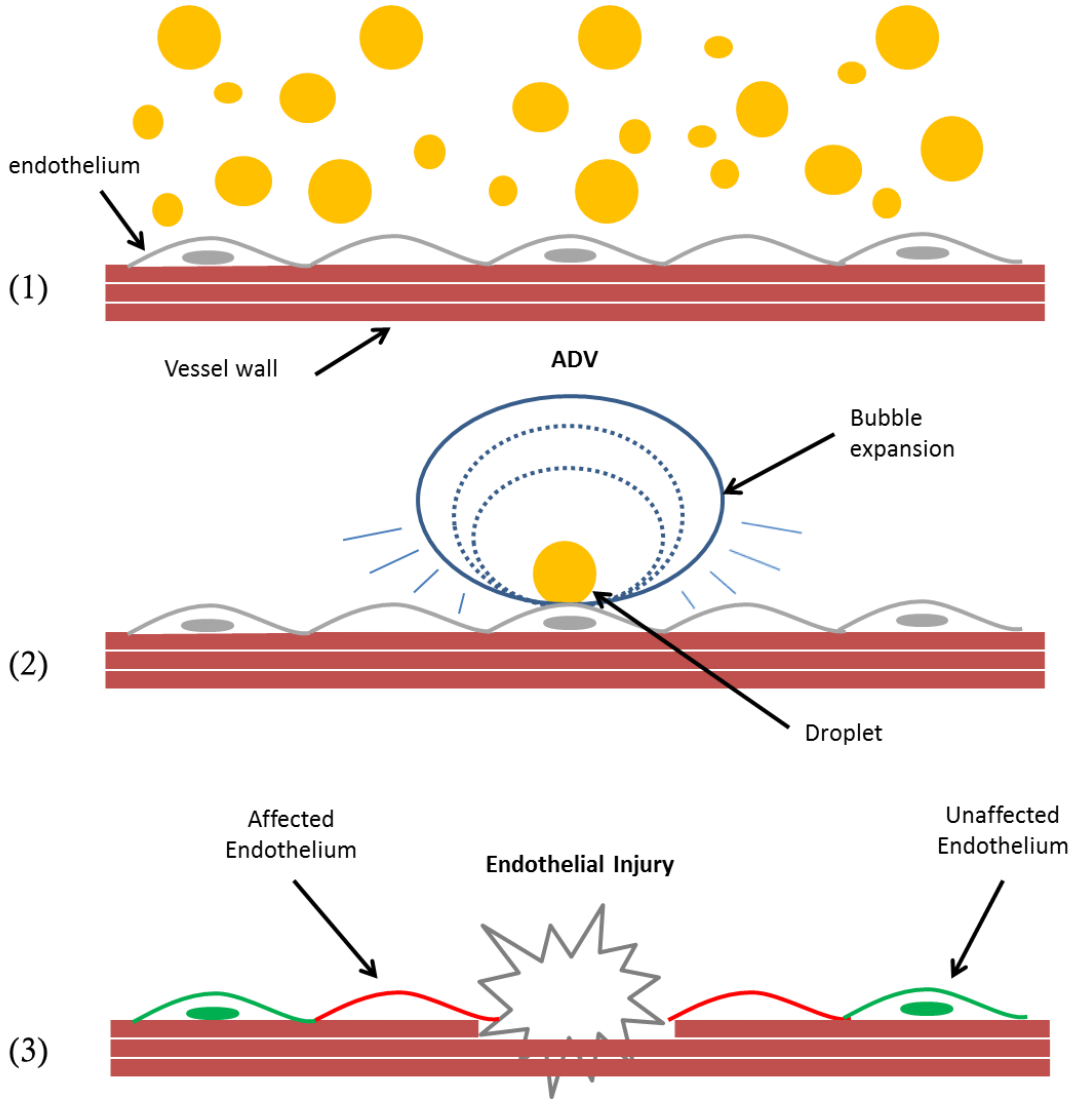

Figure 2.1: Droplets of various sizes flow inside the blood vessel (1) until an ultrasound beam triggers ADV that may occur near or at the vessel wall (2) impacting endothelial cells and ultimately important vessel functions (3). Note: droplet in (2) is the source of the final bubble and not a droplet inside a bubble.

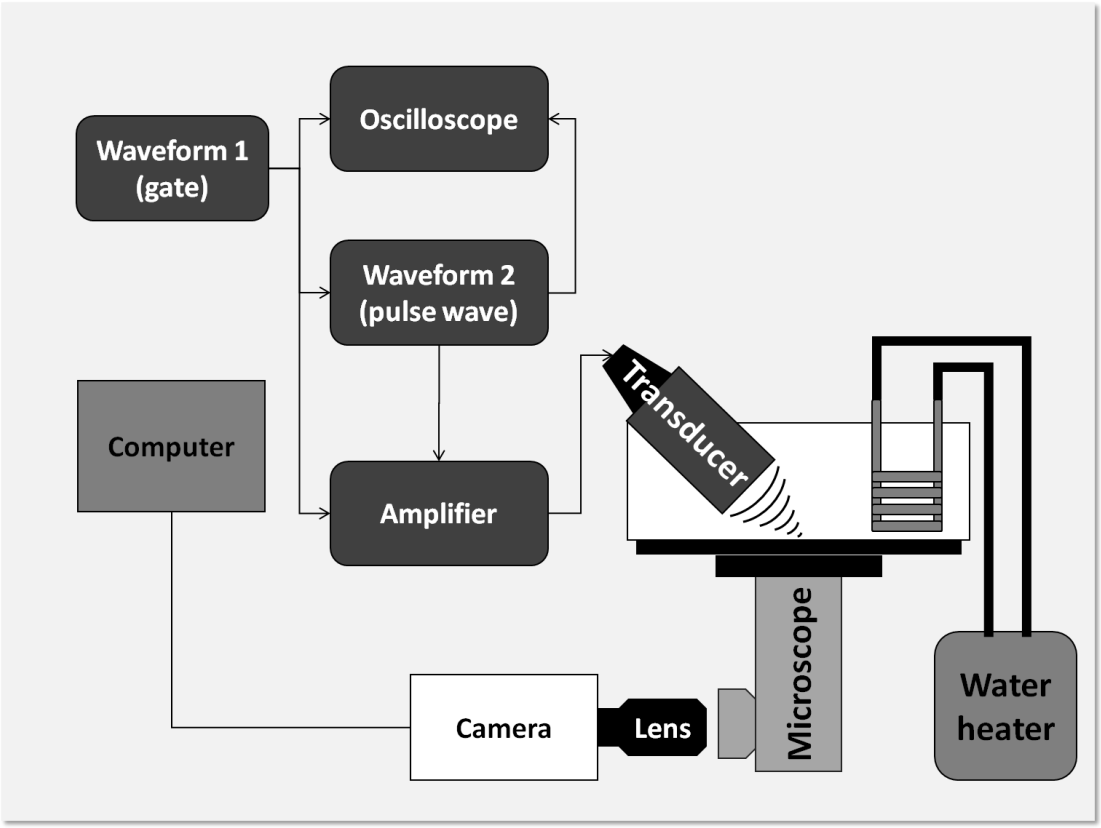

Figure 2.2: Ultrasound setup. A single element transducer is placed at an angle focused at the bottom of an OptiCell™ culture chamber. ADV events are recorded using a camera attached to an inverted microscope.

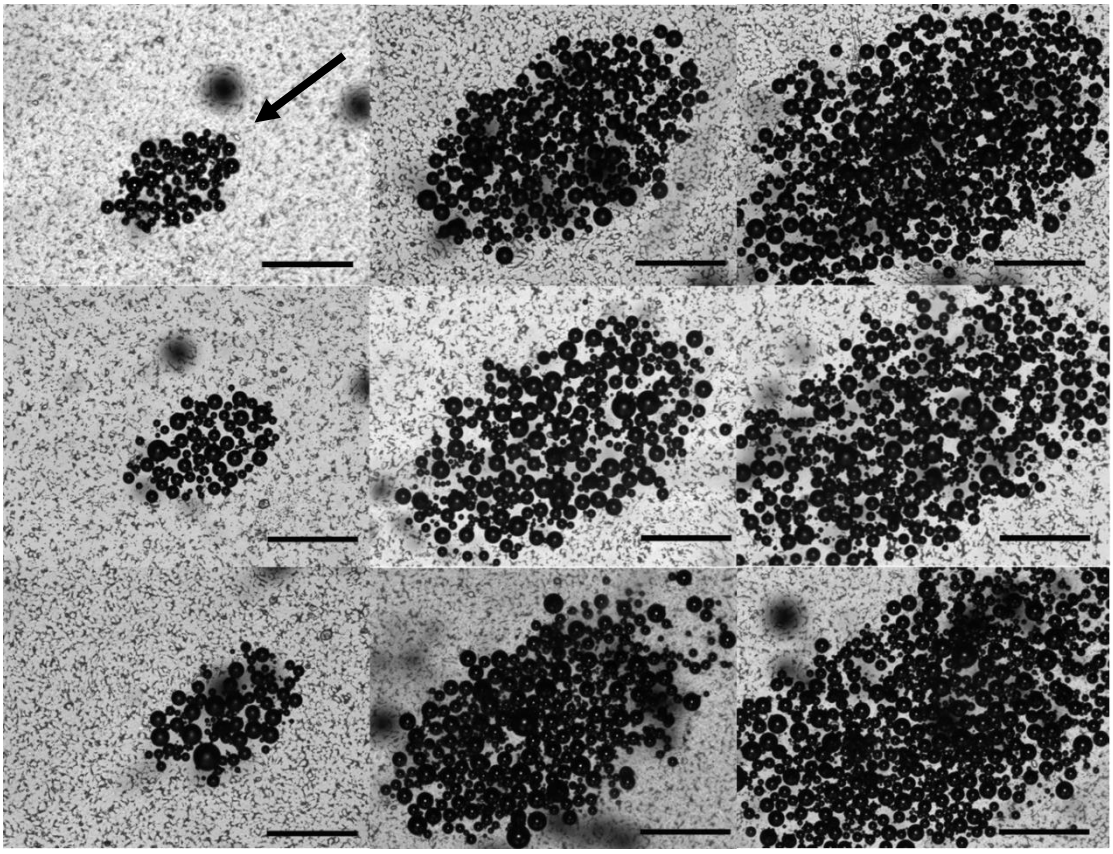

Figure 2.3: Bubble clouds as generated during ADV at 4 MPa (left column), 6 MPa (middle) and 8 MPa (right column). Rows represent number of cycles as follows: 4 (upper), 8 (middle) and 16 (bottom). The US beam travels from NE to SW (arrow). The scale bar is 500 μm.

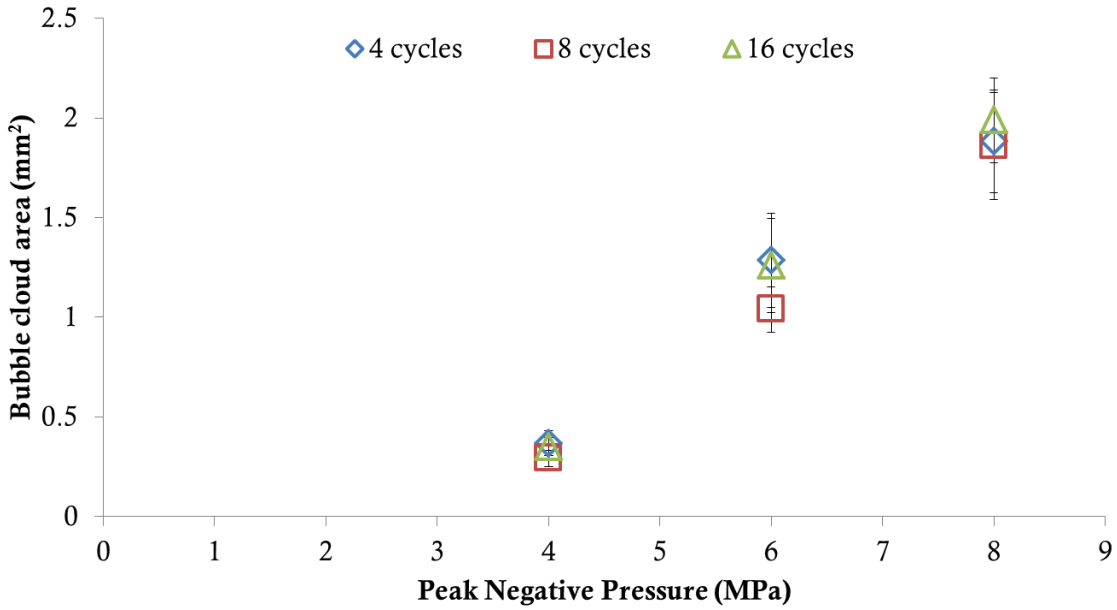

Figure 2.4: Bubble cloud area versus pulse length. Vaporization (ADV) threshold is at 4 MPa, 4 cycles. Error bars correspond to one standard deviation (n=8). Significant differences found across pressures ($p<0.05$), but not across cycles ($p>0.05$).

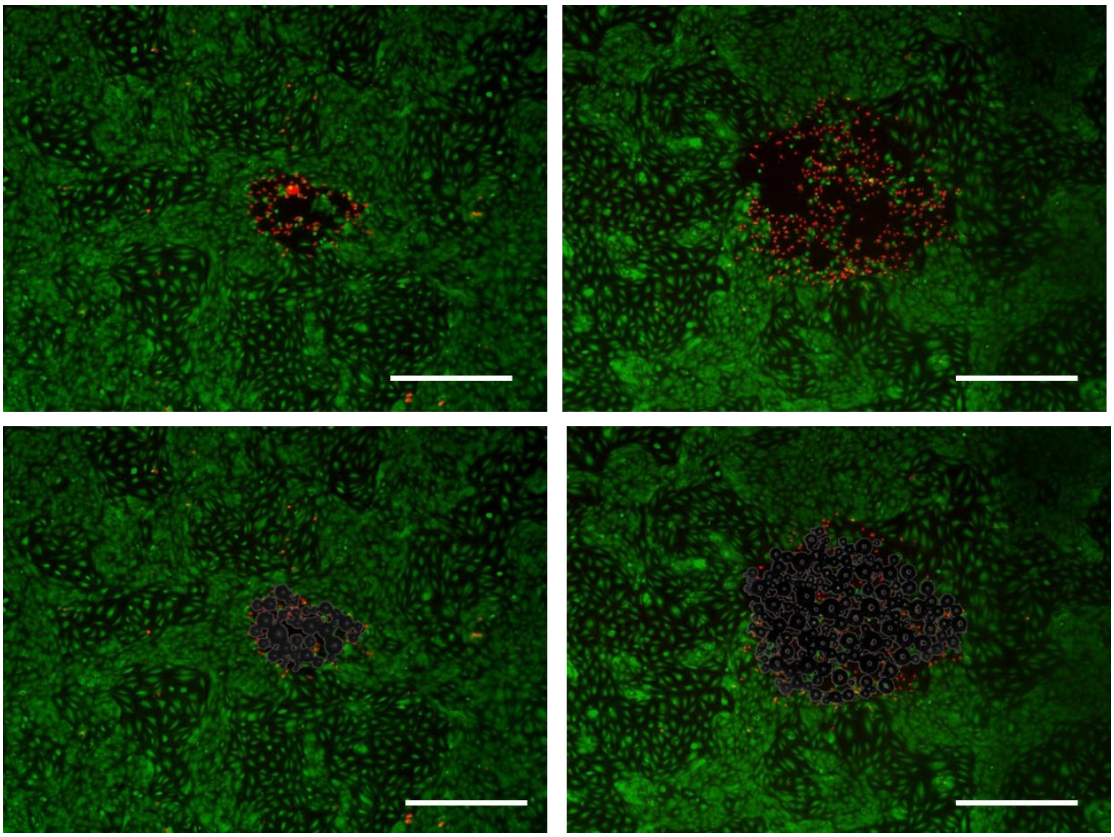

Figure 2.5: Endothelial cells stained with fluorescent dye calcein (live cells) and EthD-1 (dead cells) after ADV at 3.5 MPa (left column) and 4.5 MPa (right column). By creating an overlay of the images containing the bubble clouds (bottom row) generated during ADV we can see that the damage zones are practically the size of said bubble cloud. Note that a few cells inside this damage zones have survived ADV. The scale is 500 μm.

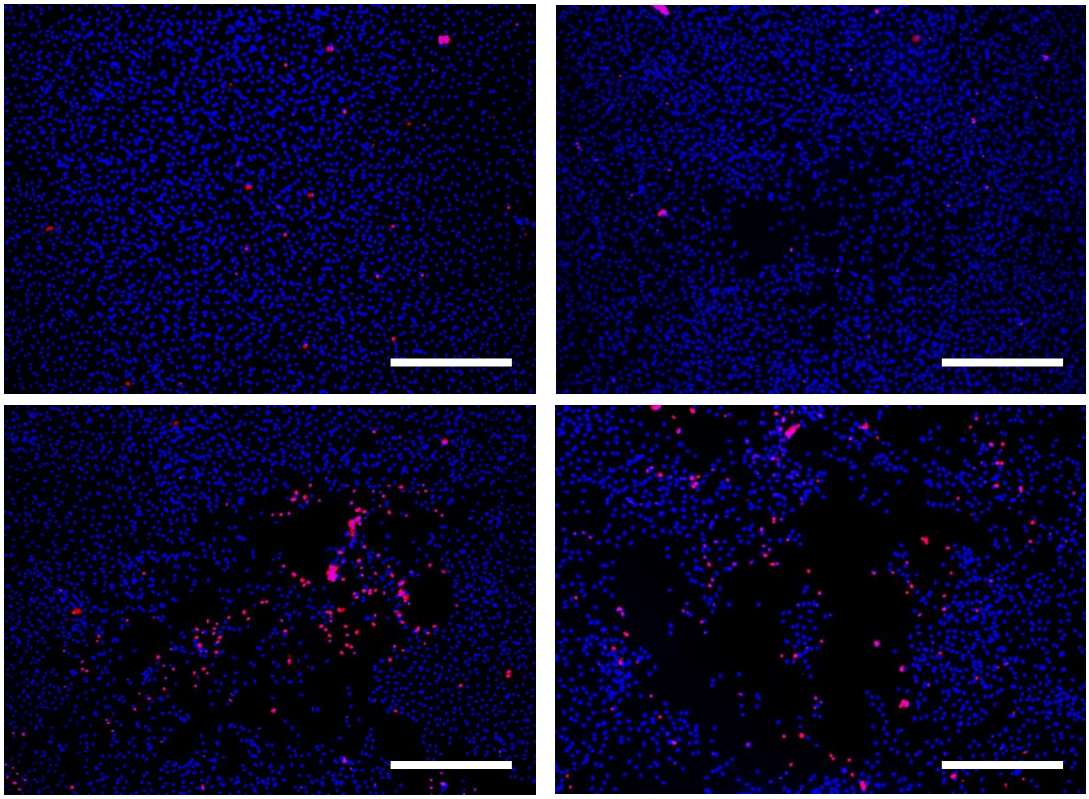

Figure 2.6: Representative images depicting cell damage after ADV compared to a control (top left). Cell death (red stain) as well as sheared off cells (empty spaces in the center) increase with pressure: 4MPa (top right), 6 MPa (bottom left) and 8 MPa (bottom right). The ultrasound pulse consisted of 8 cycles. Cells were stained with nuclei acids Hoechst (all cells) and EthD-1 (dead cells). The scale bar is 500 μm.

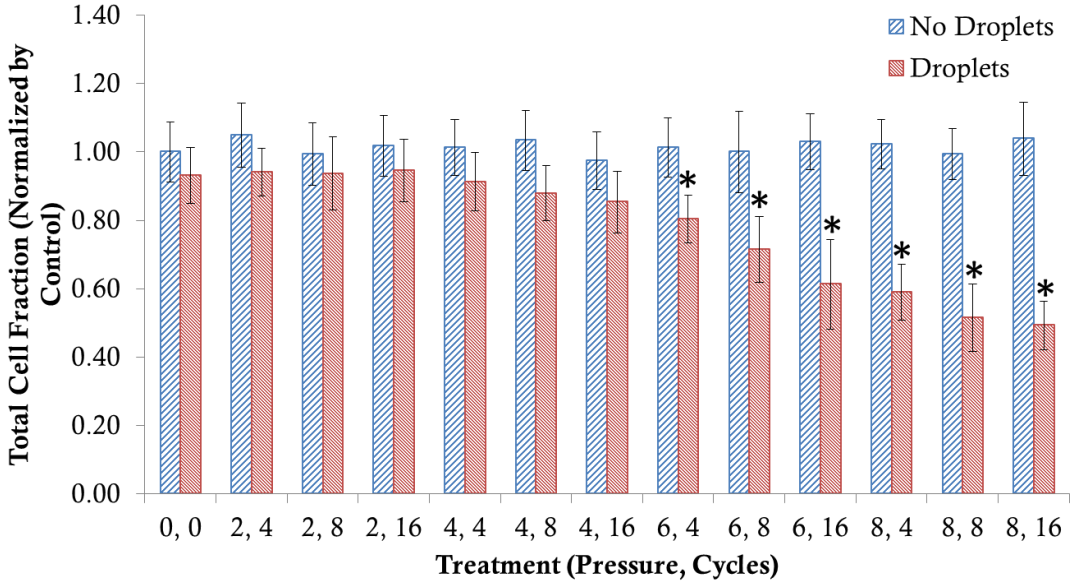

Figure 2.7: Total cell fraction as normalized by our control. The total cell fraction corresponds to the total number of cells in each treatment divided by the total number of cells in our control (0 MPa, 0 cyles, no droplets). Each treatment is described by a peak-negative pressure (MPa) and a number of cycles. Vaporization (ADV) threshold is at 4 MPa, 4 cycles. Asterisks (*) denote treatments that are significantly different from the control ($p<0.05$). Error bars correspond to one standard deviation (n=8).

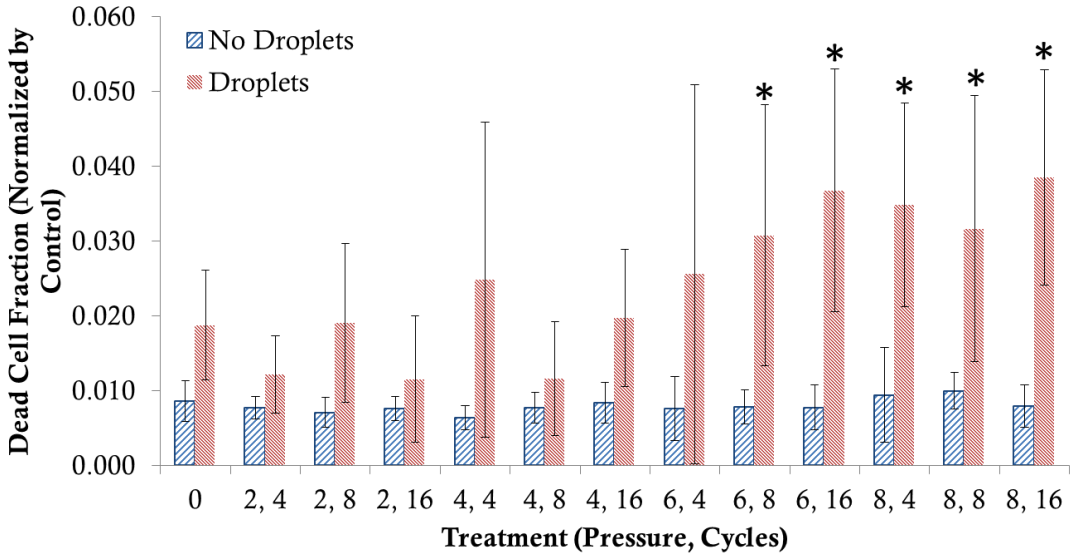

Figure 2.8: Dead cell fraction as normalized by our control. The dead cell fraction corresponds to the total number of dead cells in each treatment divided by the total number of cells in our control (0 MPa, 0 cyles, no droplets). Each treatment is described by a peak-negative pressure (MPa) and a number of cycles. Vaporization (ADV) threshold is at 4 MPa. Asterisks (*) denote treatments that are significantly different from the control ($p<0.05$). Error bars correspond to one standard deviation (n=8).

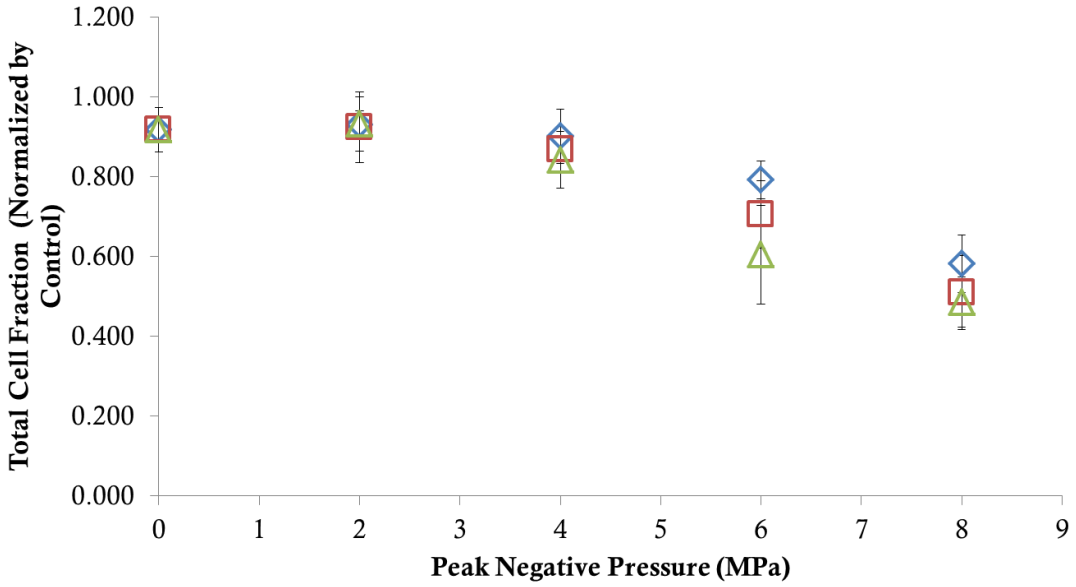

Figure 2.9: Total cell fraction as a function of peak negative pressure for 4 cycles (blue diamonds), 8 cycles (red squares) and 16 cycles (green triangles). Error bars correspond to one standard deviation (n=8). No statistical significance ($p<0.05$) was found for cycles.

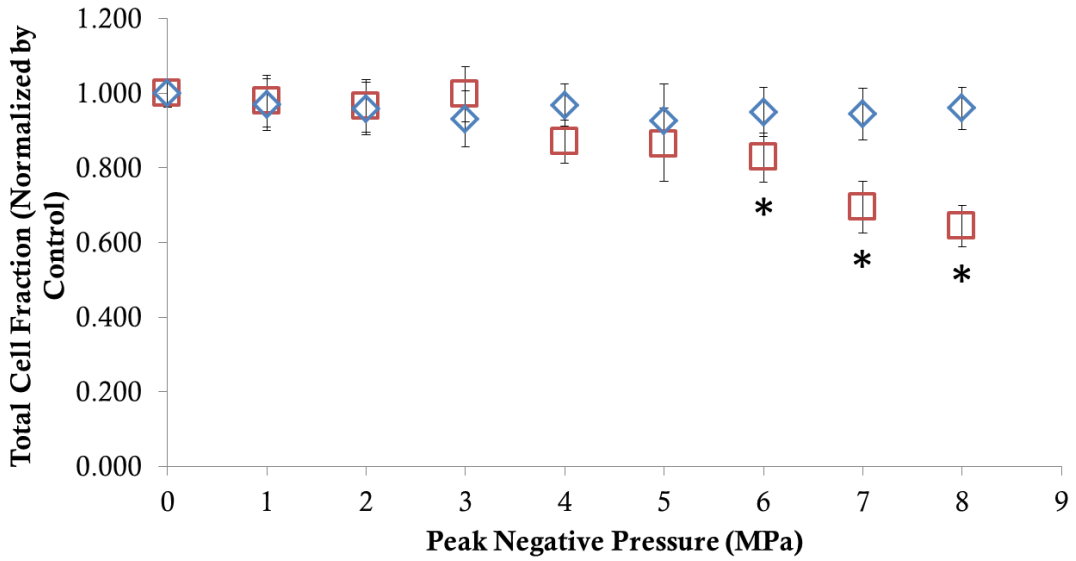

Figure 2.10: Total cell fraction as a function of peak negative pressure. The total cell fraction corresponds to the total number of cells in each treatment divided by the total number of cells in our control (0 MPa, no droplets). Red squares correspond to all treatments with droplets while blue diamonds correspond to treatments without droplets. Vaporization (ADV) threshold is at 4 MPa. Asterisks (*) denote treatments that are significantly different from the control ($p<0.05$). Error bars correspond to one standard deviation (n=8).

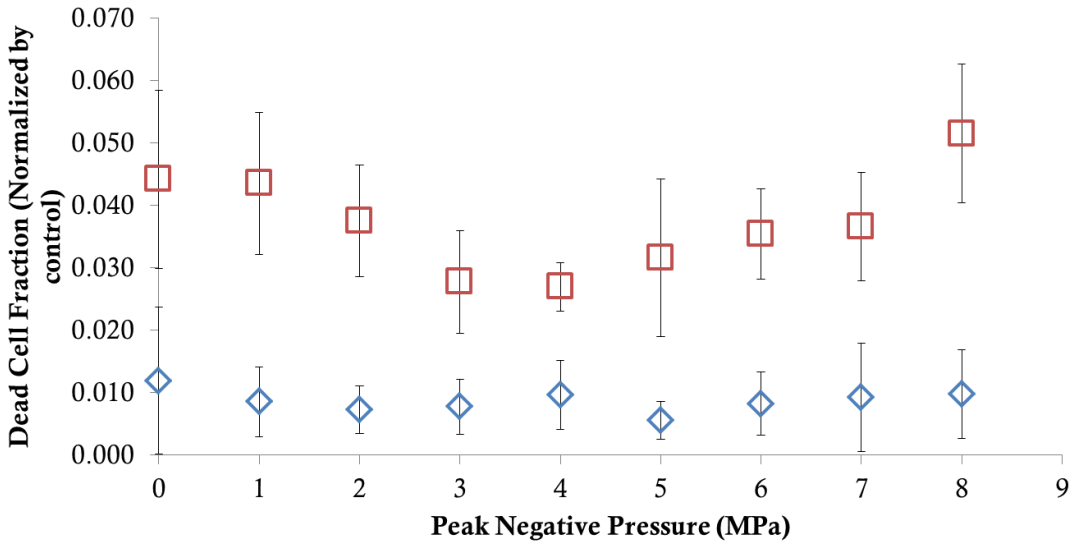

Figure 2.11: Dead cell fraction as a function of peak negative pressure. The dead cell fraction corresponds to the total number of dead cells in each treatment divided by the total number of cells in our control. Red squares correspond to all treatments with droplets while blue diamonds correspond to treatments without droplets. Vaporization (ADV) threshold is at 4 MPa. Significant differences ($p<0.05$) from our control were found for all treatments. Error bars correspond to one standard deviation (n=8).

Chapter 3

Comparison of frequency-dependent bioeffects on endothelial cells

3.1 Introduction

Acoustic cavitation refers to events where previously formed cavities (gas bodies) expand and contract in the presence of an acoustic field [60]. Two types of cavitation have been previously described and are referred to as stable and transient (inertial). As mentioned in Chapter 2, stable cavitation happens when these gas bodies undergo small oscillations for many cycles of the acoustic pressure. If the pressure is high enough, these gas bodies may collapse violently (Figure 3.1) due to inertial cavitation (IC) generating as a result, high temperatures and pressures capable of inducing bioeffects on tissue [61].

A recent study demonstrated that changes in acoustic parameters could potentially establish the likelihood of IC during ADV when insonating droplets at 3.5

MHz [53]. An important finding of this work was the relationship between the thresholds for IC and ADV and the probability of observing one event independently from the other. According to that study, ADV could take place at pressures near 3 MPa with almost zero chance of IC. In turn, IC was more probable to happen if pressures were greater than or equal to 5.7 MPa reaching an almost 100% chance of occurring if pressures were greater than 8 MPa. In addition, long pulse lengths were likely to lower the IC threshold, while keeping that of ADV relatively constant. Other acoustic parameters had little effect on both thresholds as it was the case for PRF or were kept constant as it was the case for carrier frequency. Carrier (transducer) frequency, though not investigated in that particular study, is also an important parameter that has been extensively studied in the diagnostic US field since it is known for significantly affecting the IC threshold as it is described by the mechanical index (MI) [15, 14, 61, 62]. The MI is an important metric in diagnostic US that predicts when significant bioeffects associated to transient cavitation are expected. The MI is defined as the ratio of the peak negative (rarefactional) pressure (PNP), which is derated for attenuation, and the square root of the center frequency of the ultrasound field and should not exceed a value of 1.9 (per FDA regulations) in all but ophthalmic imaging where the limit is lower [63]. The MI has also been associated with spatial peak-pulse average intensity (I_{SPPA}) for which values above 1000 W/cm^2 can be sufficient to induce transient cavitation [64].

For ADV, higher frequencies would be rather attractive as these will lower the ADV threshold making it easier to vaporize droplets, while being less likely to induce IC [53]. Unfortunately, the use of higher frequencies for GE inside the body will be limited since these are not able to overcome tissue attenuation. Therefore, the selection of an appropriate carrier frequency for our application requires a more elaborate decision-making process. This chapter explores this frequency-dependent phenomenon by comparing bioeffects generated during ADV at 3.5 MHz and 7.5 MHz under the same conditions to elucidate the role of carrier frequency in the generation of significant bioeffects and the underlying mechanism.

3.2 Materials and Methods

All descriptions for materials and methods for this chapter follow those found in Chapter 2. The following sections are briefly summarized for the benefit of the reader. For specific details of materials or equipment used (i.e. manufacturer or catalog numbers), or other procedures please refer to Chapter 2, section 2.2.

3.2.1 Cell Culture

HUVECs were cultured and maintained at 37ºC in standard culture conditions. Cells were grown in culture flasks for one passage and then transferred to OptiCell™ culture chambers previously coated with fibronectin prior to US experiments. The cells were grown to ~90% confluence and only passages one through four were used

in these experiments.

3.2.2 Droplets

Albumin-coated droplets with a DDFP core were obtained from the Department of Radiology at the University of Michigan, Ann Arbor.

3.2.3 Ultrasound Setup

An acrylic tank containing degassed water was placed on top of an inverted microscope to observe and record ADV events. A single-element 7.5 MHz (A321S, 1.9 cm-diameter, 3.81 cm-focal length, Olympus Panametrics-NDT, Waltham, MA) transducer was focused at a 40° angle to the bottom membrane of an OptiCell™ chamber located at the bottom of the tank. The US pulses were generated and controlled using two function generators and an amplifier as described in Chapter 2, section 2.2.3 and monitored using an oscilloscope.

3.2.4 Exposure Protocol

Please refer to chapter 2, section 2.2.4 for details. For this experiment PNPs ranged from 0 to 5 MPa, while pulse length was varied by changing the number of cycles to a nominal value of 4, 8 and 16. Contrary to the previously described transducer (3.5 MHz) in Chapter 2, the 7.5 MHz transducer reaches saturation close to 5 MPa. It is important to note that although the 3.5 MHz transducer was able to reach saturation much later (i.e. 8 MPa), the 7.5 MHz transducer is capable of providing a

lower ADV threshold (2 MPa versus 4 MPa).

3.2.5 Fluorescence Microscopy

The OptiCells™ culture chambers were rinsed 2x with PBS containing 2% BSA to remove any excess droplet solution. Cells were stained with nucleic acid dyes Hoechst and EthD-1 following the staining protocol, then fixed in 4% PFA and stored in HEPES with sodium azide to prevent fungal growth. Each area exposed to an ADV event was examined using a 4x magnification objective. A fluorescence image, consisting of a blue (total cell count) and a red (dead cell count) frame, was obtained for each area and recorded using MetaMorph Premier software.

3.2.6 Image Processing

Fluorescence microscopy images were cropped using a Matlab (Mathworks, Natick, MA) script according to the beam width of the new transducer in order to increase the signal-to-noise ratio of each image. These were transferred to ImageJ for image processing that included conversion to binary (black and white) and particle counting using the "Analyze Particles" tool to determine the total number of cells and the number of dead cells per frame. Overlays were created using Adobe PhotoShop.

3.2.7 Statistics

Each treatment consisted of between 6 and 9 replicates. This difference in sample size was due to imaging artifacts encountered during image acquisition. Minitab 16

(Minitab Inc., State College, PA) was used to carry out the statistical analysis. A general linear regression and an ANOVA were performed to determine significant factors affecting the response of our experiments. A Dunnet's test was also used to compare experimental groups to our control. P-values below 0.05 were considered statistically significant throughout the experiments.

3.3 Results

The results from this study are divided into three sections. The first two will be focused on the results involving the 7.5 MHz transducer alone (sections 3.3.1 and 3.3.2), while the second one will focus on making a comparison to those obtained in chapter 2, considering the change in carrier frequency (section 3.3.3). Similar to chapter 2, this chapter shows the effects of performing ADV using a single 7.5-MHz US pulse at various combinations of PNPs and pulse lengths on ECs. Damage was observed and assessed by the use of nucleic acid stains Hoechst 33342 and ethidium homodimer-1 (EthD-1).

3.3.1 Bubble Cloud

The size of the bubble cloud generated by ADV using a 7.5 MHz transducer was affected by each combination (above threshold) of pressure and pulse length (Figure 3.2). A PNP of 2 MPa and 4 cycles was not able to provide sufficient energy to vaporize the droplets, but an increase to 8 cycles provided enough acoustic energy to

initiate ADV. A general regression analysis was performed using the bubble cloud area (BCA) in mm^2 as the response. The variables Pressure and Cycles were used as predictors. The variable Cycles was used as a categorical variable after a preliminary regression analysis revealed a lack-of-fit ($p<0.05$) for the initially proposed model. This regression analysis yielded an equation for each Cycles group (Figure 3.3).

According to this model, Pressure was a significant predictor, whereas Cycles was only a significant predictor for the treatment at 16 cycles, while Pressure*Cycles was a significant predictor for both the 8-cycle and the 16-cycle treatment when compared to the 4-cycle treatment. Significant predictors are those variables that when included in a regression, significantly improve the prediction of the response. The (adj) R-Sq of this model was 92% with a non-significant lack-of-fit. However, this model is only useful for predicting BCAs only at the three levels of cycles tested, but for all values of pressure between 2 and 8 MPa.

3.3.2 Total Cell Fraction and Death Cell Fraction

The total cell fraction (TCF) from each spot was used to determine differences in cell density across the culture chamber as it was shown in chapter 2. An ANOVA of the negative control group (chamber without droplets) and the treatments with droplets, but no ADV revealed that neither Pressure nor Cycles cause a significant change in

the mean and that the cell densities for both chambers were not significantly different. Therefore an average value of the total cell count was used to normalize the data and obtain a TCF.

For the experimental group it was found that Pressure did not cause a significant change in the mean, however Cycles and an interaction between Pressure and Cycles were significant. A Dunnett's test showed that only treatments with droplets 4, 16; 5, 8 and 5, 16 (pressure, cycles) were statistically different from our control (0, 0, no droplets). Similarly, for the dead cell fraction (DCF), an ANOVA was performed. However, a preliminary analysis of the residuals revealed the need for a transformation of the data. The following analysis was performed using a power transformation (T) of our data ($T=Y^{\lambda}$) with lambda equal to 0.5 and Y equal to DCF. According to the ANOVA none of the variables used in our study affected significantly the value of DCF^0.5.

For the following section TCF was chosen over the DCF as a metric for bioeffects after our data indicated that the DCF did not seemed affected by a change in acoustic parameters (this chapter) or was maintained below 5% (Chapter 2).

3.3.3 Frequency-dependent effects

Chapter 2 showed how BCA could be predicted by only using pressure and how the pulse length (cycles) was not an important factor when vaporizing at 3.5 MHz. In

this chapter however, it was observed that both pressure and cycles were significant variables affecting the value of BCA. To investigate this, the BCA data were plotted against the spatial peak-pulse average intensity (I_{SPPA}) of each treatment, which is a quantity that takes into account both pressure and pulse length [65]. By doing so, it was found that the intensities developed under the conditions tested by the 7.5 MHz transducer ranged from 60 to 200 W/cm^2, while those from the 3.5 MHz transducer ranged from 150 to 1500 W/cm^2. This yielded two distinct curves, with both showing that BCA increased with increasing I_{SPPA}.

While ADV is a threshold phenomenon, both data sets were fitted using a sigmoid curve. Fitting any other curve (e.g. linear, exponential) would result in less than ideal results as none of these will appropriately describe the sub threshold region. In addition, these curve fits will assume infinite BCA for infinite I_{sppa}, a hypothesis that seems rather absurd and not supported by nonlinear acoustics which states that a saturation limit is expected [66]. Although there was no experimental data to validate the saturation region of the sigmoid fit for the 7.5 MHz transducer, there is no reason to believe that this transducer will behave any differently than the 3.5 MHz counterpart, which had data supporting our hypothesis. In fact, a HIFU simulator developed by the FDA [67] was used to confirm (and estimate) the saturation limit. This HIFU simulator integrates the axisymmetric KZK equations, which take into account the combined effects of nonlinearity, beam diffraction,

interference and absorption. Radial plots of pressure and intensity were generated and used to determine the radius above threshold as the input power in watts was changed.

This information provided enough evidence to confirm that in fact, the area available for vaporization offered by both transducers will saturate as the input power is increased (Figure 3.7) and that a sigmoid fit is indeed an appropriate choice. In comparison to the 3.5 MHz transducer, the 7.5 MHz transducer showed a lower maximum area. This result was no surprise since it is known that transducers of the same focal length, but higher frequencies will saturate at lower intensities [66], therefore achieving smaller areas. The sigmoidal fits yielded R-sq > 90%, which make the sigmoidal fit not only appropriate, but also an excellent predictor of BCA.

TCF data were also plotted against I_{SPPA} for both frequencies (Figure 3.9). It is worth reiterating that the TCF data was calculated taking into account the transducer beam width for both cases. This was done in order to increase the signal-to-noise ratio of the images used. Both transducers showed a decrease in TCF as the I_{SPPA} was increased within their respective ranges. Significant damage occurred at an I_{SPPA} of near 200 W/cm^2 for the 7.5 MHz transducer and 1000 W/cm^2 for the 3.5 MHz transducer, which corresponded to a near 40% and 50% of the maximum achievable areas (as estimated from the sigmoidal fits), respectively.

The relationship for the 3.5 MHz transducer was slightly nonlinear (R-sq = 0.85),

while that of the 7.5 MHz transducer was strongly nonlinear (R-sq = 0.56). The 7.5 MHz TCF data was fitted using sigmoid fit following an analogous reasoning as in the case for BCA. In short, the TCF was unaffected or slightly affected by intensity until a significant value was reached, leading to a decrease in TCF. It is expected that a minimum will be reached and be limited by the saturation area of the transducer. Although there are not data to support the second half of the sigmoid, this fit significantly improves the R-sq to a 0.7, explaining our data more accurately when compared to the linear fit. The 3.5 MHz R-sq counterpart did not improve significantly when a sigmoid fit was used (0.87 versus 0.85), however we believe it is still the most appropriate model.

To see how both transducers compare in their ability to vaporize and affect cells, a plot that included both the BCA (as a percent of the maximum achievable area) and the TCF as a function of I_{SPPA} was generated (Figure 3.10). Analogous to a pump performance and system curves, this plot lets us analyze operating conditions of each transducer with their respective losses (TCF reduction). An operating point defined as the intersection between both curves yielded a value of 68% for the 3.5 MHz transducer and a 50% for the 7.5 MHz transducer corresponding to I_{SPPA} values of 1150 W/cm^2 and 215 W/cm^2, respectively. Operating below or above this point will sacrifice either vaporization area or cell viability (or attachment), respectively resulting in less than optimal results.

The TCF data was also plotted against the BCA taking into account differences in the transducers maximum achievable areas (Figure 3.11). This was done by defining a normalized BCA as the ratio of the experimental BCA and the maximum achievable area of each transducer. The plots revealed inverse relationships for both cases, with significantly different slopes. More specifically, the 7.5 MHz transducer showed a slope equal to twice of that for the 3.5 MHz transducer.

3.4 Discussion

The results presented here demonstrate the differences in the use of a 3.5 MHz versus a 7.5 MHz transducer for ADV purposes. To our knowledge this is the first study that describes these differences applicable to ADV and ultimately GE in terms of the effects of the cloud production on endothelial cells. Firstly, it was shown that both pressure and pulse length had an important role in determining the BCA when using the 7.5 MHz transducer, while pressure was the only significant factor for the 3.5 MHz transducer. This discrepancy could be due in part to the relative contribution of each parameter to the value of intensity. Under comparable transducer geometries, as higher frequency transducers are not capable of meeting the pressures achieved by lower frequencies and can reach saturation faster, both pressure and time will have an equally important role in determining intensity. In contrast, lower frequency transducers may rely mostly on their ability to generate higher pressures.

The data showed that BCA is strongly dependent in the intensity of the transducer, making I_{sppa} a better predictor than pressure and/or cycles under the conditions tested here.

Cell damage was described by a reduction in cells attached (TCF) after the quantity DCF showed a poor role in representing these bioeffects. As vaporization was carried out cells were likely killed, sheared-off and washed away after rinsing steps were performed removing any loosely attached or floating dead cells leading to DCFs of less than 0.10. This assumption comes in part from a number of computational studies stating that those stresses (more specifically, pressures) generated during an ADV event inside an idealized blood vessel will likely be several orders of magnitude above those encountered physiologically. For a given intensity, the 7.5 MHz transducer was more damaging than the 3.5 MHz transducer generating a lower TCF value by a factor of 2. Intensities necessary to evoke transient cavitation are believed to be above 1000 W/cm^2, and while significant damage occurs at this point for the 3.5 MHz transducer, this is not the case for the 7.5 MHz transducer. A possible explanation for these effects is the fact that for higher frequencies the ADV threshold is lowered and vaporization of smaller droplets, which do not make a significant contribution to BCA, are still capable of directly affecting the cells. This was previously documented in [8], where it was shown that two different droplet populations (in size) had the same threshold for a given

frequency. Inertial or transient cavitation is also expected to occur when the MI is at or above 1.9. However, only one of the treatments included using the 7.5 MHz reached this critical value. On the other hand, the presence of IC events in the experiments including the 3.5 MHz transducer was not ruled out, as intensities greater than 1000 W/cm^2 were achieved, and MI values reached and surpassed 1.9. Therefore, it is unlikely that IC had a significant role in generating these bioeffects when using a 7.5 MHz transducer, but these may correspond to a mechanical process linked to ADV.

As mentioned in chapter 2, ADV-related events leading to cell damage may include the rapid phase transition and bubble expansion processes. These events may be responsible for evoking high shear stresses, pressures or other mechanical means for disrupting the cell integrity (i.e. cell membrane, attachment). Extremely high pressures at the wall were estimated in a numerical study that simulated a bubble expansion inside a tube [45]. These pressures were developed in time scales O(0.5 μs), which corresponded to expansion velocities at their highest. Although our experiments did not consider a tube, these time scales are so short that it may be plausible to expect a similar or higher pressure generation in our case, since vaporization happened at the wall. In addition, IC bioeffects have been well documented in the past [61, 68, 69], which are believed to be caused mainly by either thermal or mechanical or even chemical means as it is the production of highly

reactive chemicals capable of affecting cells [69].

Cell lysis is perhaps the most extensively studied bioeffect because of the significant reduction in viability observed in most IC experiments [69]. Depleting a test sample of most cells will make it almost impossible to quantify other effects induced by less harmful mechanisms associated with IC. Nevertheless, if cell viability is sustained other bioeffects may include changes in morphology, cell permeability and growth rate.

We believe that the effects presented here are mainly attributed to ADV. The close proximity of the DDFP droplets to the cell monolayer makes the latter more susceptible to the direct effects from a vaporization event causing cell damage and eventually loss in cell attachment. The results obtained from the 7.5 MHz transducer are in good agreement with this hypothesis as this transducer was not capable of generating intensities or MI values above those reported for the onset of IC and yet induced greater effects when compared to the 3.5 MHz transducer. Nevertheless, IC could still be a possible explanation for other bubble-ultrasound related bioeffects, but predominantly after vaporization has taken place. A possible explanation for this hypothesis is the fact that during ADV the bubble is at a high internal pressure (near 50 atm). In addition, ADV (mainly the liquid consumption phase) may be over in less than 1 μs, thus bubbles of resonant size may come out of resonance before significant pressures have time to act upon them. If cells are lysed

and detached during a vaporization event, there will be no cells present to account for bioeffects associated to IC. The 7.5 MHz transducer has the ability to lower the ADV threshold while providing vaporization of smaller droplets compared to the 3.5 MHz transducer [8]. These smaller droplets, which may not significantly contribute to vaporization area, may still be responsible for the difference in bioeffects seen for both transducers. As a result, the 7.5 MHz transducer experiences a relatively lower effectiveness to provide significant vaporization and minimizing cell damage.

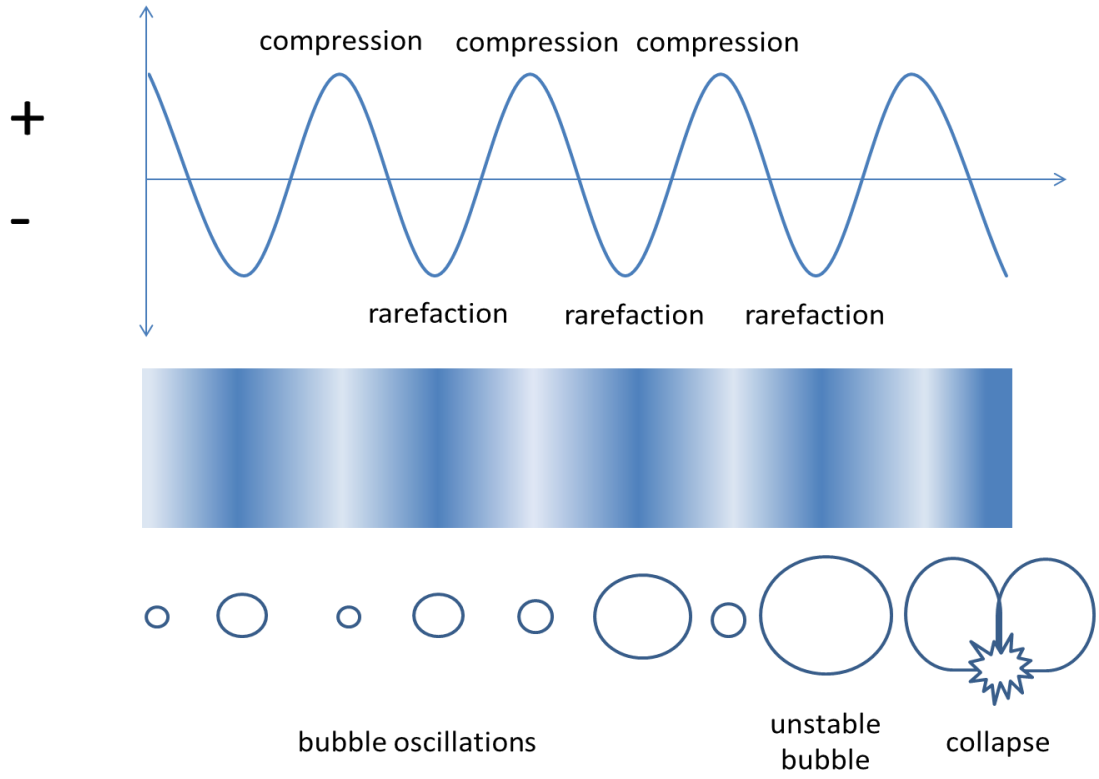

Figure 3.1: Acoustic cavitation. Bubbles endure several oscillations until a bubble grows in an unstable manner in the presence of an acoustic field. If the acoustic pressure is sufficiently high these bubbles may collapse violently. Peak positive pressures correspond to the compression phase, whereas peak negative pressures correspond to the rarefaction phase.

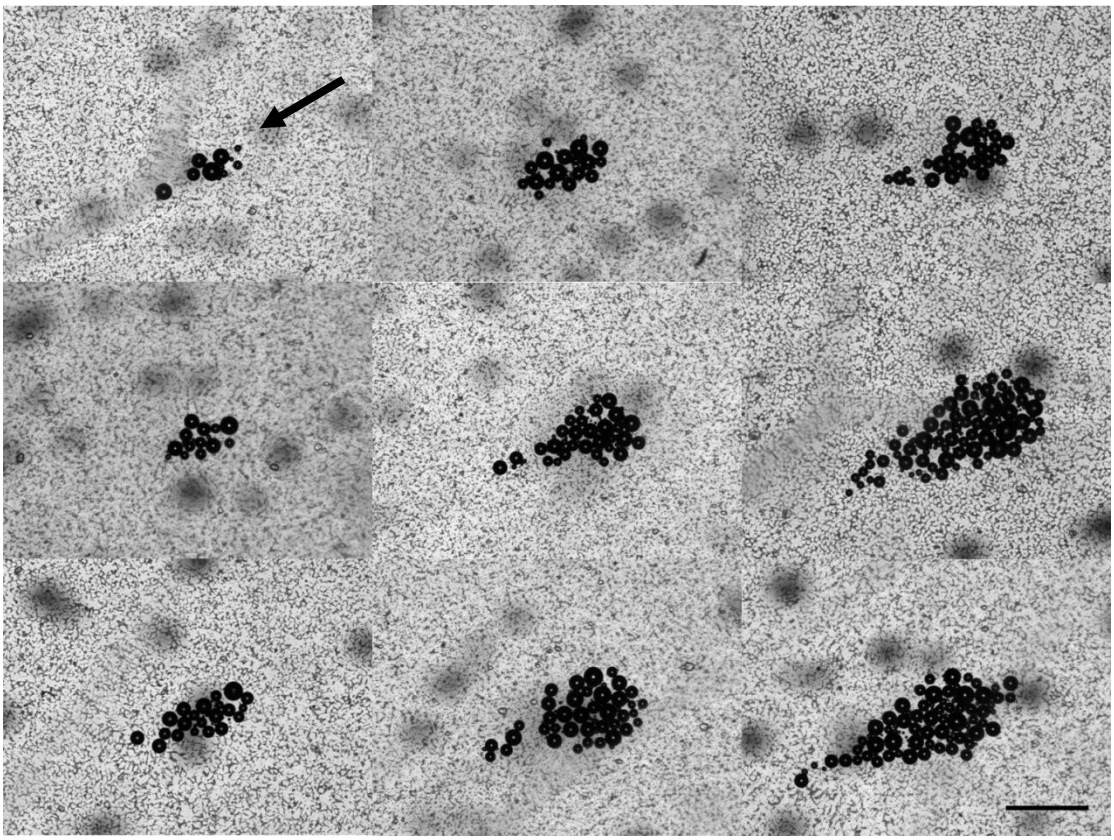

Figure 3.2: Bubble clouds as generated during ADV at 3 MPa (upper row), 4 MPa (middle) and 5 MPa (bottom row). Columns represent number of cycles as follows: 4 (left), 8 (middle) and 16 (right). The US beam travels from NE to SW (arrow). The scale bar is 500 μm.

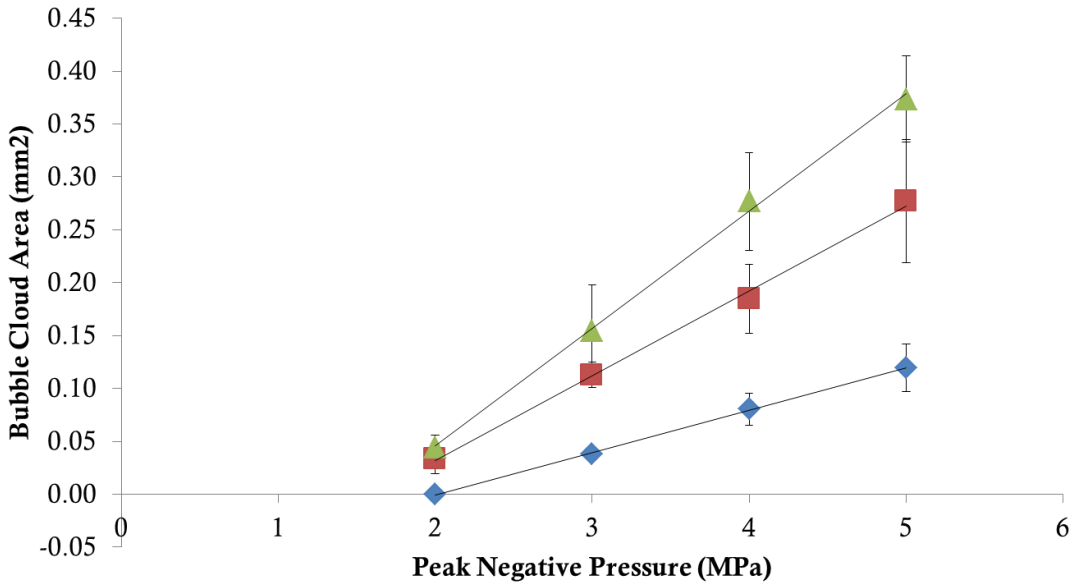

Figure 3.3: Bubble cloud area in mm^2 for different pressure-cycle combinations using a 7.5 MHz transducer: 4 cycles (diamonds), 8 cycles (squares) and 16 cycles (triangles). The ADV threshold is 2 MPa, 8 cycles. The error bars correspond to one standard deviation (n=5). Below threshold the value of bubble cloud area is 0.

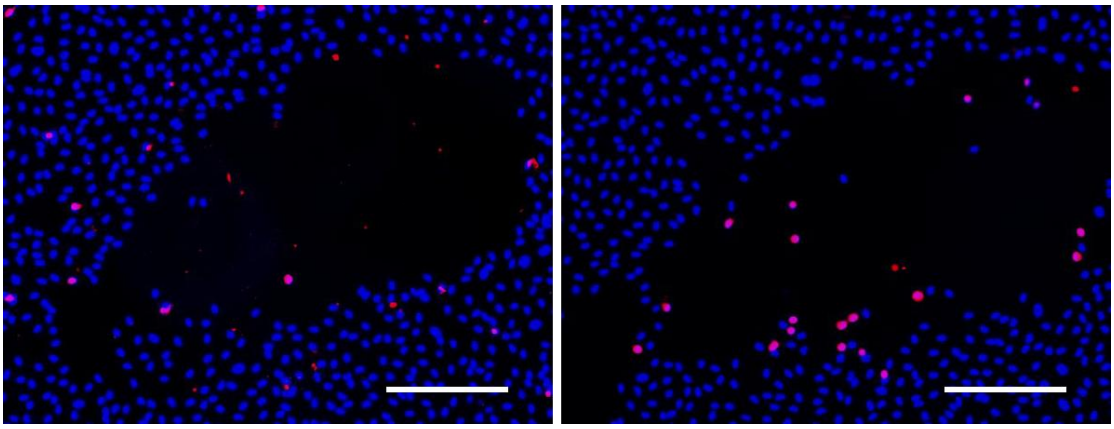

Figure 3.4: Representative images depicting cell damage after ADV using a 7.5 MHz transducer at 4 MPa, 16 cycles (left) and 5 MPa, 16 cycles (right). Cells are stained with nucleic acid stain Hoechst, while dead cells are stained red with EthD-1. The scale bar is 250 μm.

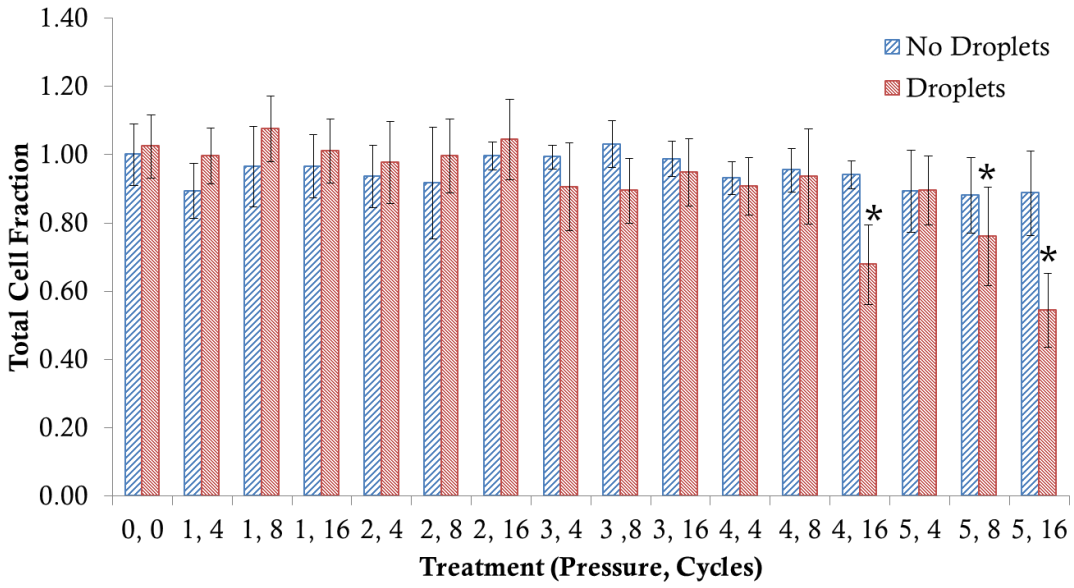

Figure 3.5: Total cell fraction as normalized by our control. The total cell fraction corresponds to the total number of cells in each treatment divided by the total number of cells in our control (0 MPa, 0 cyles, no droplets). Each treatment is described by a peak-negative pressure (MPa) and a number of cycles. Vaporization (ADV) threshold is at 2 MPa, 8 cycles. Asterisks (*) denote treatments that are significantly different from the control ($p<0.05$). Error bars correspond to one standard deviation (n=5).

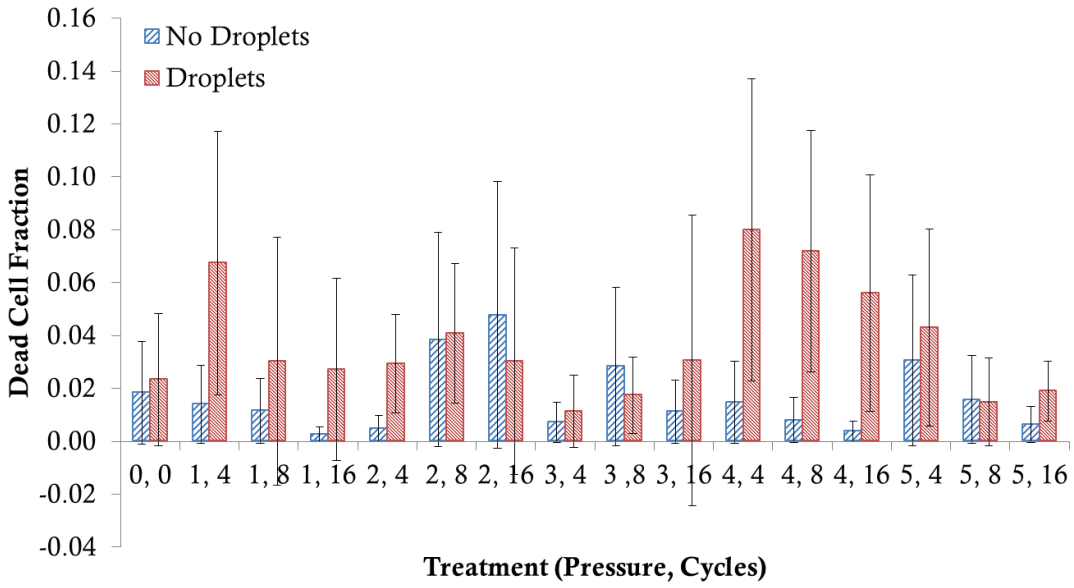

Figure 3.6: Dead cell fraction as normalized by our control. The dead cell fraction corresponds to the total number of dead cells in each treatment divided by the total number of cells in our control (0 MPa, 0 cyles, no droplets). Each treatment is described by a peak-negative pressure (MPa) and a number of cycles. Vaporization (ADV) threshold is at 2 MPa, 8 cycles. No significant difference was found between experimental treatments and our control. Error bars correspond to one standard deviation (n=5).

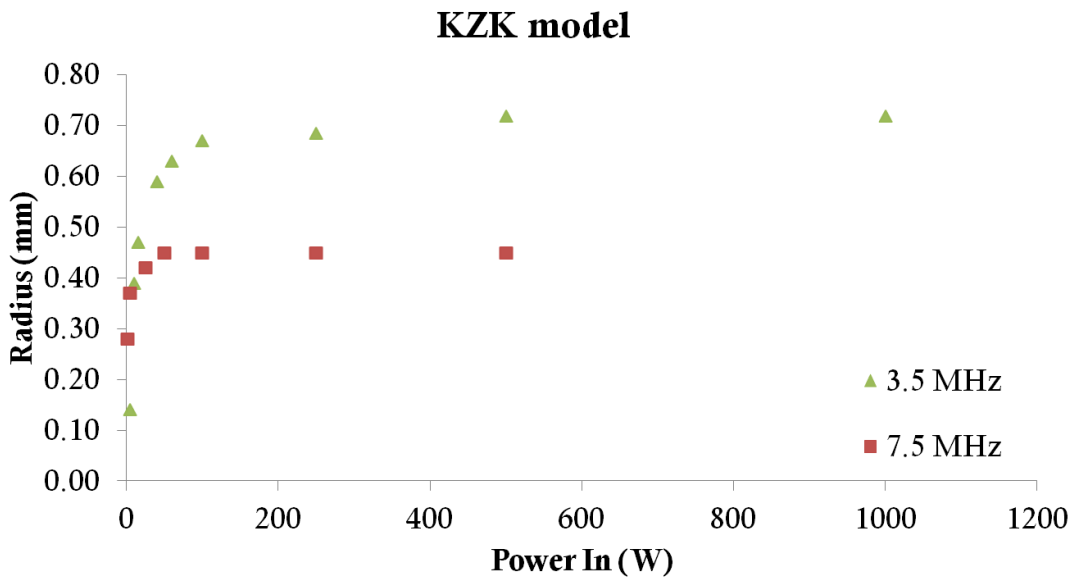

Figure 3.7: The KZK model shows how a saturation point is reached for both transducers as the input power (W) to the transducer is increased. The y-axis shows the radius above threshold for each transducer.

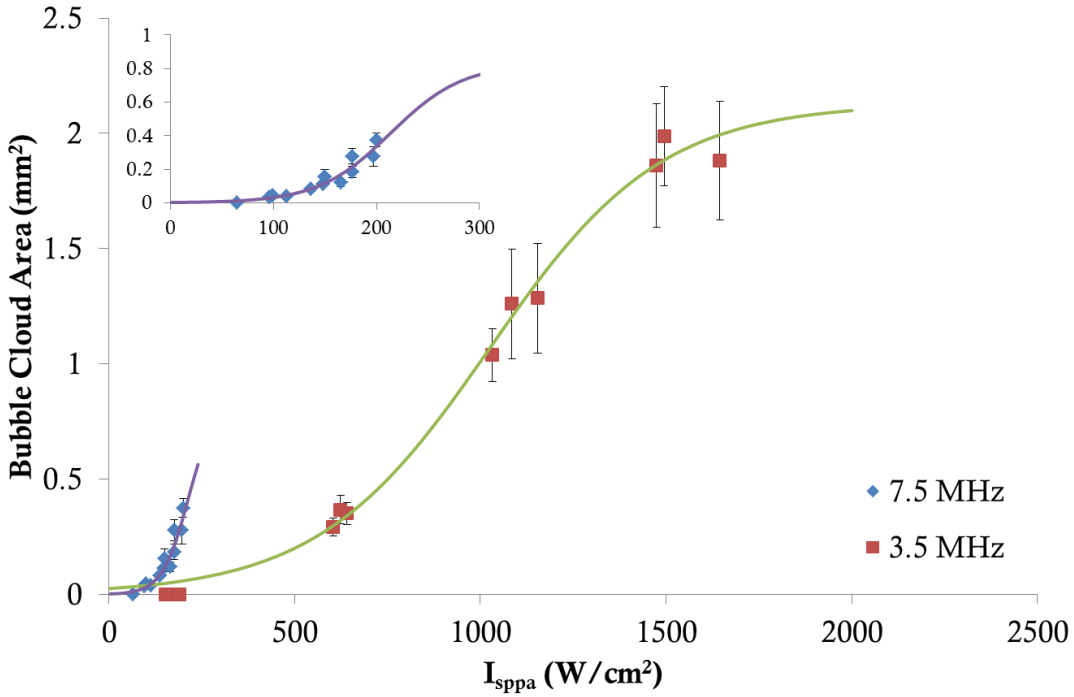

Figure 3.8: Bubble cloud area (mm^2) plotted against the spatial peak-pulse average intensity (I_{sppa}) for the 3.5 MHz and 7.5 MHz transducers. Both transducers show a sigmoidal behavior which is characteristic of a threshold phenomenon reaching a saturation point. The saturation point corresponds to the maximum achievable insonation area for each transducer as obtained using the FDA's HIFU simulator. The sigmoid fit agrees favorably with the data as the R-sq for the 3.5 MHz and 7.5 MHz fits are 0.99 and 0.91, respectively. The insert on the top left takes a closer look at the fit for the 7.5 MHz.

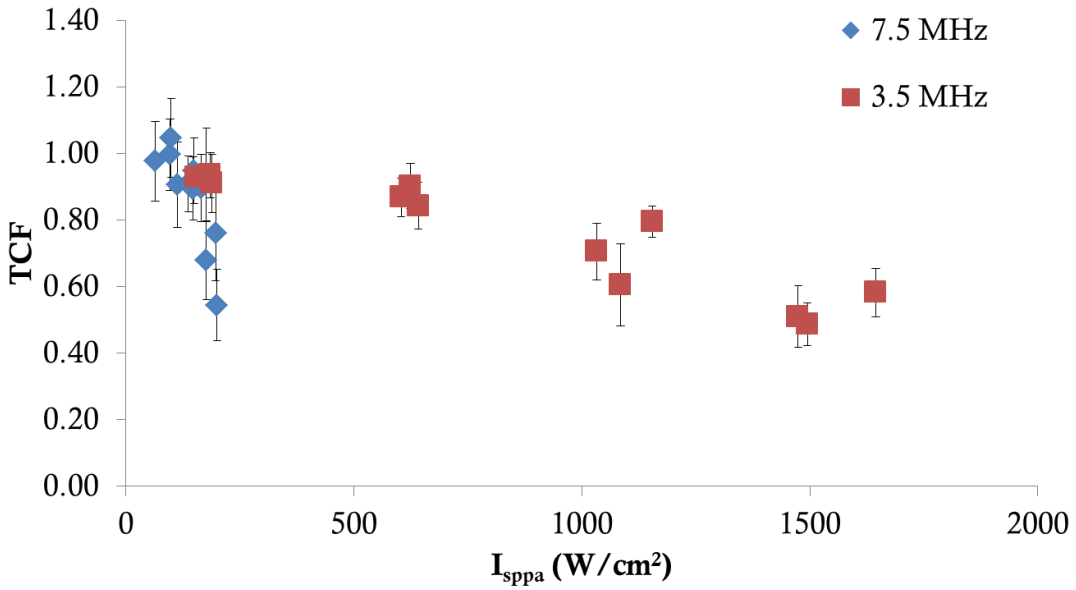

Figure 3.9: Total cell fraction (TCF) plotted against the spatial peak-pulse average intensity (I_{sppa}) for the 3.5 MHz and 7.5 MHz transducers. Both transducers show a decrease in cell fraction as the intensity is increased within their respective ranges. The behavior for the 3.5 MHz transducer is slightly nonlinear (R-sq = 0.85), while that of the 7.5 MHz transducer is strongly nonlinear (R-sq = 0.56). A TCF of 1 indicates a sample with no sheared-off cells.

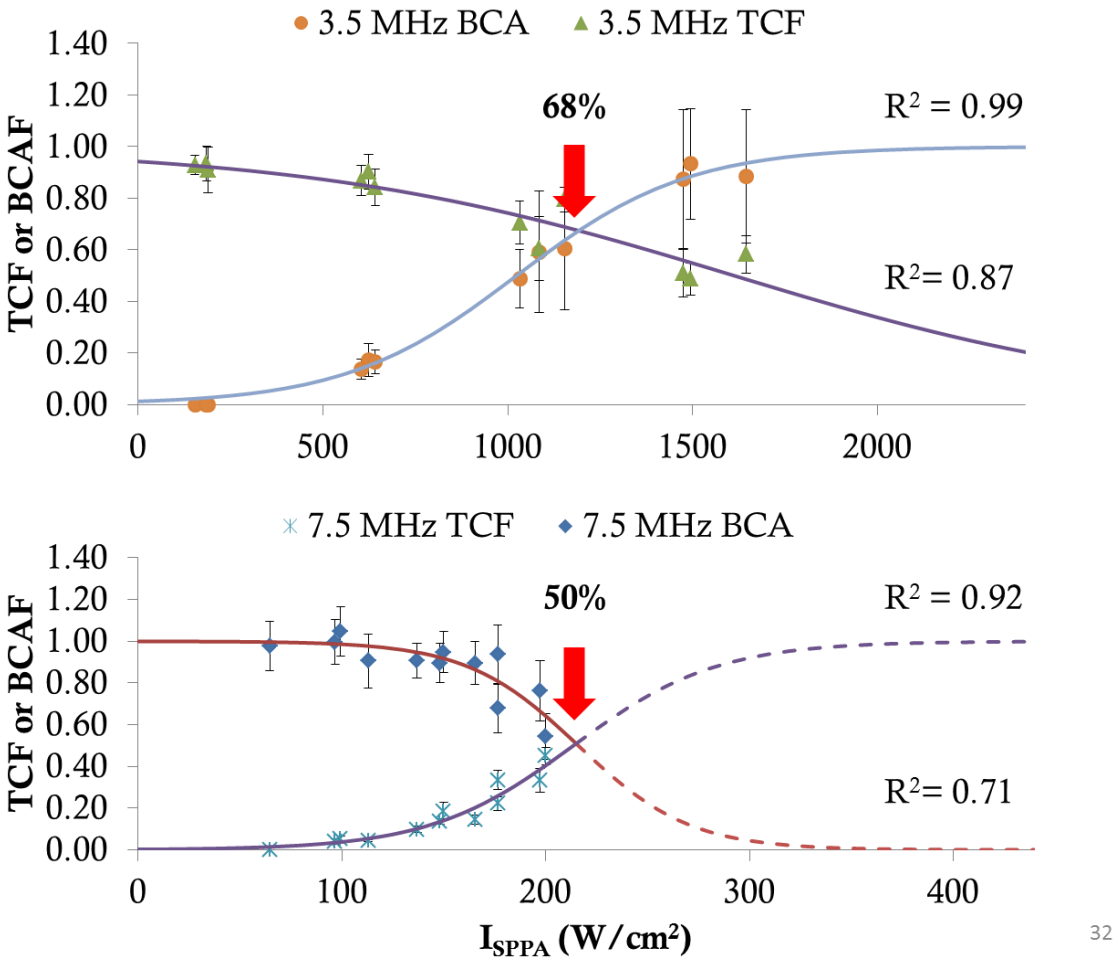

Figure 3.10: The plot above presents the total cell fraction (TCF, triangles and diamonds) and a normalized bubble cloud area (NBCA, circles and stars) plotted against the spatial peak-pulse average intensity (I_{sppa}) for each transducer. Top plot corresponds to the 3.5 MHz transducer; bottom corresponds to the 7.5 MHz transducer. The NBCA corresponds to the experimental BCA divided by the maximum achievable area obtained from the sigmoid fit of the experimental data (see Figure 3.8)

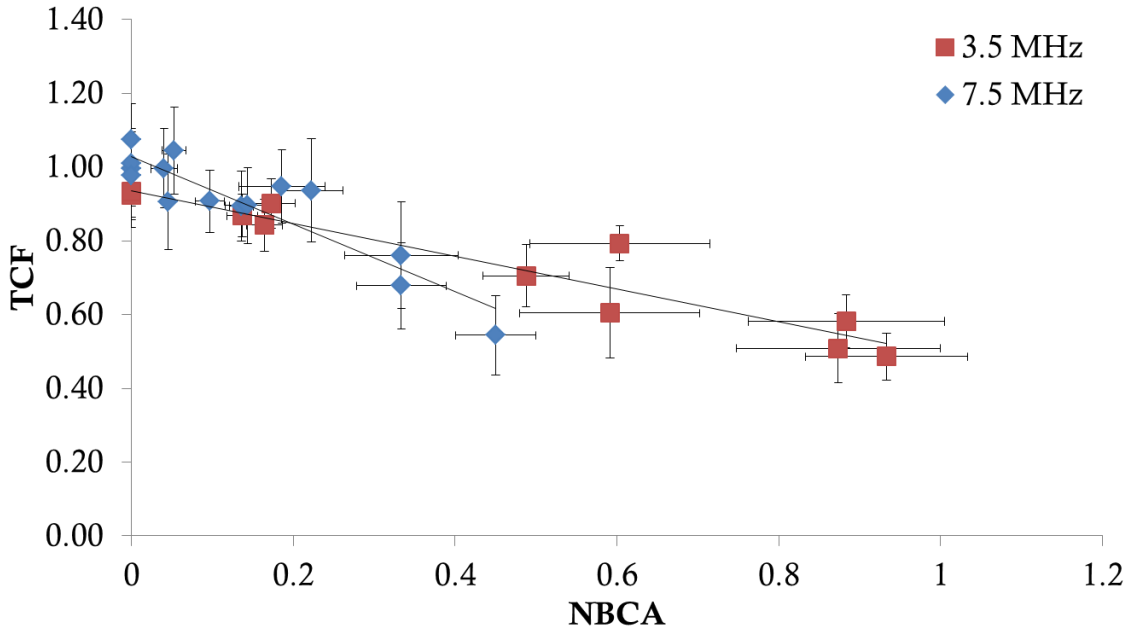

Figure 3.11: Total cell fraction (TCF) plotted against a normalized bubble cloud area (NBCA). The BCA was normalized to account for each transducer maximum achievable area for vaporization as obtained from the sigmoid fit.

Chapter 4

Vaporization proximity and confinement effects

4.1 Introduction

Chapters 2 and 3 focused their attention on characterizing the bioeffects of ADV on ECs when varying different acoustic parameters. This was however, presented as a *worst case* scenario since only droplets in direct contact with the monolayer were considered. A direct inverse relationship between total cell fraction (TCF) and bubble cloud area (BCA) indicated that those events leading to bubble formation and further expansion were likely the cause of cell injury. We also presented evidence that suggested that the 7.5 MHz transducer will be more damaging (relative to its own beam width) when compared to the 3.5 MHz transducer probably due to its capability to lower the ADV threshold, hence vaporizing a greater number of droplets.

While finding droplets in close proximity to the vessel wall (i.e. endothelium) is not

entirely improbable, factors such as droplet density and blood vessel size relative to beam size will be important in determining the extent and location of damage. For example, a beam whose width is similar to the diameter of the targeted vessel will be able to provide vaporization at any point inside the vessel including those near the vessel wall (Figure 4.1(a)). If on the contrary, the beam width is smaller than the targeted vessel, vaporization – and as a result – damage could be localized to avoid (Figure 4.1(b)) or include (Figure 4.1(c)) the vessel wall, depending on the application. In addition to the relative location of the droplet inside the blood vessel, the relative size of the droplet is also important. As mentioned in the previous chapters, recent studies have investigated the role of initial droplet size in the development of pressures and shear stresses [12, 13, 45]. These computational studies determined that the generation of stresses could change dramatically when going from rigid [12] to flexible [13] tube walls. They also found that both peak shear stresses and peak pressures increase with increasing R_d/R_v [45], where R_d is the radius of the droplet and R_v is the radius of the vessel (tube). Therefore, for a given droplet population, significant bioeffects may be generated in small blood vessels.

These studies assumed vaporization in the center of the tubes and neglected background flow. The present study presents vaporization occurring in the wall opposite to the EC monolayer (Figure 4.2(b) and Figure 4.2(c)). While it is understood that location of vaporization may also play an important role the

generation of shear stresses and pressures, containing droplets in the center of acoustically transparent tubes coated with ECs was a challenge. We believe that although the absolute magnitude of shear stresses and pressures will be altered by this idealized experimental setup, relevant trends related to bubble expansion and fluid inertia should still hold. Significant pressures and shear stresses were found to occur at extremely short times O(0.5μs) regardless of the droplet size. Therefore, damage associated with ADV in our current setup can also be informative. It is known that physiologically ECs are exposed to shear stresses in the range of 1-20 dyne/cm^2 with local increases – in certain areas of the vasculature – between 30 and 100 dyne/cm^2 [70, 71, 72]. Therefore, significant deviations from these values would translate to major bioeffects that may include altered responses to physiological events or even cell detachment and lysis.

The objective of this chapter is to investigate how vaporization proximity as well as the relative level of confinement of vaporization affects ECs in a case-by-case basis. The level of confinement will be assessed by changing R_d/R_v, while proximity will be explained by comparing these results to those obtained in chapters 2 and 3. Both cases presented show vaporization away from the EC monolayer. The first case presents vaporization with $R_d/R_v = 0.01$ (open environment), while the second case presents vaporization for $R_d/R_v = 0.03$ (confined environment). For purposes of this study an open environment was defined as a situation where bubbles were

vaporized and fully expanded to its spherical shape in any direction, while a confined environment represented a situation where bubbles were only allowed to expand in one direction (Figure 4.2 and Figure 4.3).

4.2 Materials and Methods

4.2.1 Cell Culture

HUVECs were cultured and maintained at 37ºC in standard culture conditions. Cells were grown in culture flasks for one passage and then transferred to OptiCell™ culture chambers previously coated with fibronectin prior to US experiments. The cells were grown to ~90% confluence and only passages one through four were used in these experiments.

4.2.2 Ultrasound Setup

A similar setup to the one described in chapters 2 and 3 was used for these experiments. Briefly, an acrylic tank containing degassed, warm (37ºC) water was placed on top of an inverted microscope to observe and record ADV events. A single-element 3.5 MHz (A381S, 1.9 cm-diameter, 3.81 cm-focal length, Olympus Panametrics-NDT, Waltham, MA) transducer was focused at a 40º angle to the bottom membrane of an OptiCell™ chamber located at the bottom of the tank. US pulses were generated and controlled using two function generators and an amplifier as described in Chapter 2, section 2.2.3.

4.2.3 Exposure Protocol

OptiCells™ are composed of two flexible, 75 μm-thick polystyrene membranes separated by 2 mm. The recommended maximum volume is 10 mL. Withdrawal of fluid beyond this point (< 10mL) would result in partial collapse of the membranes, which is the basis for this experiment. In the experimental group, two OptiCells™ were used to define two gap separations (300 and 100 μm approximately) that defined an open and a confined environment. One OptiCell™ was used as a negative control. In the experimental group ADV was carried out in those areas of the center of the OptiCells™ were the gap separation was kept constant. The gap between the membranes was calculated as follows: total volume of 4 mL inside the OptiCell™ corresponding to a gap separation of 100 μm and 6 mL corresponding to 300 μm. The gap separation was verified by focusing the bottom and top membranes using the Z-direction motor of the microscope and determining the change in focal distance. A gap separation lower than 100 μm was particularly hard to achieve. A gap distance of 200 μm was initially proposed, but the error in the measurement (±50 μm) did not allow for three mutually exclusive gap separations. These two gap separations (along with an average droplet radius of 1.5 μm) yielded an R_d/R_v value of 0.03 and 0.01, respectively. ADV was generated using an 8-cycle pulse (3.3 μs) and 7 MPa of acoustic pressure (peak rarefactional). Images from the areas where ADV took place as well as other areas with no ADV were obtained to

account for the effects of fluid withdrawal from the culture chamber.

4.2.4 Fluorescence Microscopy

The OptiCells™ culture chambers were rinsed 2x with PBS containing 2% BSA to remove any excess droplet solution. Cells were stained with nucleic acid dye Hoechst following the staining protocol, then fixed in 4% PFA and stored in HEPES with sodium azide to prevent fungal growth. Each area exposed to an ADV event was examined using a 4x magnification objective. A fluorescence image consisting was obtained for each area and recorded using MetaMorph Premier software.

4.2.5 Image Processing

Fluorescence microscopy images were transferred to ImageJ for image processing that included conversion to binary (black and white) and particle counting using the "Analyze Particles" tool to determine the total number of cells and the number of dead cells per frame.

4.2.6 Statistics

All cases studied consisted of at least 10 replicates. Minitab 16 was used to carry out the statistical analysis. Statistical significance of effects was assessed by performing a students's t-test. P-values below 0.05 were considered statistically significant throughout the experiments.

4.3 Results

4.3.1 Confinement

As mentioned earlier in this chapter, confinement was described by the ability of the bubble cloud to contacting the opposite wall of the OptiCell™ chamber, where the ECs were attached. A confined environment had an average R_d/R_v ratio of 0.03, while an open environment had an average value of 0.01. This ratio was obtained using an average droplet radius of 1.5 μm, however higher ratios will exist throughout the chamber given the polydispersity of the droplet distribution.

The results obtained from this experiment were presented in the form of total cell fraction (TCF) as it was done in the previous chapters. As this chapter only addresses the effects of high pressures and shear stresses due to bubble expansion, cell detachment and not cell death was investigated. Cell death was ruled a non-significant metric of damage as it was revealed by the results of chapters 2 and 3 that it was kept at or below 5% with rather high standard deviations. Figure 4.4 shows representative images of the overall effects of performing ADV in either scenario. As it can be seen in the figure, there is a significant reduction in cell density when ADV is performed in a confined environment. Quantitative results are shown in Figure 4.5. These results were normalized using our negative control, where cells were maintained in normal growth conditions with no US exposure or

droplet solution. By doing so, the effects of fluid withdrawal from the chamber were also taken into account. These results showed that when compared to our negative control, fluid withdrawal had no effect in cell attachment in either case maintaining a TCF of near 1. Our experimental group showed that for the case where vaporization happened in an open environment (R_d/R_v = 0.01) cell detachment was not significantly different from our negative control. However, when vaporization happened in a confined environment (R_d/R_v = 0.03), it led to significantly more damage, reducing the TCF to less than 0.1.

4.3.2 Proximity

This section utilizes the results obtained from the current study and compares them to those obtained in the previous chapters for similar conditions (Figure 4.6). Chapters 2 and 3 discussed the effects of vaporizing droplets in direct contact to the EC monolayer. This chapter showed results of two cases where vaporization occurred away from the monolayer, but in environments that allowed bubbles to either expand in any direction or to be confined in one direction. Figure 4.7 summarizes these results as cases (a), (b) and (c). These results indicated that all cases were statistically different from each other showing a greater damage for the case where ADV occurred in a confined space, namely 0.6, 1 and 0.1 TCF, respectively.

4.4 Discussion

ADV is a phenomenon that allows for local vaporization of liquid droplets and subsequent embolism of the gas bubbles. Depending on the circumstances vaporization can occur far, near or even at the endothelial surface. All of these situations present different consequences in terms of bioeffects induced to the vessel wall. Vessel rupture and petechial hemorrhage has been observed in vivo by [52]. The results presented here show a small portion of all the possible bioeffects associated with shear stresses and pressures generated during vaporization. However, they provide the reader a better understanding of how this process may affect ECs inside the blood vessels. Studies carried out in [12, 13, 45] showed how shear stresses and pressures developed inside tubes for different initial droplet sizes and determined that peak shear stress increase with droplet size. These peak shear stresses were found to be between 35 and 80 dyne/cm^2 for droplet to tube ratios of 0.078 and 0.144, respectively. These shear stresses corresponded to conditions where fluid velocities inside the tube were at a maximum. The same trend was observed here, although our ratios were well below those mentioned earlier. A possible explanation for this is our inclusion of hundreds of droplets (bubbles) as opposed to the one modeled in these studies. Multiple bubbles might have coalesced rapidly – matching their maximum expansion ratios – resulting in larger bubbles capable of significantly increasing the fluid velocity inside the chamber.

This could have resulted in the generation of shear stresses capable of denuding the ECs from the membrane. In the same manner, another explanation for the observed damages is the development of high pressures during bubble expansion, which can reach up to 80,000 bar in 2 μs. Shear stresses, on the other hand, will require longer times to develop due to the viscous resistance of the fluid. Thus, we believe that since these peak pressures occur at a much faster time scale than the peak shear stresses, they may be responsible for injuring cells or even rupturing the blood vessel before damages associated to shear stresses can be translated the endothelium. Shear stress will then be responsible for removing loosely attached dead cells explaining the reduced count of these throughout our experiments.

Both proximity and confinement of vaporization pose challenges that may not be easily controlled due to the polydispersity of the droplet population. Monodispersity of droplets could immensely aid in the prediction of damages, but producing such a solution with the required sizes and quantity is rather difficult. In addition, the ultimate goal of the application will dictate which blood vessels will be targeted, putting small arterioles and capillaries at higher risk. Therefore, reduced damage could be achieved if vaporization is localized as further away from the endothelium (center of blood vessel) and making an appropriate selection of the transducer and acoustic parameters.

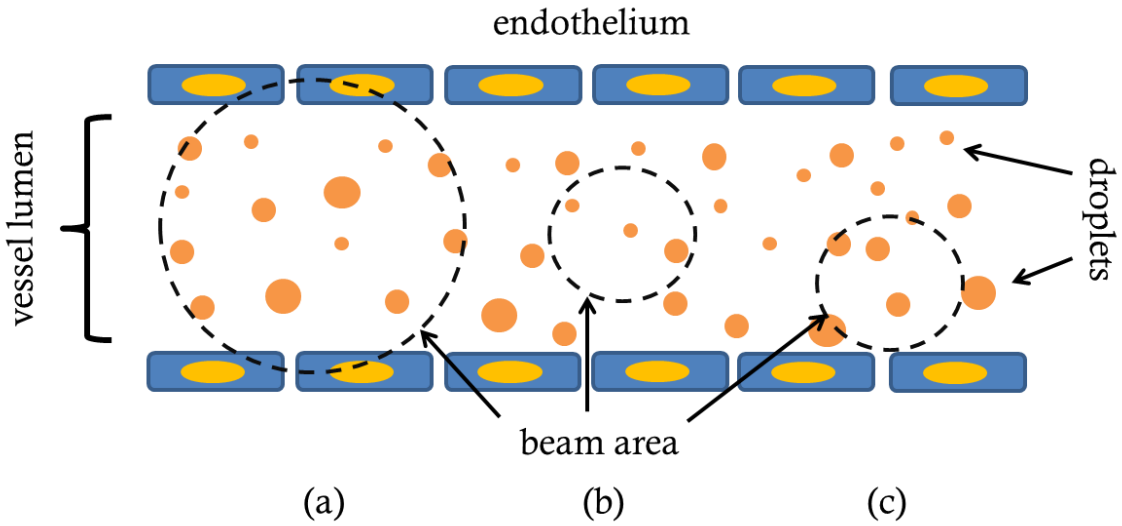

Figure 4.1: Blood vessel size relative to beam size. Larger beam sizes will facilitate vaporization anywhere along the span of the vessel diameter (a), while smaller beam sizes will aid in the localization of damage (b and c).

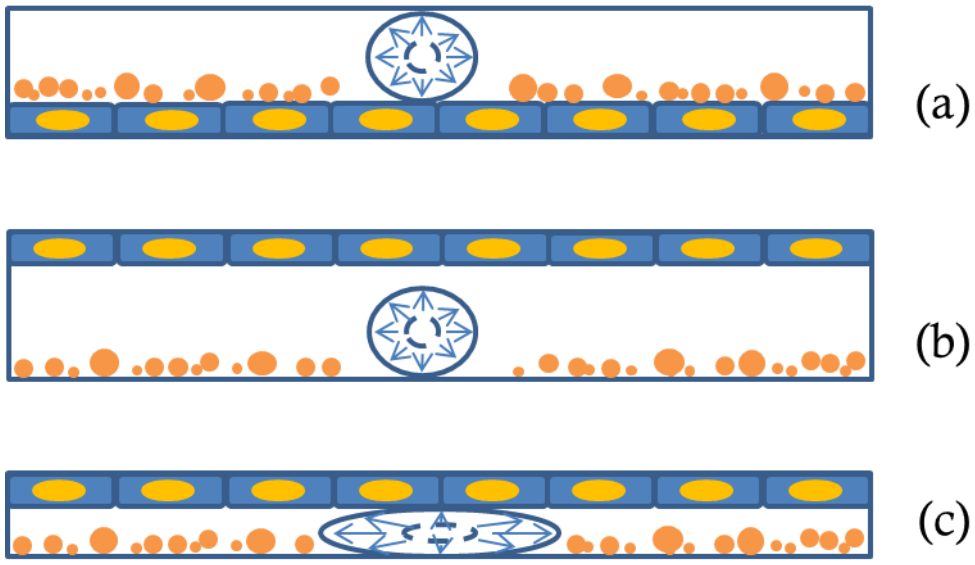

Figure 4.2: Diagram depicting three cases where ADV could take place inside blood vessels using OptiCell™ chambers. Vaporization in direct contact with the endothelium (a), vaporization near the endothelium in an open space (b) and vaporization near the endothelium in a confined space (c).

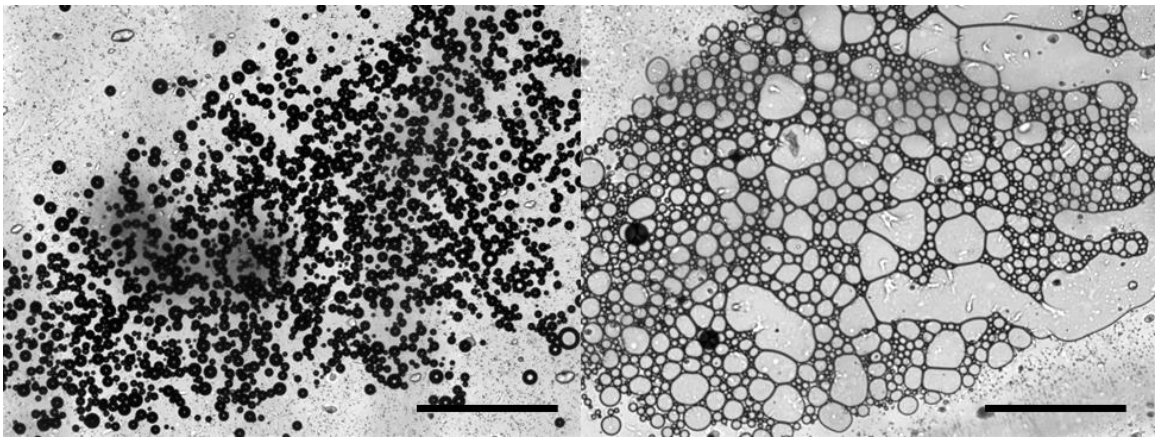

Figure 4.3: ADV inside an open (left) versus confined (right) environments. An open environment is defined as a situation where bubbles can be vaporized and expand fully to its spherical shape in any direction. A confined environment represents a situation where bubbles are only allowed to expand in one direction. In both cases vaporization occurred in the wall opposite to the EC monolayer. Scale bar is 500 μm.

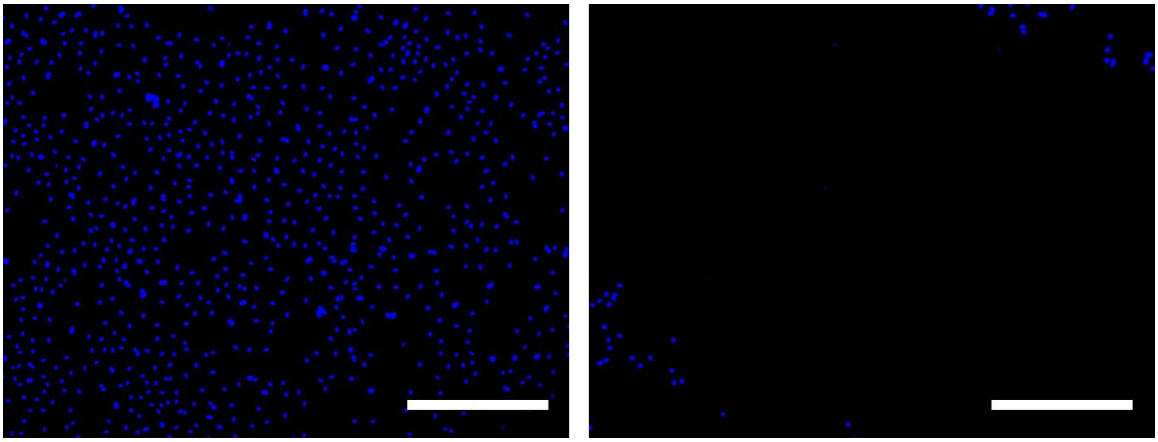

Figure 4.4: Fluorescence images depicting cell density after ADV in an open environment (left) and confined environment (right). Cells were stained with fluorescent dye Hoechst. Scale bar is 500 μm.

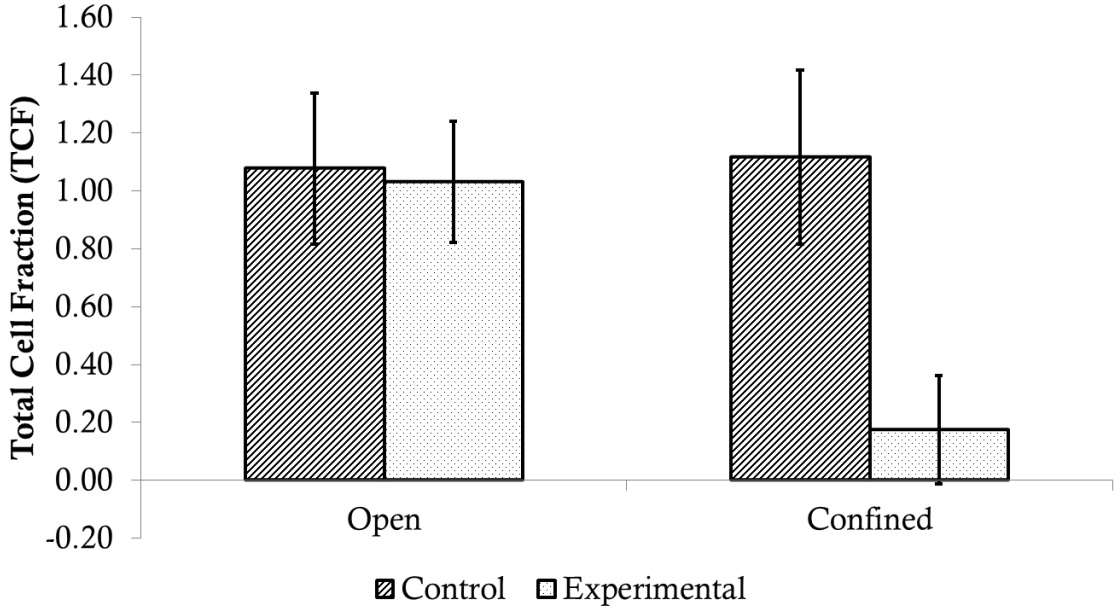

Figure 4.5: Total cell fraction after ADV for an open versus a confined environment. Control group (line hatch) represents the treatments with droplets, but no ADV. All data is normalized to our negative control (no droplets, no ultrasound). Open case corresponds to $R_d/R_v = 0.01$, while confined case corresponds to $R_d/R_v = 0.03$

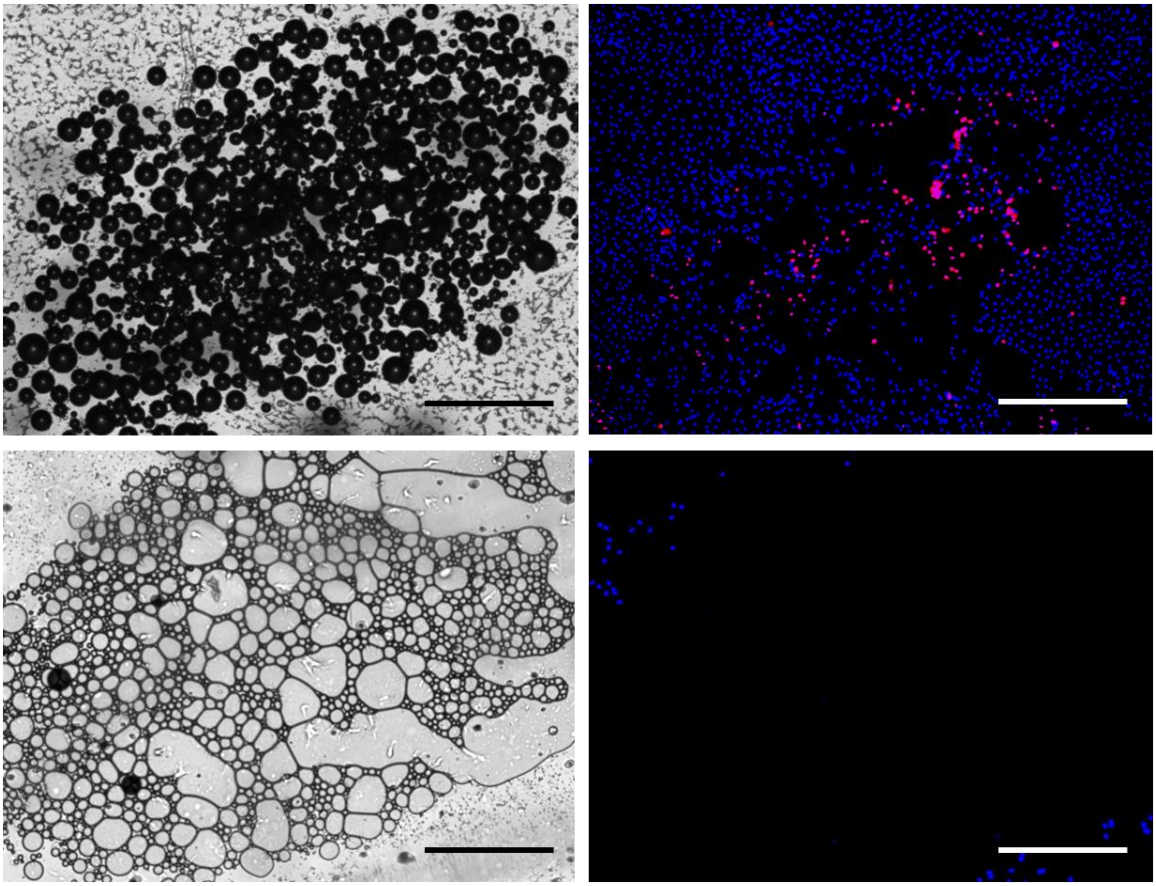

Figure 4.6: ADV and associated damages for vaporization at the EC monolayer (top row) versus vaporization away from the EC monolayer, but in confined environment (bottom row). Scale is 500 μm.

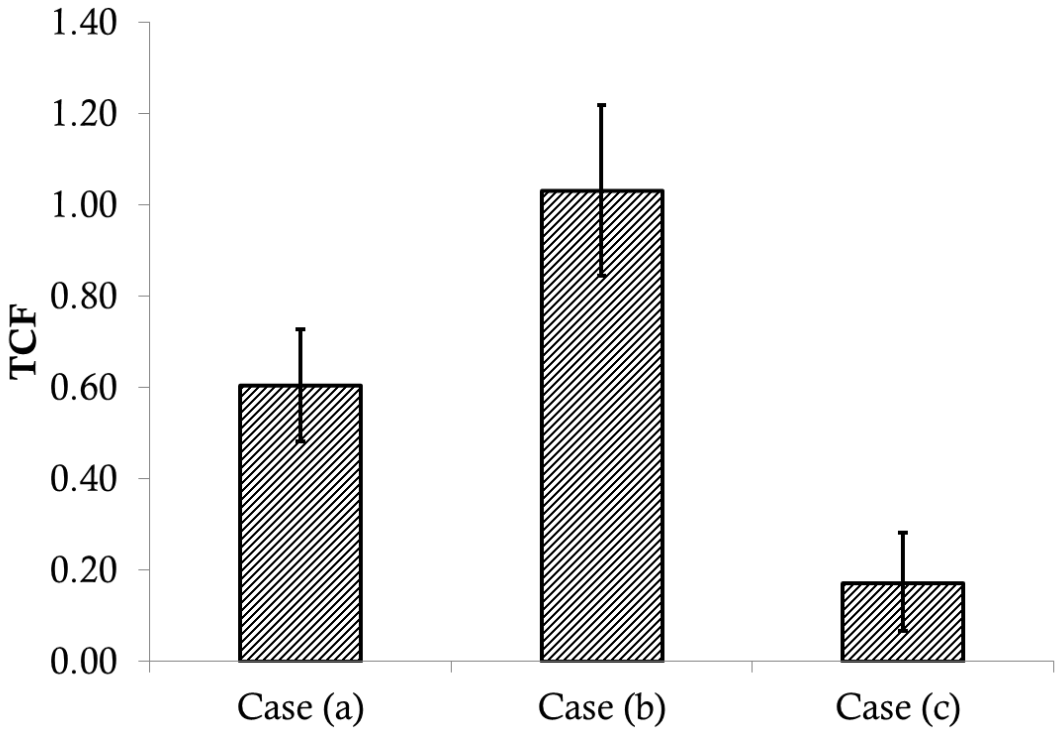

Figure 4.7: Total cell fraction (TCF) for the cases presented in Figure 4.2. Case (a) corresponds to vaporization at the EC monolayer as presented in chapters 2 and 3. Cases (b) and (c) correspond to vaporization in an open environment ($R_d/R_v = 0.03$) and closed environment ($R_d/R_v = 0.01$), respectively.

Chapter 5

Conclusions

This dissertation has presented the effects of ADV on an idealized endothelial monolayer while varying acoustic parameters, such as pressure, pulse length and carrier frequency. Proximity and confinement of ADV were also investigated. To the best of our knowledge this is the first study that shows the ADV-endothelial interaction and effects under acoustic conditions applicable to GE and the implications of such effects during and after treatment. For the conditions tested in this study, these are the main findings of this work:

- ADV in direct contact with ECs will cause cell damage and detachment.
- Cell damage is dependent on the BCA
- Damage to ECs is highly localized. No damage was found beyond the BCA when vaporization happened in direct contact with the cells.
- A combination of pressure, pulse length and frequency determine the BCA and hence the degree of damage.

    - Greater spatial peak intensities (determined by pressure amplitude and time) translate to grater effects.
    - The pressure contribution to BCA changes with frequency. Greater contribution is seen for lower frequencies and vice versa.
    - BCAs are limited by the size of the beam width.
- For a given intensity, the 7.5 MHz transducer caused more damage than the 3.5 MHz transducer relative to their own beam widths.
- Droplet size to gap size ratio is important in the generation of pressures and stresses capable of affecting ECs.
    - Greater ratios translated to greater effects.
- Vaporizing away from the ECs, but in a confined environment produces greater effects than vaporizing in direct contact to the cells.
- High pressures may have a major role in cell damage when compared to shear stresses. Shear stresses may become more important at longer time scales.
- Though unlikely for the 7.5 MHz transducer, IC is still a possible cause of death, especially for the 3.5 MHz transducer.

Under physiological conditions, EC will sense shear stresses and other mechanical stimuli to respond to meet metabolic needs [38]. They can also adapt by upregulating growth factors, cytoskeletal reorganization, among other activities. However, if these stresses are altered beyond physiological conditions ECs functions

could be impaired [23]. Risks of thrombus formation, fat accumulation, and atherosclerosis are major consequences of endothelial dysfunction from which GE could benefit. Damage to the endothelium could induce thrombosis at the site of vaporization providing additional occlusion to those affected vessels. Controlled impairment of endothelial functions like permeability could also aid in the delivery of drugs or other substances that will need to cross the endothelial barrier during treatments. In other words, if controlled, not only could ADV provide a localized embolus to a specific location in the vasculature, but could also provide a mechanism for triggering local drug delivery following occlusion given that cell viability can be sustained.

Our data have shown that ADV events occurring in close proximity to ECs as well as in confined environments will cause a decrease cell viability and/or attachment. However cell repopulation can happen depending on the growth conditions. In summary, we have found a range of results that provide an insight into the potential bioeffects of GE during ADV that not only could help us prevent damage, but could aid in the optimization of this therapy and other clinical applications.

Chapter 6

Recommendations and Future Work

The results presented in this dissertation were obtained from controlled *in vitro* experiments simulating a worst-case scenario. *In vivo* situations are often times difficult to mimic. The addition of all the necessary parameters to closely simulate these conditions does not allow for a controlled experiment. Therefore, several variables were not considered to facilitate the explanation of our results. This study presented an *idealized* model in which a monolayer of HUVECs attached to fibronectin was used in a static environment. Flow of bulk fluid, RBCs and transport of macromolecules are a few of the characteristics of a blood vessel that were omitted in this study. In particular, flow was not considered as the flow in target vessels is much slower than the firing frequency of the US. Also, the endothelium is supported by an extracellular matrix composed of a mesh of different proteins and other different layers of cells with different mechanical properties. We believe that the anchor these cells are attached to is an important parameter in

determining the likelihood of cell detachment and as such would have different effects depending on its composition. Laminin, collagen, proteoglycans and other important growth factors are some of the additional proteins that make up the basement membrane where endothelial cells are attached to. In addition, the cellular response from ECs may vary depending on their origin in the vascular tree as well as their initial pathological state [39]. ECs showing an initial diseased state may be more vulnerable to cellular injury and altered response when compared to a healthy cell population.

A proposed extension to this work is the study of how droplets behave in flow at physiological conditions and how these lead to interaction between the droplet albumin shell and the endothelium. Preliminary studies showed that ECs have an affinity for albumin-coated DDFP droplets (Figure 6.1) , perhaps due to an albumin receptor previously described elsewhere [57, 73]. Albumin is the major blood protein in charge of controlling the oncotic pressure influencing transendothelial fluxes of water and other small molecules across the vessel wall. It can also be transported across the endothelium, may reduce platelet adhesion and restrict surface binding of other plasma proteins. A group from the Yale School of Medicine found a 60-kDa *endothelial* glycoprotein that is believed to be directly involved in a specific interaction with albumin [73]. Activation of this glycoprotein (gp60) led to albumin uptake by the endothelium of microvessels as well as transport via a transcellular

pathway [58]. These characteristics make an albumin-coated droplet a great candidate for direct interaction with the endothelium facilitating vaporization *at* the endothelial surface and perhaps aiding in other therapies as localized drug delivery. A flow chamber has previously been used for this purpose (Figure 6.2) and preliminary results point at a settlement of these droplets in slow flow (low shear) conditions allowing for these to interact with the endothelium and eventually attaching to the endothelial surface (Figure 6.3).

It would also be pertinent to include an *in vivo* experiment in which significant vaporization is carried out inside an animal model to quantify the number of circulating endothelial cells in blood. Circulating endothelial cells (CEC) have been used in the past as an indicator of vascular disease, endothelial dysfunction and cancer. CECs can be found in the bloodstream and can be quantified by a number of methods including immunocytochemistry and flow cytometry. Quantifying CECs after ADV events can asses both the likelihood and strength of ADV events taking place near the endothelium. A high number of CEC compared to controls will be an indication that ADV has indeed hindered the EC attachment to the vascular wall and hence its function.

Ultra-high speed experiments in which ADV events are limited to a single cell could also aid in the elucidation of the actual mechanism of injury. This method may allow us to observe any indication of cavitation (collapse or jet formation) or perhaps how bubble expansion directly affects the cell membrane. Other parameters

like droplet size are believed to affect the degree of damage and should also be studied. However, for this case a monodisperse solution of droplets may be needed. Monodisperse droplet solutions are currently being developed, but high throughput to meet the desired concentrations is still a challenge. This study only considered one pulse, but in fact longer pulses or the inclusion of pulse repetition frequency (PRF) may be needed in clinical practice to increase the number of vaporized droplets in the vasculature and increase the probability of occlusion. However idealized this model is to address the many questions regarding the effectiveness of ADV and GE as a whole, this has served as a platform for subsequent studies aiming for the optimization of not only GE, but other related therapies.

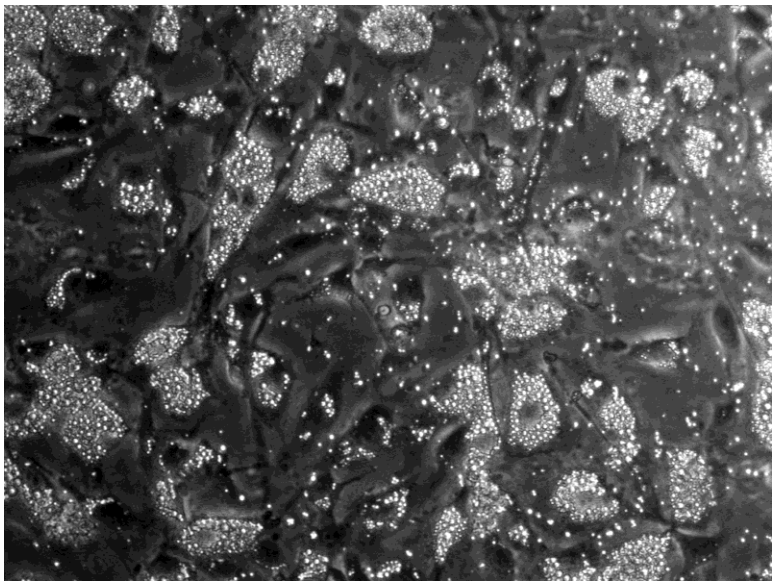

Figure 6.1: Endothelial cell culture with a solution of albumin-coated DDFP droplets. After two rinses with PBS droplets were removed from intercellular spaces but remained attached on the cell surface. Addition of free albumin to the PBS solution aided in the detachment of these droplets perhaps due to competition.

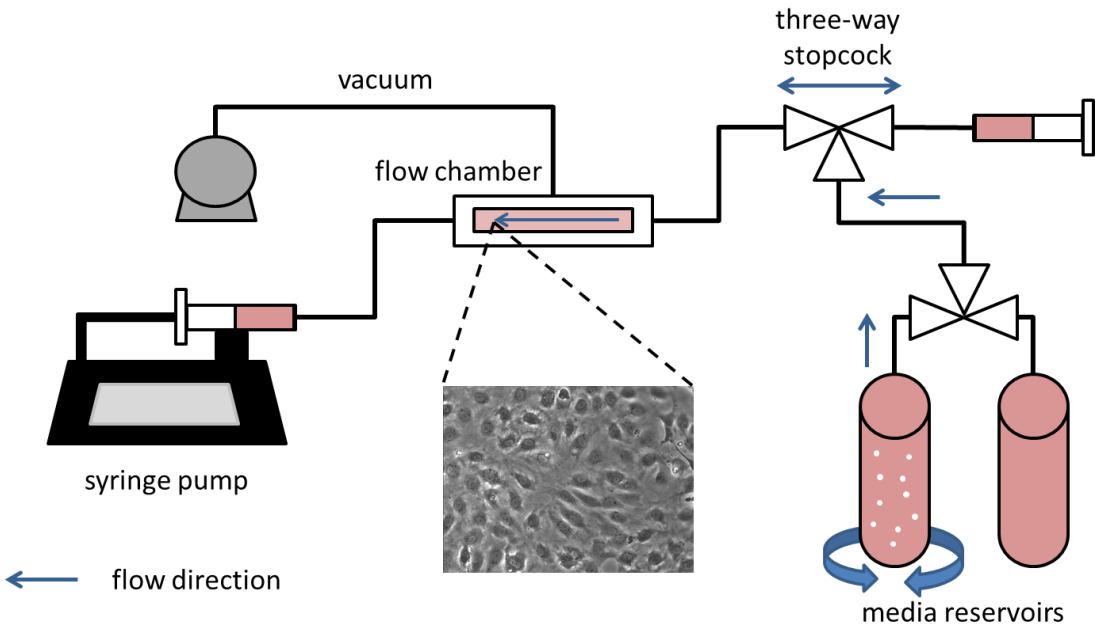

Figure 6.2: Proposed setup for the study of droplet-endothelial interaction. A syringe pump will withdraw cell media from one of the reservoirs to prime the lines and the channel. A second reservoir connected through a three-way valve and containing the droplet solution continuously stirred will be used to introduce them into the system. An extra three-way valve connected to a syringe may be used to remove air bubbles from the system.

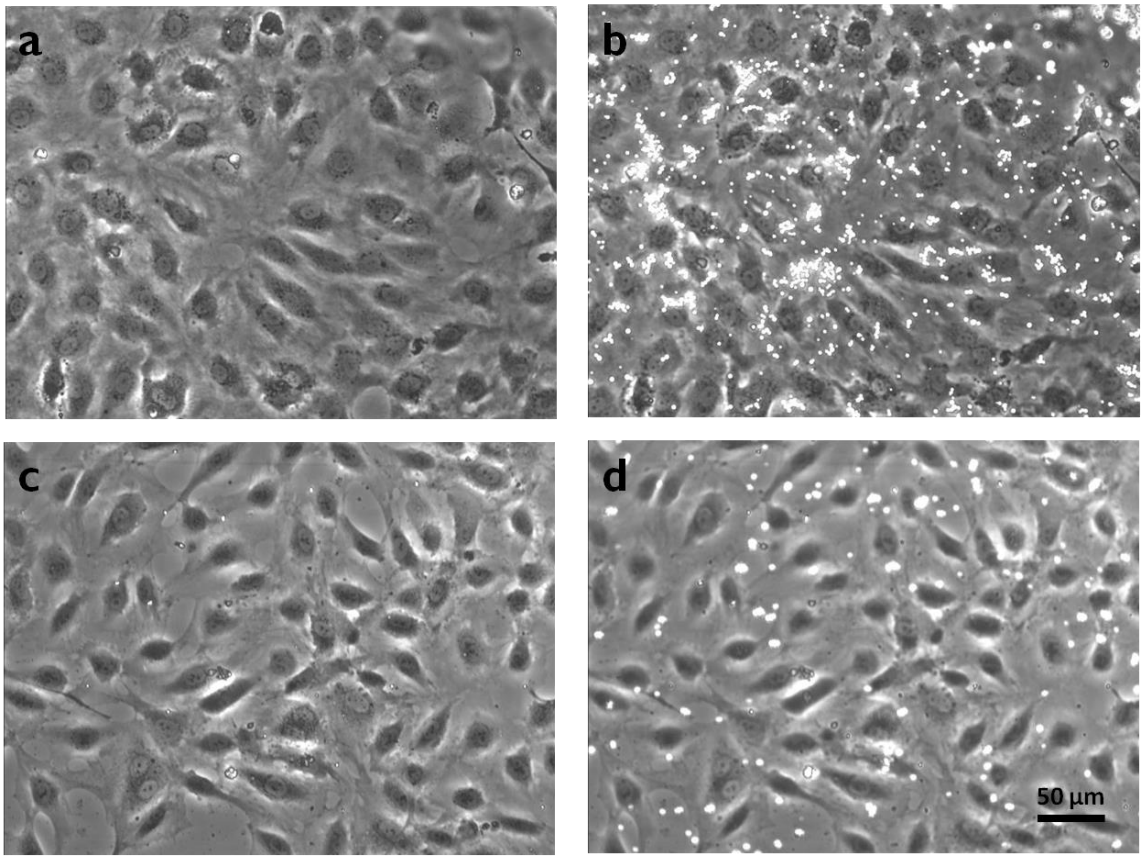

Figure 6.3: Preliminary results depicting the effects of shear stress in droplet settlement under flow conditions. Before and after pictures show results for 2 dyne/cm^2 (a and b) and 4 dyne/cm^2 (c and d).

Appendix A
Statistical Analysis - Chapter 2

General Regression Analysis: BCA versus Pressure, Cycles

```
Regression Equation

BCA  =  -0.799869 + 0.320643 Pressure + 0.0037073 Cycles + 0.000588616
       Pressure*Cycles

87 cases used, 1 cases contain missing values

Coefficients

Term               Coef   SE Coef       T     P
Constant        -0.799869  0.110180  -7.2596  0.000
Pressure         0.320643  0.020342  15.7623  0.000
Cycles           0.003707  0.010459   0.3545  0.724
Pressure*Cycles   0.000589  0.001927   0.3055  0.761
```

Interpretation: We reject the null hypothesis that the pressure coefficient = 0. Pressure is a significant factor in the linear model and strongly changes the response, BCA (bubble cloud area). There's not enough evidence to reject the null hypothesis that the coefficient for Cycles or Pressure*Cycles = 0. Therefore, these do not contribute to our model.

```
Summary of Model

S = 0.202975    R-Sq = 93.30%       R-Sq(adj) = 93.05%
PRESS = 3.75391  R-Sq(pred) = 92.64%
```

Interpretation: This model can explain 93% of the variation in BCA. The extra 7% is not explained by this model and may be due to other sources of variations not accounted for in the model and error.

```
Analysis of Variance

Source           DF   Seq SS   Adj SS   Adj MS       F        P
Regression        3  47.5801  47.5801  15.8600  384.962  0.000000
  Pressure        1  47.4824  10.2359  10.2359  248.450  0.000000
  Cycles          1   0.0938   0.0052   0.0052    0.126  0.723900
  Pressure*Cycles   1   0.0038   0.0038   0.0038    0.093  0.760746

Error            83   3.4195   3.4195   0.0412
  Lack-of-Fit     8   1.5004   1.5004   0.1876    7.330  0.000000
  Pure Error      75   1.9191   1.9191   0.0256
Total            86  50.9996
```

Interpretation: Confirmation of the linear model. The regression fits our data ($p<0.05$), pressure is a significant factor affecting the response ($p<0.05$), while other factors or interactions are not important ($p>0.05$). However, due to a lack-of-fit in the regression model, another model may be more adequate. This is in part due to the lack of error in the measurements for one pressure value where all responses were equal to 0. For our experiments, BCA is a threshold phenomenon, dependent on pressure, thus the BCA below the threshold are known and equal to 0.

```
Fits and Diagnostics for Unusual Observations

Obs     BCA     Fit    SE Fit   Residual  St Resid
 61  1.70473  1.18190  0.0248204   0.522824   2.59528  R
 73  1.39593  1.89994  0.0616738  -0.504009  -2.60633  R
 75  2.30320  1.79894  0.0534196   0.504254   2.57510  R
 84  2.27048  1.83261  0.0379038   0.437875   2.19591  R

R denotes an observation with a large standardized residual.
```

The following model fixes the lack-of-fit encountered in the first model by excluding BCA = 0 and parameters that were not significant in predicting the value of BCA.

Note that 25 observations have been deleted.

```
Regression Equation

BCA  =  -1.21491 + 0.393339 Pressure

63 cases used, 25 cases contain missing values
Coefficients

Term         Coef    SE Coef        T     P
Constant  -1.21491  0.0956495  -12.7017  0.000
Pressure   0.39334  0.0153193   25.6760  0.000

Summary of Model

S = 0.196145    R-Sq = 91.53%       R-Sq(adj) = 91.39%
PRESS = 2.48821  R-Sq(pred) = 91.02%

Analysis of Variance

Source        DF   Seq SS   Adj SS   Adj MS       F        P
Regression     1  25.3635  25.3635  25.3635  659.259  0.000000
  Pressure     1  25.3635  25.3635  25.3635  659.259  0.000000
Error         61   2.3468   2.3468   0.0385
```

```
  Lack-of-Fit   1   0.0607   0.0607   0.0607    1.593  0.211771
  Pure Error   60   2.2861   2.2861   0.0381
Total          62  27.7103
```

Interpretation: This is a better model that fits and explains our data. The lack-of-fit is not significant; therefore this is a more adequate model.

```
Fits and Diagnostics for Unusual Observations

Obs      BCA      Fit     SE Fit   Residual  St Resid
 46  1.56605  1.14512  0.0247167   0.420933   2.16328  R
 47  1.55069  1.14512  0.0247167   0.405565   2.08430  R
 61  1.70473  1.14512  0.0247167   0.559605   2.87594  R
 73  1.39593  1.93180  0.0389851  -0.535871  -2.78764  R
 78  1.48633  1.93180  0.0389851  -0.445468  -2.31735  R

R denotes an observation with a large standardized residual.
```

Interpretation: These observations with large residuals are likely to be outliers.

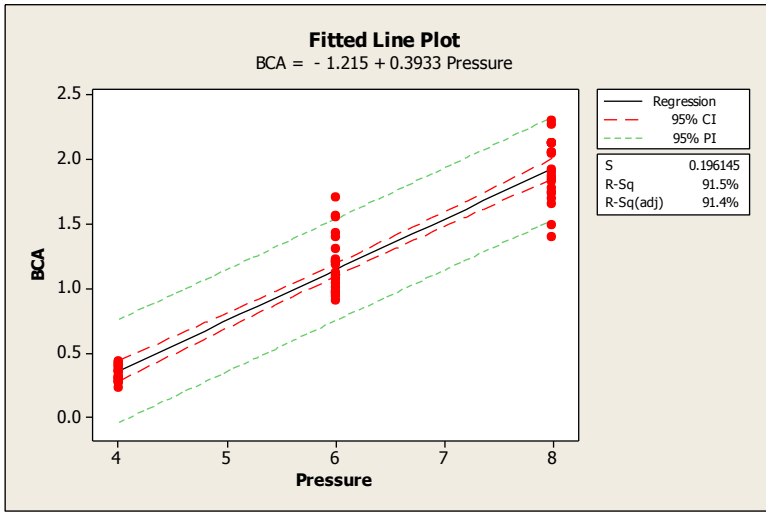

Figure A.A. 1: This figure shows the fitted line through the data with 95% confidence interval (CI) and 95 % prediction interval (PI). The confidence interval gives us information on probability of finding the mean, while the prediction interval gives us probability of finding the scattered data. We can explain ~91% of the variation with this model. Close to 9 % is due to other factors and error.

We can use this model to estimate the value of BCA at pressures between 4 and 8 MPa.

General Regression Analysis: tcc versus press, cyc in R

```
Call:
lm(formula = tcc ~ press * cyc * drop, data = pcd)

Residuals:
    Min      1Q  Median      3Q     Max
-669.68  -96.12   16.90  123.11  455.10

Coefficients:
              Estimate Std. Error t value Pr(>|t|)
(Intercept)    2678.2220    64.1534  41.747  < 2e-16 ***
press           -1.9057    13.9015  -0.137  0.89113
cyc             -2.8449     7.4194  -0.383  0.70187
drop           -96.0977    87.7277  -1.095  0.27490
press:cyc        0.6562     1.5088   0.435  0.66418
press:drop     -86.1627    19.0498  -4.523 1.14e-05 ***
cyc:drop        33.1371    10.1478   3.265  0.00132 **
press:cyc:drop  -9.5386     2.0633  -4.623 7.48e-06 ***
---
Signif. codes:  0 ‘***’ 0.001 ‘**’ 0.01 ‘*’ 0.05 ‘.’ 0.1 ‘ ’ 1

Residual standard error: 200.3 on 169 degrees of freedom
  (2 observations deleted due to missingness)
Multiple R-squared:  0.8272,    Adjusted R-squared:   0.82
F-statistic: 115.5 on 7 and 169 DF,  p-value: < 2.2e-16
```

Interpretation: Pressure (press), cycles (cyc) and droplets (drop) do not contribute to our regression model ($p>0.05$). This does not mean that they have no effect in the response, tcc (total cell count). Other parameters are better at explaining the changes in tcc. We reject the null hypothesis that the coefficients are equal to zero

for the following interaction terms: press*drop, cyc*drop and press*cyc*drop. These terms have a strong significant effect on estimating our response. We can explain 82% of the variation with this model, while the rest is due to other factors not included in the model and error. This regression significantly fits our data ($p<0.05$).

```
> anova(model1)
Analysis of Variance Table
Response: tcc
              Df   Sum Sq  Mean Sq  F value    Pr(>F)
press          1  7601046  7601046 189.3951 < 2.2e-16 ***
cyc            1    66893    66893   1.6668    0.1985
drop           1 16070320 16070320 400.4238 < 2.2e-16 ***
press:cyc      1   767023   767023  19.1119 2.148e-05 ***
press:drop     1  7055861  7055861 175.8107 < 2.2e-16 ***
cyc:drop       1    39483    39483   0.9838    0.3227
press:cyc:drop 1   857742   857742  21.3723 7.481e-06 ***
Residuals    169  6782523    40133
---
Signif. codes:  0 ‘***’ 0.001 ‘**’ 0.01 ‘*’ 0.05 ‘.’ 0.1 ‘ ’ 1
```

Interpretation: Pressure and droplets significantly affect the tcc ($p<0.05$). Note how these have an effect on the response, but cannot be used to estimate the value of tcc in the regression. Cyc and cyc*drop are not significant, meaning that changing cycles have no effect on the response even in the presence of droplets. However, there is an interaction between pressure and the other two variables.

One-way ANOVA: Total Cells versus Treatment in Minitab 16

Treatment (coded)	Treatment (P,N)	Droplets
0	0	0
2	2, 4	0
3	2, 8	0
1	2, 16	0
5	4, 4	0
6	4, 8	0
4	4, 16	0
8	6, 4	0
9	6, 8	0
7	6, 16	0
11	8, 4	0
12	8, 8	0
10	8, 16	0
13	0	1
15	2, 4	1
16	2, 8	1
14	2, 16	1
18	4, 4	1
19	4, 8	1
17	4, 16	1
21	6, 4	1
22	6, 8	1
20	6, 16	1
24	8, 4	1
25	8, 8	1
23	8, 16	1

Source	DF	SS	MS	F	P
Treatment	25	34096931	1363877	40.04	0.000
Error	151	5143960	34066		
Total	176	39240891			

S = 184.6 R-Sq = 86.89% R-Sq(adj) = 84.72%

All treatments have been code to be compared to our control

```
                    Individual 95% CIs For Mean Based on
                    Pooled StDev
Level  N   Mean  StDev  -------+---------+---------+---------+--
 0     7  2637.9  165.7                        (--*--)
 1     7  2684.7  166.4                         (--*-)
 2     6  2767.3  177.7                          (--*--)
 3     7  2623.0  174.9                        (-*--)
 4     6  2571.3  155.7                       (--*--)
 5     6  2673.3  132.6                        (--*--)
 6     5  2727.2  159.1                         (---*--)
 7     6  2717.2  131.7                         (--*--)
 8     8  2670.4  155.4                         (-*--)
 9     6  2637.0  264.8                        (--*--)
10     6  2739.7  220.6                          (--*--)
11     6  2697.2   83.1                         (--*--)
12     6  2622.7  104.6                       (--*--)
13     8  2455.8  148.8                     (-*--)
14     8  2494.0  182.3                     (--*-)
15     7  2484.4   97.7                    (--*-)
16     8  2471.1  235.9                     (-*--)
17     7  2251.4  189.9                 (--*--)
18     7  2409.6  180.5                    (--*--)
19     7  2319.0  154.4                  (-*--)
20     7  1615.4  328.6        (-*--)
21     8  2118.5  126.3                (-*--)
22     7  1885.0  226.7            (--*-)
23     7  1298.9  168.4  (--*--)
24     7  1555.6  193.9      (--*--)
25     7  1360.1  248.1   (--*--)
                    -------+---------+---------+---------+--
                       1500     2000     2500     3000

Pooled StDev = 184.6

Grouping Information Using Dunnett Method
```

Level	N	Mean	Grouping
0 (control)	7	2637.9	A
2	6	2767.3	A
10	6	2739.7	A
6	5	2727.2	A
7	6	2717.2	A
11	6	2697.2	A
1	7	2684.7	A
5	6	2673.3	A
8	8	2670.4	A
9	6	2637.0	A
3	7	2623.0	A
12	6	2622.7	A
4	6	2571.3	A
14	8	2494.0	A
15	7	2484.4	A
16	8	2471.1	A
13	8	2455.8	A
18	7	2409.6	A
19	7	2319.0	A
17	7	2251.4	A
21	8	2118.5	
22	7	1885.0	
20	7	1615.4	
24	7	1555.6	
25	7	1360.1	
23	7	1298.9	

Means not labeled with letter A are significantly different from control level mean.

The following treatments were significantly different from the control: all treatments with 6 and all treatments with 8.

```
Dunnett's comparisons with a control

Family error rate = 0.05
Individual error rate = 0.0031

Critical value = 3.01
Control = level (0) of Treatment
```

General Regression Analysis: dcc versus press, cyc in R

```
Call:
lm(formula = dcc ~ press * cyc * drop, data = pcd)

Residuals:
   Min     1Q  Median     3Q    Max
-68.830 -11.802  -2.965   6.577 131.045

Coefficients:
             Estimate Std. Error t value Pr(>|t|)
(Intercept)   21.76423    9.64741   2.256   0.0254 *
press          0.02414    2.04796   0.012   0.9906
cyc           -0.33140    1.08777  -0.305   0.7610
drop          23.00973   12.94145   1.778   0.0772 .
press:cyc      0.05977    0.21920   0.273   0.7854
press:drop     3.68790    2.76793   1.332   0.1846
cyc:drop      -2.27016    1.48769  -1.526   0.1289
press:cyc:drop  0.53667    0.29897   1.795   0.0745 .
---
Signif. codes:  0 ‘***’ 0.001 ‘**’ 0.01 ‘*’ 0.05 ‘.’ 0.1 ‘ ’ 1

Residual standard error: 28.56 on 167 degrees of freedom
  (4 observations deleted due to missingness)
Multiple R-squared:  0.4812,    Adjusted R-squared:  0.4594
F-statistic: 22.13 on 7 and 167 DF,  p-value: < 2.2e-16
```

Interpretation: We fail to reject the null hypothesis that the coefficients are equal to zero. We cannot fit a line through our data. We can only explain 46% of the

variation with this model.

```
> anova(model2)
Analysis of Variance Table

Response: dcc
             Df Sum Sq Mean Sq  F value    Pr(>F)
press         1  21747   21747  26.6603 6.833e-07 ***
cyc           1     42      42   0.0518   0.82018
drop          1  82210   82210 100.7834 < 2.2e-16 ***
press:cyc     1   4069    4069   4.9884   0.02685 *
press:drop    1  15649   15649  19.1847 2.089e-05 ***
cyc:drop      1      3       3   0.0032   0.95508
press:cyc:drop  1   2628    2628   3.2222   0.07446 .
Residuals   167 136224     816
---
Signif. codes:  0 ‘***’ 0.001 ‘**’ 0.01 ‘*’ 0.05 ‘.’ 0.1 ‘ ’ 1
```

Interpretation: Pressure significantly affectsBCA the response, dcc (dead cell count). The means for the group containing droplets and that without droplets are significantly different (drop $p<0.05$). Pressure interacts with both cycles and droplets.

One-way ANOVA: Dead Cells versus Treatment in Minitab 16

```
Source      DF      SS    MS     F      P
Treatment   25  137934  5517  6.60  0.000
Error      149  124639   837
Total      174  262573

S = 28.92   R-Sq = 52.53%   R-Sq(adj) = 44.57%

Individual 95% CIs For Mean Based on Pooled StDev
```

```
Level  N   Mean  StDev  --+---------+---------+---------+-------
 0     6  23.00   7.29    (------*-----)
 1     7  20.71   4.03    (-----*-----)
 2     6  18.33   5.50   (-----*------)
 3     7  20.29   4.31    (-----*-----)
 4     6  17.33   4.68  (------*------)
 5     6  21.50   5.36   (------*------)
 6     6  23.50   7.34    (------*-----)
 7     6  20.67  12.58   (------*------)
 8     8  20.88   6.17    (-----*-----)
 9     6  21.00   8.69   (------*------)
10     6  27.00  17.87     (------*-----)
11     6  25.50   6.44     (-----*------)
12     6  21.00   8.32   (------*------)
13     8  50.13  19.61           (----*-----)
14     7  30.86  22.65      (-----*-----)
15     6  32.50  13.92      (-----*------)
16     8  50.88  28.42           (-----*----)
17     7  52.71  24.62           (-----*-----)
18     7  66.43  56.38              (-----*-----)
19     7  31.00  20.23      (-----*-----)
20     7  98.29  43.39                    (-----*-----)
21     8  67.88  62.75               (----*-----)
22     7  82.14  46.67                  (-----*------)
23     7 103.00  38.54                       (-----*------)
24     7  93.14  36.48                    (------*-----)
25     7  84.71  47.48                   (-----*-----)
                  --+---------+---------+---------+-------
                    0       35       70      105

Pooled StDev = 28.92
```

Same as before, all treatments have been coded to be compared to our control.

Grouping Information Using Dunnett Method

Level	N	Mean	Grouping
0 (control)	6	23.00	A
23	7	103.00	
20	7	98.29	
24	7	93.14	
25	7	84.71	
22	7	82.14	
21	8	67.88	A
18	7	66.43	A
17	7	52.71	A
16	8	50.88	A
13	8	50.13	A
15	6	32.50	A
19	7	31.00	A
14	7	30.86	A
10	6	27.00	A
11	6	25.50	A
6	6	23.50	A
5	6	21.50	A
12	6	21.00	A
9	6	21.00	A
8	8	20.88	A
1	7	20.71	A
7	6	20.67	A
3	7	20.29	A
2	6	18.33	A
4	6	17.33	A

Means not labeled with letter A are significantly different from control level mean.

The following treatments were significantly different from the control: 6, 8; 6, 16 and all treatments with 8.

```
Dunnett's comparisons with a control

Family error rate = 0.05
Individual error rate = 0.0033

Critical value = 2.99

Control = level (0) of Treatment
```

Appendix B
Statistical Analysis - Chapter 3

General Regression Analysis: NBCA versus Pressure, Cycle

Regression Equation

BCA = -0.0396519 + 0.0206116 Pressure - 0.00894162 Cycle + 0.00591338 Pressure*Cycle

Coefficients

Term	Coef	SE Coef	T	P
Constant	-0.0396519	0.0423412	-0.93649	0.353
Pressure	0.0206116	0.0107619	1.91524	0.060
Cycle	-0.0089416	0.0035897	-2.49089	0.015
Pressure*Cycle	0.0059134	0.0009316	6.34747	0.000

Summary of Model

S = 0.0380491 R-Sq = 89.10% R-Sq(adj) = 88.58%
PRESS = 0.100580 R-Sq(pred) = 87.79%

Analysis of Variance

Source	DF	Seq SS	Adj SS	Adj MS	F	P
Regression	3	0.734028	0.734028	0.244676	169.006	0.0000000
Pressure	1	0.409925	0.005310	0.005310	3.668	0.0600778
Cycle	1	0.265773	0.008982	0.008982	6.205	0.0154341

```
  Pressure*Cycle   1  0.058330  0.058330  0.058330   40.290  0.0000000
Error            62  0.089759  0.089759  0.001448
  Lack-of-Fit     7  0.032532  0.032532  0.004647    4.466  0.0005415
  Pure Error     55  0.057228  0.057228  0.001041
Total            65  0.823788Fits and Diagnostics for Unusual Observations

Obs     NBCA      Fit    SE Fit   Residual  St Resid
 49  0.314321  0.393411  0.0125392  -0.079089  -2.20160  R
 64  0.338533  0.228408  0.0079917   0.110125   2.96031  R
 65  0.351069  0.228408  0.0079917   0.122661   3.29730  R

R denotes an observation with a large standardized residual.
```

This model tries to predict the value of bubble cloud area (BCA) given the parameters Pressure and Cycle. P-values below 0.05 tell us which parameters contribute significantly to the model. Cycle and Pressure*Cycle contribute significantly. Pressure alone or the constant do not contribute significantly in making a prediction of BCA. A negative constant would be absurd to consider in this model given that when both Pressure and Cycle are equal to zero this would yield a negative BCA, which is not physically possible. This term should be removed from the model. The (adj) R-Sq tells us that we can explain ~88% of the variation in BCA with this model. The rest of the variation can be explained by other parameters not accounted for in this model and other uncontrollable sources of error. Further investigation and analysis would be needed to determine other sources of the variation. The ANOVA table tells us which parameters caused a significant effect on the mean of the response (BCA). Parameters with p-values

below 0.05 significantly affect the mean. A significant interaction tells us that the change in the mean is different depending on the selected levels (values) for both Pressure and Cycle. In other words the effects of Pressure depend on the value of Cycle. A lack-of-fit test reveals that the model presented here may not be adequate. Mainly that a linear regression does not adequately fit the data. Higher order terms (quadratic) should be considered to fix this model in order to make better predictions, but further investigation and resources may be needed. Lastly, three observations with rather large residuals may suggest the presence of outliers (mistyped data, different units). After checking the input data it was determined that this are in fact the true measured values.

General Regression Analysis: BCA versus Pressure, Cyc

```
Regression Equation

Cyc
4    BCA  =  -0.0837196 + 0.0407188 Pressure

8    BCA  =  -0.128751 + 0.0801653 Pressure

16   BCA  =  -0.176862 + 0.111143 Pressure


Coefficients

Term              Coef    SE Coef        T     P
Constant     -0.0837196  0.0367809  -2.27617  0.026
Pressure      0.0407188  0.0090094   4.51957  0.000
Cyc
```

```
  8          -0.0450314  0.0423220  -1.06402  0.292
  16         -0.0931429  0.0423220  -2.20081  0.032
Pressure*Cyc
  8           0.0394465  0.0106601   3.70038  0.000
  16          0.0704246  0.0106601   6.60637  0.000


Summary of Model

S = 0.0312096     R-Sq = 92.91%       R-Sq(adj) = 92.31%
PRESS = 0.0701498  R-Sq(pred) = 91.48%


Analysis of Variance

Source         DF    Seq SS    Adj SS    Adj MS       F        P
Regression      5  0.765345  0.765345  0.153069  157.148  0.000000
  Pressure      1  0.409925  0.019896  0.019896   20.427  0.000030
  Cyc           2  0.310846  0.005529  0.002765    2.838  0.066403
  Pressure*Cyc  2  0.044574  0.044574  0.022287   22.881  0.000000
Error          60  0.058442  0.058442  0.000974
  Lack-of-Fit   5  0.001215  0.001215  0.000243    0.233  0.946181
  Pure Error   55  0.057228  0.057228  0.001041
Total          65  0.823788

Fits and Diagnostics for Unusual Observations

Obs      BCA      Fit    SE Fit    Residual  St Resid
 13  0.236667  0.156568  0.0069787   0.0800989   2.63315  R
 31  0.347248  0.267711  0.0069787   0.0795365   2.61466  R
 49  0.314321  0.378855  0.0106601  -0.0645335  -2.20006  R
 61  0.211548  0.272076  0.0106601  -0.0605278  -2.06350  R
 64  0.338533  0.272076  0.0106601   0.0664575   2.26565  R
 65  0.351069  0.272076  0.0106601   0.0789934   2.69302  R

R denotes an observation with a large standardized residual.
```

General Regression Analysis: TCF versus Pressure, Cycles, Drop

Regression Equation

Drop
0 TCF = 0.987007 - 0.0130922 Pressure + 0.000764843 Cycles - 0.00032345 Pressure*Cycles

1 TCF = 1.07345 - 0.00828487 Pressure + 0.0143335 Cycles - 0.00804414 Pressure*Cycles

194 cases used, 43 cases contain missing values

Coefficients

Term	Coef	SE Coef	T	P
Constant	0.987007	0.0183809	53.6974	0.000
Pressure	-0.013092	0.0089759	-1.4586	0.146
Cycles	0.000765	0.0029480	0.2594	0.796
Drop				
1	0.086441	0.0250837	3.4461	0.001
Pressure*Cycles	-0.000323	0.0010869	-0.2976	0.766
Pressure*Drop				
1	0.004807	0.0120694	0.3983	0.691
Cycles*Drop				
1	0.013569	0.0041541	3.2663	0.001
Pressure*Cycles*Drop				
1	-0.007721	0.0014635	-5.2754	0.000

Summary of Model

S = 0.0938903 R-Sq = 55.09% R-Sq(adj) = 53.39%
PRESS = 1.79328 R-Sq(pred) = 50.88%

Analysis of Variance

Source	DF	Seq SS	Adj SS	Adj MS	F	P
Regression	7	2.01093	2.01093	0.287276	32.5880	0.000000
Pressure	1	1.00487	0.01875	0.018755	2.1275	0.146365
Cycles	1	0.02855	0.00059	0.000593	0.0673	0.795579
Drop	1	0.03379	0.10469	0.104688	11.8756	0.000703
Pressure*Cycles	1	0.36897	0.00078	0.000781	0.0886	0.766345
Pressure*Drop	1	0.31768	0.00140	0.001399	0.1586	0.690862
Cycles*Drop	1	0.01173	0.09405	0.094049	10.6687	0.001297
Pressure*Cycles*Drop	1	0.24533	0.24533	0.245334	27.8302	0.000000
Error	186	1.63966	1.63966	0.008815		
Lack-of-Fit	24	0.35103	0.35103	0.014626	1.8387	0.014336
Pure Error	162	1.28864	1.28864	0.007955		
Total	193	3.65059				

Fits and Diagnostics for Unusual Observations

Obs	TCF	Fit	SE Fit	Residual	St Resid	
2	0.87678	1.07345	0.0170686	-0.196671	-2.13019	R
33	0.98262	1.16579	0.0306133	-0.183171	-2.06368	R
54	1.23697	1.02880	0.0220665	0.208165	2.28100	R
59	0.84518	1.04986	0.0115058	-0.204678	-2.19652	R
68	1.10585	0.89181	0.0177995	0.214034	2.32172	R
77	0.81833	1.00940	0.0141308	-0.191073	-2.05851	R
89	0.48657	0.75482	0.0206602	-0.268248	-2.92882	R
96	1.08373	0.89756	0.0131453	0.186164	2.00250	R
97	1.12638	0.89756	0.0131453	0.228818	2.46132	R
106	0.37915	0.61783	0.0285832	-0.238682	-2.66881	R
117	0.61927	0.82493	0.0177127	-0.205653	-2.23041	R
138	0.79661	0.98701	0.0183809	-0.190393	-2.06783	R
160	0.77266	0.97568	0.0125363	-0.203024	-2.18189	R
166	0.79063	0.97745	0.0156414	-0.186821	-2.01798	R
183	0.76816	0.96177	0.0119287	-0.193602	-2.07885	R
221	0.74870	0.90791	0.0337830	-0.159210	-1.81743	X
223	0.98678	0.90791	0.0337830	0.078876	0.90039	X
224	0.92689	0.90791	0.0337830	0.018980	0.21666	X
227	0.77116	0.90791	0.0337830	-0.136749	-1.56103	X

R denotes an observation with a large standardized residual.
X denotes an observation whose X value gives it large leverage.

Results for: Control

General Regression Analysis: TCF versus Pressure, Cycles

Regression Equation

TCF = 0.987007 - 0.0130922 Pressure + 0.000764843 Cycles - 0.00032345 Pressure*Cycles

90 cases used, 29 cases contain missing values

Coefficients

Term	Coef	SE Coef	T	P
Constant	0.987007	0.0174721	56.4904	0.000
Pressure	-0.013092	0.0085321	-1.5345	0.129
Cycles	0.000765	0.0028022	0.2729	0.786
Pressure*Cycles	-0.000323	0.0010331	-0.3131	0.755

Summary of Model

S = 0.0892482 R-Sq = 8.68% R-Sq(adj) = 5.49%
PRESS = 0.751784 R-Sq(pred) = -0.22%

Analysis of Variance

Source	DF	Seq SS	Adj SS	Adj MS	F	P
Regression	3	0.065110	0.065110	0.0217033	2.72475	0.049136
Pressure	1	0.064303	0.018755	0.0187546	2.35455	0.128589
Cycles	1	0.000026	0.000593	0.0005934	0.07450	0.785554
Pressure*Cycles	1	0.000781	0.000781	0.0007807	0.09801	0.754984
Error	86	0.685011	0.685011	0.0079652		
Lack-of-Fit	12	0.117304	0.117304	0.0097754	1.27421	0.251993
Pure Error	74	0.567707	0.567707	0.0076717		
Total	89	0.750121				

Fits and Diagnostics for Unusual Observations

Obs	TCF	Fit	SE Fit	Residual	St Resid	
20	0.796615	0.987007	0.0174721	-0.190393	-2.17539	R
42	0.772656	0.975681	0.0119165	-0.203024	-2.29538	R
48	0.790625	0.977446	0.0148681	-0.186821	-2.12294	R
65	0.768164	0.961767	0.0113389	-0.193602	-2.18698	R
117	0.733724	0.914727	0.0183779	-0.181003	-2.07250	R

R denotes an observation with a large standardized residual.

Results for: Experimental

General Regression Analysis: TCF versus Pressure, Cycles

Regression Equation

TCF = 1.07345 - 0.00828487 Pressure + 0.0143335 Cycles - 0.00804414 Pressure*Cycles

104 cases used, 14 cases contain missing values

Coefficients

Term	Coef	SE Coef	T	P
Constant	1.07345	0.0177623	60.4341	0.000
Pressure	-0.00828	0.0083966	-0.9867	0.326
Cycles	0.01433	0.0030458	4.7061	0.000
Pressure*Cycles	-0.00804	0.0010199	-7.8870	0.000

Summary of Model

S = 0.0977062 R-Sq = 66.78% R-Sq(adj) = 65.78%
PRESS = 1.04149 R-Sq(pred) = 63.76%

Analysis of Variance

Source	DF	Seq SS	Adj SS	Adj MS	F	P
Regression	3	1.91910	1.91910	0.639700	67.0088	0.000000
Pressure	1	1.27891	0.00929	0.009294	0.9736	0.326175
Cycles	1	0.04635	0.21143	0.211426	22.1469	0.000008
Pressure*Cycles	1	0.59384	0.59384	0.593843	62.2053	0.000000
Error	100	0.95465	0.95465	0.009547		
Lack-of-Fit	12	0.23372	0.23372	0.019477	2.3774	0.010511
Pure Error	88	0.72093	0.72093	0.008192		
Total	103	2.87375				

Fits and Diagnostics for Unusual Observations

Obs	TCF	Fit	SE Fit	Residual	St Resid	
2	0.87678	1.07345	0.0177623	-0.196671	-2.04699	R
54	1.23697	1.02880	0.0229634	0.208165	2.19191	R
59	0.84518	1.04986	0.0119735	-0.204678	-2.11074	R
68	1.10585	0.89181	0.0185229	0.214034	2.23105	R
89	0.48657	0.75482	0.0214999	-0.268248	-2.81444	R
97	1.12638	0.89756	0.0136795	0.228818	2.36519	R
106	0.37915	0.61783	0.0297449	-0.238682	-2.56458	R
117	0.61927	0.82493	0.0184326	-0.205653	-2.14330	R

R denotes an observation with a large standardized residual.

Grouping Information Using Dunnett Method

Level	N	Mean	Grouping
1 (control)	23	1.00000	A
20	6	1.13481	
21	4	1.10269	A
17	27	1.08028	A
18	4	1.05845	A
19	6	1.05161	A
23	4	1.05095	A
10	3	1.03071	A
22	5	1.03033	A

```
24           5  0.99968  A
 5           4  0.99652  A
 9           4  0.99277  A
29           6  0.98841  A
 8           4  0.98753  A
 2           5  0.96582  A
 4           5  0.96402  A
28           5  0.95703  A
25           5  0.95513  A
13           6  0.95409  A
31           6  0.94471  A
26           4  0.94352  A
11           4  0.94074  A
 6           5  0.93647  A
12           5  0.93168  A
15           4  0.92389  A
 7           3  0.91691  A
 3           6  0.89370  A
16           5  0.88047  A
14           4  0.85838  A
32           5  0.80284
27           6  0.71511
30           6  0.57372

Means not labeled with letter A are significantly different from control
level mean.

Dunnett's comparisons with a control

Family error rate = 0.05
Individual error rate = 0.0018

Critical value = 3.18
Control = level (1) of Treatment
```

Intervals for treatment mean minus control mean

```
Level                  Lower               Center                    Upper
--+---------+---------+---------+-------
 2    -0.17413  -0.03418   0.10577              (-----*----)
 3    -0.23632  -0.10630   0.02371            (----*----)
 4    -0.17593  -0.03598   0.10397              (-----*----)
 5    -0.15713  -0.00348   0.15017               (-----*-----)
 6    -0.20348  -0.06353   0.07642             (----*-----)
 7    -0.25720  -0.08309   0.09101           (------*------)
 8    -0.16612  -0.01247   0.14118              (------*-----)
 9    -0.16088  -0.00723   0.14642               (-----*-----)
10    -0.14339   0.03071   0.20481               (------*------)
11    -0.21291  -0.05926   0.09439            (------*-----)
12    -0.20827  -0.06832   0.07163             (----*-----)
13    -0.17593  -0.04591   0.08411              (----*----)
14    -0.29527  -0.14162   0.01203          (-----*-----)
15    -0.22976  -0.07611   0.07754             (-----*-----)
16    -0.25948  -0.11953   0.02042           (----*-----)
17    -0.00020   0.08028   0.16075                    (--*--)
18    -0.09520   0.05845   0.21210                (-----*-----)
19    -0.07841   0.05161   0.18162                 (----*----)
20     0.00479   0.13481   0.26482                    (----*-----)
21    -0.05096   0.10269   0.25633                   (-----*-----)
22    -0.10962   0.03033   0.17028                (----*-----)
23    -0.10270   0.05095   0.20460                (-----*-----)
24    -0.14027  -0.00032   0.13963              (-----*-----)
25    -0.18482  -0.04487   0.09508              (----*-----)
26    -0.21013  -0.05648   0.09717             (-----*-----)
27    -0.41490  -0.28489  -0.15487       (-----*----)
28    -0.18292  -0.04297   0.09698              (----*-----)
29    -0.14160  -0.01159   0.11843               (-----*----)
30    -0.55629  -0.42628  -0.29626   (----*----)
31    -0.18531  -0.05529   0.07472              (----*----)
32    -0.33711  -0.19716  -0.05721          (----*-----)
                              --+---------+---------+---------+-------
                             -0.50     -0.25      0.00      0.25
```

General Regression Analysis: DCF^0.5 versus Pressure, Cycles, Drop

Regression Equation

Drop
0 DCF^0.5 = 0.0885781 + 0.0046958 Pressure - 0.000241549 Cycles -
           0.000282005 Pressure*Cycles

1 DCF^0.5 = 0.12295 + 0.0134112 Pressure + 0.00144206 Cycles -
           0.000805295 Pressure*Cycles

Coefficients

Term	Coef	SE Coef	T	P
Constant	0.0885781	0.0140989	6.28264	0.000
Pressure	0.0046958	0.0068781	0.68272	0.495
Cycles	-0.0002415	0.0022260	-0.10851	0.914
Drop				
1	0.0343720	0.0199318	1.72448	0.086
Pressure*Cycles	-0.0002820	0.0007867	-0.35844	0.720
Pressure*Drop				
1	0.0087154	0.0096976	0.89872	0.370
Cycles*Drop				
1	0.0016836	0.0031600	0.53280	0.595
Pressure*Cycles*Drop				
1	-0.0005233	0.0011261	-0.46469	0.643

Summary of Model

S = 0.0816880 R-Sq = 12.22% R-Sq(adj) = 9.53%
PRESS = 1.62611 R-Sq(pred) = 6.59%

Analysis of Variance

Source	DF	Seq SS	Adj SS	Adj MS	F	P
Regression	7	0.21265	0.21265	0.0303788	4.55254	0.000089
Pressure	1	0.01708	0.00311	0.0031103	0.46610	0.495477
Cycles	1	0.00214	0.00008	0.0000786	0.01177	0.913685

```
  Drop                 1  0.17701  0.01984  0.0198441  2.97383  0.085971
  Pressure*Cycles        1  0.00639  0.00086  0.0008574  0.12848  0.720341
  Pressure*Drop          1  0.00808  0.00539  0.0053897  0.80770  0.369745
  Cycles*Drop            1  0.00051  0.00189  0.0018943  0.28387  0.594691
  Pressure*Cycles*Drop       1   0.00144   0.00144   0.0014409   0.21594
0.642596
Error                229  1.52810  1.52810  0.0066729
  Lack-of-Fit           24  0.30087  0.30087  0.0125361  2.09407  0.003085
  Pure Error           205  1.22723  1.22723  0.0059865
Total                236  1.74075

Fits and Diagnostics for Unusual Observations

Obs   DCF^0.5      Fit    SE Fit  Residual  St Resid
 37  0.331178  0.138908  0.0096048  0.192270   2.37015  R
 42  0.326732  0.138908  0.0096048  0.187824   2.31535  R
 46  0.339895  0.141455  0.0119318  0.198439   2.45557  R
 54  0.322226  0.147076  0.0165087  0.175149   2.18930  R
 71  0.362787  0.147603  0.0141753  0.215185   2.67481  R
 86  0.308310  0.148129  0.0176117  0.160181   2.00811  R
 89  0.333378  0.148129  0.0176117  0.185249   2.32238  R
 91  0.344170  0.169479  0.0156842  0.174692   2.17907  R
 92  0.346288  0.169479  0.0156842  0.176810   2.20548  R
 97  0.324487  0.162362  0.0111582  0.162125   2.00346  R
 99  0.333378  0.162362  0.0111582  0.171016   2.11334  R
135  0.299739  0.088578  0.0140989  0.211161   2.62436  R
172  0.350409  0.085081  0.0165184  0.265328   3.31658  R
182  0.319097  0.091525  0.0090665  0.227572   2.80319  R
198  0.276346  0.093965  0.0087710  0.182381   2.24564  R
229  0.286979  0.105451  0.0203239  0.181528   2.29436  R

R denotes an observation with a large standardized residual.
```

General Regression Analysis: TCF versus NBCA, Freq

Weighted analysis using weights in Weight

Regression Equation

Freq
0   TCF = 1.0281 - 0.175594 NBCA

1   TCF = 0.93824 - 0.186347 NBCA

Coefficients

Term	Coef	SE Coef	T	P
Constant	1.02810	0.0256005	40.1593	0.000
Freq				
1	-0.08986	0.0310388	-2.8950	0.008
NBCA	-0.17559	0.0271881	-6.4585	0.000
Freq*NBCA				
1	-0.01075	0.0318473	-0.3376	0.739

Summary of Model

S = 0.701335   R-Sq = 89.35%   R-Sq(adj) = 87.96%
PRESS = 18.3296 R-Sq(pred) = 82.74%

Analysis of Variance

Source	DF	Seq SS	Adj SS	Adj MS	F	P
Regression	3	94.892	94.8924	31.6308	64.3071	0.000000
Freq	1	12.278	4.1225	4.1225	8.3813	0.008165
NBCA	1	82.558	20.5170	20.5170	41.7122	0.000001
Freq*NBCA	1	0.056	0.0561	0.0561	0.1140	0.738704
Error	23	11.313	11.3130	0.4919		
Lack-of-Fit	18	10.756	10.7557	0.5975	5.3602	0.036046
Pure Error	5	0.557	0.5574	0.1115		
Total	26	106.205				

Fits and Diagnostics for Unusual Observations

Obs	TCF	Fit	SE Fit	Residual	St Resid	
15	0.543804	0.607237	0.0516042	-0.063433	-1.13872	X
16	0.929513	0.938240	0.0175505	-0.008728	-0.46704	X
22	0.792606	0.689793	0.0162534	0.102812	3.55943	R

R denotes an observation with a large standardized residual.
X denotes an observation whose X value gives it large leverage.

Appendix C
Statistical Analysis - Chapter 4

Two-Sample T-Test and CI

```
Sample   N   Mean  StDev  SE Mean
1       16  1.080  0.300    0.075
2       16  1.120  0.300    0.075


Difference = mu (1) - mu (2)
Estimate for difference:  -0.040
95% CI for difference:  (-0.257, 0.177)
T-Test of difference = 0 (vs not =): T-Value = -0.38  P-Value = 0.709  DF
= 30
```

Two-Sample T-Test and CI

```
Sample   N   Mean  StDev  SE Mean
1       16  1.080  0.300    0.075
2       16  1.030  0.190    0.048


Difference = mu (1) - mu (2)
Estimate for difference:  0.0500
95% CI for difference:  (-0.1328, 0.2328)
T-Test of difference = 0 (vs not =): T-Value = 0.56  P-Value = 0.578  DF =
25
```

Two-Sample T-Test and CI

```
Sample   N   Mean  StDev  SE Mean
1       16  1.120  0.300    0.075
2       16  0.170  0.110    0.028


Difference = mu (1) - mu (2)
Estimate for difference:  0.9500
95% CI for difference:  (0.7822, 1.1178)
T-Test of difference = 0 (vs not =): T-Value = 11.89  P-Value = 0.000  DF
= 18
```

Two-Sample T-Test and CI

```
Sample   N   Mean  StDev  SE Mean
1        9  0.600  0.120    0.040
2       16  1.030  0.190    0.048


Difference = mu (1) - mu (2)
Estimate for difference:  -0.4300
95% CI for difference:  (-0.5588, -0.3012)
T-Test of difference = 0 (vs not =): T-Value = -6.92  P-Value = 0.000  DF
= 22
```

Two-Sample T-Test and CI

```
Sample   N   Mean  StDev  SE Mean
1        9  0.600  0.120    0.040
2       16  0.170  0.110    0.028


Difference = mu (1) - mu (2)
Estimate for difference:  0.4300
95% CI for difference:  (0.3265, 0.5335)
T-Test of difference = 0 (vs not =): T-Value = 8.86  P-Value = 0.000  DF =
15
```

Appendix D
Transducer Calibration Plots

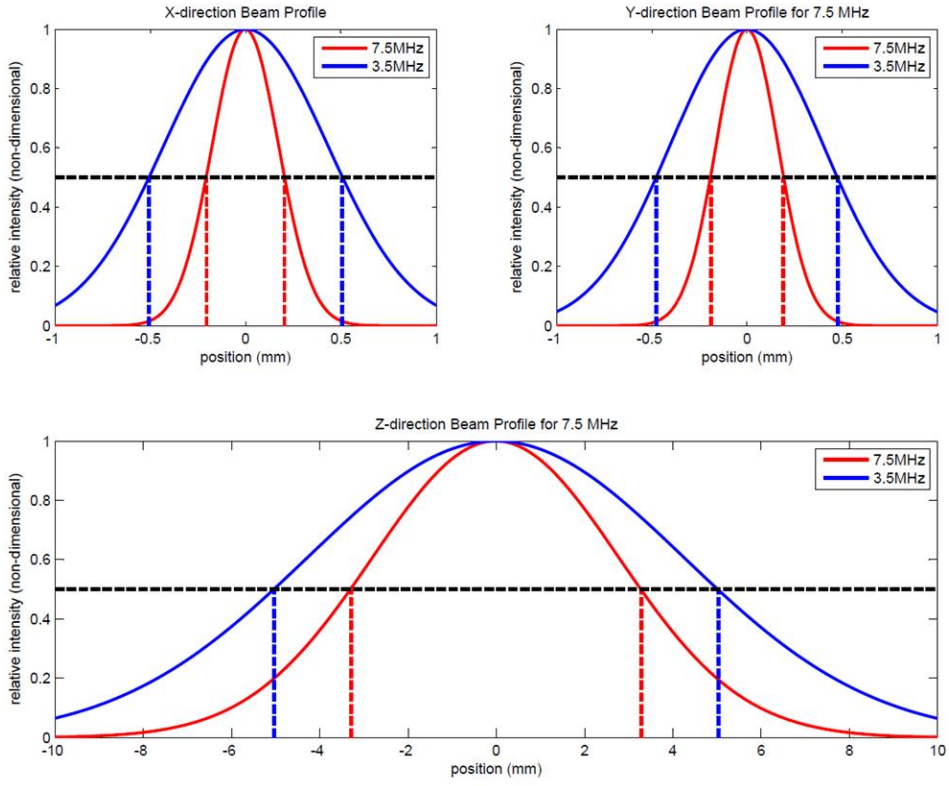

Figure A.D. 1: Beam profiles for both transducers. The y-axis corresponds to a normalized intensity using the maximum value at the origin.

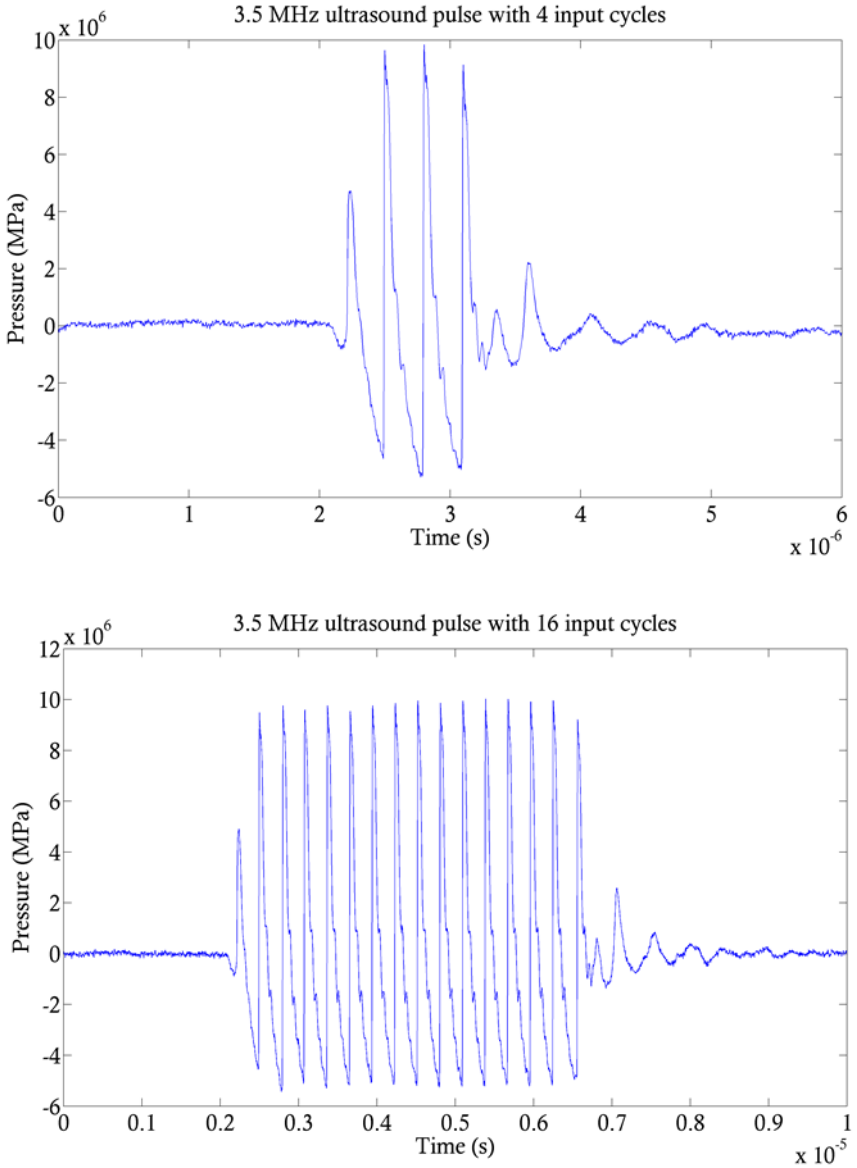

Figure A.D. 2: Ultrasound pulse for the 3.5 MHz transducer with a 4 (top) and 16 (bottom) input cycle. The y-axis shows pressure at the focus of the transducer. Note that the output signal shows one less cycle compared to the input due to ring-up/ring down artifacts.

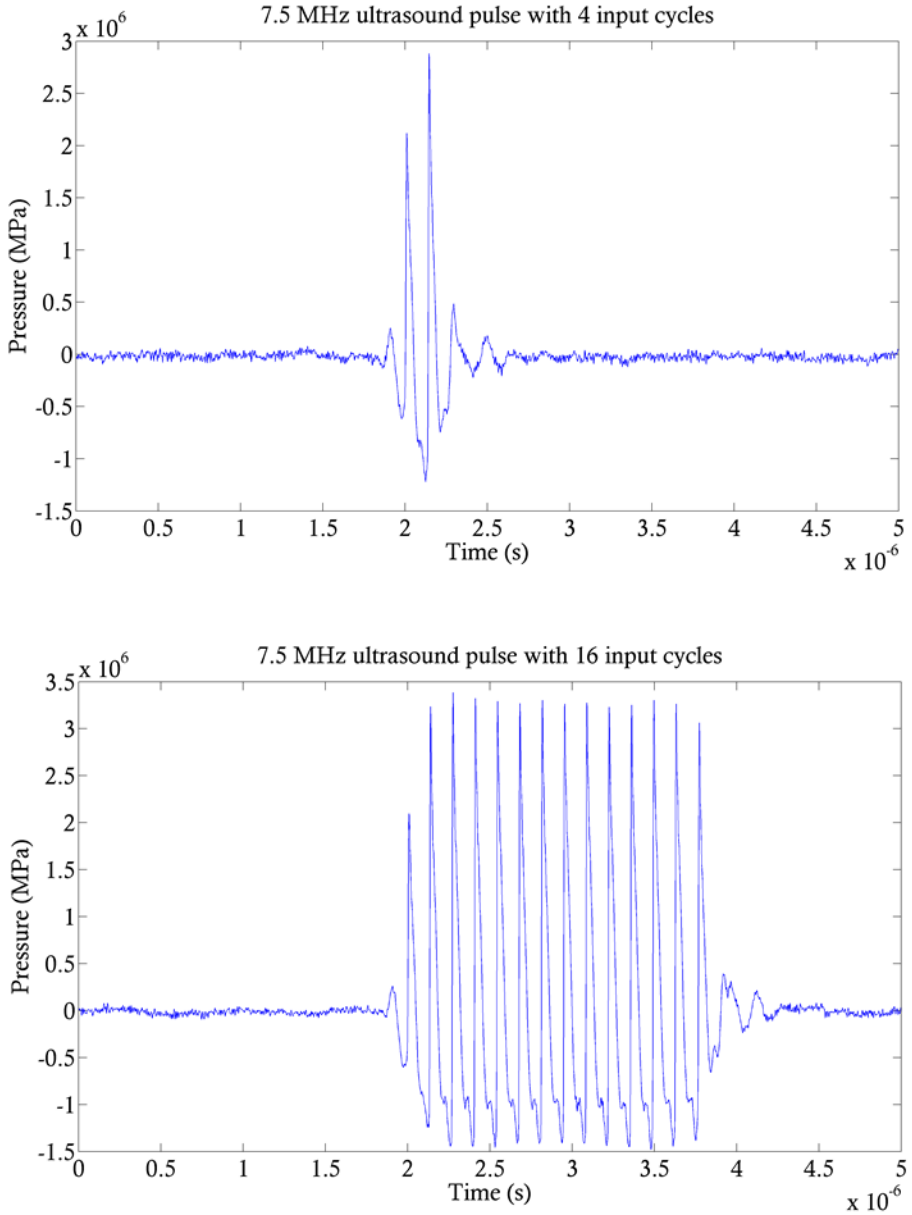

Figure A.D. 3: Ultrasound pulse from the 7.5 MHz transducer with 4 (top) and 16 (bottom) input cycles. The y-axis shows pressure at the focus of the transducer. Note that the output signal shows three less cycles compared to the input due to ring-up/ring-down artifacts.

References

[1] O. Laccourrey, A. Laurent, M. Polivka, M. Wassef, L. Domas and D. G. a. J. Merland, "Biodegradable starch microspheres for cerebral arterial embolization," *Invest Radiol,* vol. 28, pp. 150-154, 1993.

[2] T. Boehm, J. Folkman, T. Browder and M. O'Reilly, "Antiangiogenic therapy for experimental cancer does not induce acquired drug resistance," *Nature,* pp. 404-407, 1997.

[3] D. M. Coldwell, K. R. Stokes and W. F. Yakes, "Embolotherapy: Agents, Applications and Techniques," *Radiographics,* vol. 14, no. 3, pp. 623-643, 1994.

[4] N. Nakagawa and W. Castaneda-Zuniga, Transcatheter chemoembolization for hepatocellular carcinoma and other promising transarterial therapies, vol. 3, Baltimore: Interventional Radiology, 1997.

[5] J. Bull, "Cardiovascular bubble dynamics," *Critical Reviews in Biomedical Engineering,* vol. 33, no. 4, pp. 299-346, 2005.

[6] J. Bull, "The application of microbubbles for targeted drug delivery," *Expert Opinion on Drug Delivery,* vol. 4, no. 5, pp. 475-493, 2007.

[7] Z. Wong and J. Bull, "Microbubbles and microdroplets for drug delivery," *Journal of Drug Delivery Science and Technology,* vol. 21, no. 5, pp. 355-367, 2011.

[8] O. Kripfgans, J. Fowlkes, D. Miller, O. Eldevik and P. Carson, "Acoustic Droplet

Vaporization For Therapeutic and Diagnostic Applications," *Ultrasound in Med. & Biol.*, vol. 26, no. 7, pp. 1177-1189, 2000.

[9] T. Giesecke and K. Hynynen, "Ultrasound-mediated cavitation thresholds of liquid perfluorocarbon droplets in vitro," *Ultrasound in Med. & Biol.*, vol. 29, no. 9, pp. 1359-1365, 2003.

[10] O. Kripfgans, M. Fabiilli, P. Carson and J. Fowlkes, "On the Acoustic Vaporization of Micrometer-sized Droplets," *J. Acoust. Soc. Am*, vol. 116, no. 1, pp. 272-281, 2004.

[11] O. Kripfgans, J. Fowlkes, M. Woydt, O. Eldevik and P. Carson, "In vivo droplet vaporization for occlusion therapy and phase aberration correction," *IEEE Trans. Ultrason. Ferroelec. Freq. Control*, vol. 49, no. 6, pp. 726-738, 2002.

[12] T. Ye and J. Bull, "Direct numerical simulations of microbubble expansion in gas embolotherapy," *J. Biomech. Eng.*, pp. 745-758, 2004.

[13] T. Ye and J. Bull, "Microbubble expansion in a flexible tube," *J. Biomech. Eng.*, pp. 554-563, 2006.

[14] D. Miller, M. Averkiou, A. Brayman, E. Carr Everbach, C. Holland, J. Wible and J. Wu, "Bioeffects considerations for diagnostic ultrasound contrast agents," *J Ultrasound Med*, vol. 27, pp. 611-632, 2008.

[15] R. Apfel and C. Holland, "Gauging the likelihood of cavitation from short-pulse, low-duty cycle diagnostic ultrasound," *Ultrasound in Med & Biol*, vol. 17, no. 2, pp. 179-185, 1991.

[16] D. M. Skyba, R. J. Price, A. Z. Linka, T. C. Skalak and S. Kaul, "Direct In Vivo Visualization of Intravascular Destruction of Microbubbles by Ultrasound and its Local Effects on Tissue," *Circulation*, vol. 98, pp. 290-293, 1998.

[17] A. B. Fisher, S. Chien, A. I. Barakat and R. M. Nerem, "Endothelial cellular

response to altered shear stress," *Am J Physiol Lung Cell Mol Physiol,* vol. 281, 2001.

[18] S. Chien, "Effects of Disturbed Flow on Endothelial Cells," *Ann Biomed Eng,* vol. 36, no. 4, pp. 554-62, 2008.

[19] A. Rahim, S. Taylor, N. Bush, G. ter Haar, J. Bamber and C. Porter, "Physical parameters affecting ultrasound/microbubble-mediated gene delivery efficiency in vitro," *Ultrasound in Med. & Biol.,* pp. 1269-1279, 2006.

[20] D. Mukherjee, J. Wong, B. Griffin, S. Ellis, T. Porter, S. Sen and J. Thomas, "Ten-fold augmentation of endothelial uptake of vascular endothelial growth factor with ultrasound after systemic administration," *J. Am. Coll. Cardiol.,* pp. 1678-1686, 2000.

[21] J. Song, M. Qi, S. Kaul and R. Price, "Stimulation of arteriogenesis in skeletal muscle by microbubble destruction with ultrasound," *Circulation,* pp. 1550-1555, 2002.

[22] B. Meijering, R. Henning, W. van Gilst, I. Gavrilovic, A. van Wamel and L. Deelman, "Optimization of ultrasound and microbubbles targeted gene delivery to cultured primary endothelial cells," *Journal of Drug Targeting,* pp. 664-671, 2007.

[23] J. Park, Z. Fan and C. Deng, "Effects of shear stress cultivation on cell membrane disruption and intracellular calcium concentration in sonoporation of endothelial cells," *Journal of Biomechanics,* pp. 164-169, 2011.

[24] S. Bao, B. Thrall and D. Miller, "Transfection of a reporter plasmid into cultured cells by sonoporation in vitro," *Ultrasound in Med. & Biol.,* pp. 953-959, 1997.

[25] D. Miller, S. Pislaru and J. Greenleaf, "Sonoporation: Mechanical DNA delivery by ultrasonic cavitation," *Somatic Cell and Molecular Genetics,* pp. 115-134, 2002.

[26] A. Rahim, S. L. Taylor, N. L. Bush, G. R. Haar, J. C. Bamber and C. D. Porter,

"Physical parameters affecting ultrasound/microbubble mediated gene delivery efficieny in vitro," *Ultrasound in Med and Biol,* vol. 32, no. 8, pp. 1269-1279, 2006.

[27] M. Fabiilli, K. Haworth, I. Sebastian, O. Kripfgans, P. Carson and J. Fowlkes, "Delivery of chlorambucil using an acosutically-triggered perfluoropentane emulsion," *Ultrasound in Med. & Biol.,* pp. 1364-1375, 2010.

[28] L. Juffermans, A. van Dijk, C. Jongenelen, B. Drukarch, A. Reijerkerk, H. de Vries, O. Kamp and R. Musters, "Ultrasound and microbubble-induced intra- and intercellular bioeffects in primary endothelial cells," *Ultrasound in Med. and Biol.,* pp. 1917-1927, 2009.

[29] L. J. Juffermans, P. A. Dijkmans, R. J. Musters, C. A. Visser and O. Kamp, "Transient permeabilization of cell membranes by ultrasound-exposed microbubbles is related to formation of hydrogen peroxide," *Am J Physiol Heart Circ Physiol,* vol. 291, no. 4, pp. H1595-601, 2006.

[30] A. van Wamel, A. Bouakaz, M. Versluis and N. De Jong, "Micromanipulation of endothelial cell: ultrasound-microbubble-cell interactions," *Ultrasound in Med and Biol,* vol. 30, no. 9, pp. 1255-1258, 2004.

[31] P. Marmottant and S. Hilgenfeldt, "Controlled vesicle deformation and lysis by sinlge oscillating bubbles," *Nature,* vol. 423, pp. 153-156, 2003.

[32] R. Price, D. Skyba, S. Kaul and T. Skalak, "Delivery of colloidal particles and red blood cells to tissue through microvessel ruptures created by targeted microbubble destruction with ultrasound," *Circulation,* vol. 98, pp. 1264-1267, 1998.

[33] K. Hynyen, N. McDannold, N. Sheikov, F. Jolesz and N. Vykhodtseva, "Local and reversible blood-brain barrier disruption by noninvasive focused ultrasound at frquencies suitable for transkull sonications," *Neuroimage,* vol. 24, no. 1, pp. 12-20, 2005.

[34] A. Mesiwala, L. Farrell, H. Wenzel, D. Silbergeld, L. Crum, H. Winn and P. Mourad, "High-intensity focused ultrasound selectively disrupts the blood-brain barrier in vivo," *Ultrasound Med. & Biol.*, vol. 28, no. 3, pp. 389-400, 2002.

[35] K. Hynynen, N. McDannold, N. Vykhodtseva and F. Jolesz, "Non-invasive opening of BBB by focused ultrasound," *Acta Neurochir Supll,* vol. 86, pp. 555-558, 2003.

[36] R. M. Nerem, "Hemodynamics and the Vascular Endothelium," *J Biomech Eng,* vol. 115, no. 4B, pp. 510-514, 1993.

[37] P. F. Davies and S. C. Tripathi, "Mechanical Stress Mechanisms and the Cell: An Endothelial Paradigm," *Circ Res,* vol. 72, pp. 239-245, 1993.

[38] B. Sumpio, J. Riley and A. Dardik, "Cells in focus: endothelial cell," *The International Journal of Biochemistry & Cell Biology,* pp. 1508-1512, 2002.

[39] S. Kumar, D. West and A. Ager, "Heterogenicity in endothelial cells from large vessels and microvessels," *Differentiation,* pp. 57-70, 1987.

[40] D. H. Endemann and E. L. Schiffrin, "Endothelial Dysfunction," *J Am Soc Nephrol,* vol. 15, pp. 1983-1993, 2004.

[41] J. Davignon and P. Ganz, "Role of Endothelial Dysfunction in Atherosclerosis," *Circulation,* 2004.

[42] A. C. Dudley and M. Klagsbrun, "Tumor endothelial cells join the resistance-Review," vol. 15, no. 15, 2009.

[43] Y.-Q. Xiong, H.-C. Sun, W. Zhang, X.-D. Zhu, P.-Y. Zhuang, J.-B. Zhang, L. Wang, W.-Z. Wu, L.-X. Qin and Z.-Y. Tang, "Human Hepatocellular Carcinoma Tumor–derived Endothelial Cells Manifest Increased Angiogenesis Capability and Drug Resistance Compared with Normal Endothelial Cells," *Clinical Cancer Research,* vol. 15, no. 15, 2009.

[44] A. Qamar, W. Z, J. Fowlkes and J. Bull, "Dynamics of acoustic droplet vaporization

in gas embolotherapy," *Applied Physics Letters,* p. 143702, 2010.

[45] A. Qamar, Z. Wong, J. Fowlkes and J. Bull, "Evolution of acoustically vaporized microdroplets in gas embolotherapy," *Journal of Biomechanical Engineering,* vol. 134, pp. 031010-1-13, 2012.

[46] M. S. Plesset and A. Prosperetti, "Bubble dynamics and cavitation," *Annu. Rev. Fluid Mech.,* vol. 9, pp. 145-185, 1977.

[47] T. G. Leighton, The Acoustic Bubble, Academic Press, 1994.

[48] M. Minnaert, "On musical air-bubbles and the sound of running water," *Philosophical Magazine,* vol. 16, no. 104, pp. 235-248, 1933.

[49] D. B. Khismatullin, "Resonance frequency of microbubbles: Effect of viscosity," *J. Acoust. Soc. Am.,* vol. 116, no. 3, pp. 1463-1473, 2004.

[50] S. Hilgenfeldt, D. Lohse and M. Zomack, "Response of bubbles to diagnostic ultrasound: a unifying theoretical approach," *Eur. Phys. J. B,* vol. 4, pp. 247-255, 1998.

[51] J. E. Parsons, C. A. Cain and J. B. Fowlkes, "Cost-effective assempbly of a basic fber-optic hydrophone for measurement of high-amplitude therapeutic ultrasound fields," *J Acoust Soc Am,* vol. 119, no. 3, pp. 1432-40, 2006.

[52] S. Samuel, A. Duprey, M. Fabiilli, J. Bull and J. Fowlkes, "In vivo microscopy of targeted vessel occlusion employing acoustic droplet vaporization," *Microcirculation,* vol. 19, pp. 501-509, 2012.

[53] M. Fabiilli, K. Haworth, N. Fakhri, O. Kripfgans, P. Carson and J. Fowlkes, "The role of inertial cavitation in acoustic droplet vaporization," *IEEE Transactions on Ultrasonics, Ferrolectrics and Frequency Control,* pp. 1006-1017, 2009.

[54] A. H. Lo, O. D. Kripfgans, P. L. Carson, E. D. Rothman and J. B. Fowlkes, "Acoustic droplet vaporization threshold: effects of pulse duration and contrast

agent," *IEEE Trans. Ultrason. Ferroelect. Freq. Contr.,* vol. 54, no. 5, pp. 933-946, 2007.

[55] Z. Xu, T. L. Hall, J. B. Fowlkes and C. A. Cain, "Effects of acoustic parameters on bubble cloud dynamics in ultrasound tissue errosio (histotripsy)," *J. Acoust. Soc. Am.,* vol. 122, no. 1, pp. 229-36, 2007.

[56] Z. Xu, M. Raghavan, T. L. Hall, M. A. Mycek and J. B. Fowlkes, "Evolution of bubble clouds induced by pulsed cavitational ultrasound therapy-histotripsy," *IEEE Trans Ultrason. Ferroelectr. Freq. Control.,* vol. 55, no. 5, pp. 1122-32, 2008.

[57] N. Ghinea, M. Eskenasy, M. Simionescu and N. Simionescu, "Endothelial albumin binding proteins are membrane-associated components exposed on the cell surface," *J Biol Chem,* vol. 264, pp. 4755-4758, 1989.

[58] S. Vogel, R. Minshall, M. Pilipovic, C. Tiruppathi and A. Malik, "Albumin uptake and transcytosis in endothelial cells in vivo induced by albumin-binding protein," *Am J Physiol Lung Cell Mol Physiol,* vol. 281, pp. L1512-L1522, 2001.

[59] S. Siddiqui, Z. Siddiqui and A. Malik, "Albumin endocytosis in endothelial cells induces TGF-Beta receptor II signaling," *Am J Physiol Lung Cell Mol Physiol,* vol. 286, pp. L1016-1026, 2004.

[60] E. Neppiras, "Acoustic Cavitation," *Physics Reports,* vol. 61, no. 3, pp. 159-251, 1980.

[61] D. Dalecki, "Mechanical bioeffects of ultrasound," *Annu Rev Biomed Eng,* vol. 6, pp. 229-248, 2004.

[62] C. Holland and R. Apfel, "An improved theory for the prediction of microcavitation thresholds," *IEEE Trans Ultrason. Ferroelectr. Freq. Control,* vol. 36, no. 2, pp. 204-208, 1989.

[63] R. a. G. H. Phillips, "Information for Manufaturers Seeking Marketing Clearance of

Diagnostic Ultrasound Systems and Transducers," US Department of Health and Human Services, Food and Drug Administration, Silver Spring, MD, 2008.

[64] J. Bushberg, J. Seibert, E. Leidholdt and J. Boone, "Acoustic Power and Bioeffects," in *The Essential Physics of Medical Imaging*, Lippincott Williams & Wilkins, 2011.

[65] P. Lewin and M. Ziskin, "Measurment Techniques," in *Ultrasonic Exposimetry*, Boca Raton, FL., CRC Press, Inc., 1993, pp. 122-124.

[66] F. A. Duck, "Acoustic saturation and output regulation," *Ultrasound in Med. & Biol.*, vol. 25, no. 6, pp. 10009-1018, 1999.

[67] J. Soneson, "HIFU simulator v1.2 user's manual," FDA, 2011.

[68] S. Hsu and T. Huang, "Bioeffect of ultrasound on endothelial cells in vitro," *Biomolecular Engineering*, pp. 99-104, 2004.

[69] M. W. Miller, D. L. Miller and A. A. Brayman, "A review of in vitro bioeffects of inertial ultrasonic cavitation from a mechanistic perspective," *Ultrasound in Med. & Biol.*, vol. 22, no. 9, pp. 1131-1154, 1996.

[70] A. M. Malek, S. L. Alper and S. Izumo, "Hemodynamic shear stress and its role in atherosclerosis," *JAMA*, vol. 282, no. 21, pp. 2035-2042, 1999.

[71] Y. S. Li, J. H. Haga and S. Chien, "Molecular basis of the effects of shear stress on vascular endothelial cells," *J Biomech*, vol. 38, no. 10, pp. 1949-71, 2005.

[72] C. F. J. Dewey, S. R. Bussolari, M. A. Gimbrone and P. F. Davies, "The dynamic response of vascular endothelial cells to fluid shear stress," *J Biomech Eng*, vol. 103, no. 3, pp. 177-85, 1981.

[73] J. E. Schnitzer, W. W. Carley and G. E. Palade, "Albumin interacts specifically with a 60-kDa microvascular endothelial glycoprotein," *Proc. Natl. Acad. Sci.*, vol. 85, pp. 6773-6777, 1988.

[74] M. Zhang, M. L. Fabiilli, K. J. Haworth, J. B. Fowlkes, O. D. Kripfgans, W. W.

Roberts, K. A. Ives and P. L. Carson, "Initial Investigation of Acoustic Droplet Vaporization for Occlusion in Canine Kidney," *Ultrasound in Med. & Biol.*, vol. 36, no. 10, pp. 1691-1703, 2010.

[75] P. Hwang and W. Teague, "Low-frequency resonant scattering of bubble clouds," *J. Atmos. Oceanic Technol.*, vol. 17, no. 6, pp. 847-853, 2000.

[76] F. Dunn, J. E. Lohnes and F. J. Fry, "Frequency dependence of threshold ultrasonic dosages for irreversible structural changes in mammalian brain," *J. Acoust. Soc. Am.*, vol. 58, no. 2, pp. 512-514, 1975.

[77] C. X. Deng, Q. Xu, R. E. Alpfel and C. K. Holland, "In vitro measuerements of inertial cavitation thresholds in human blood," *Ultrasound in Med. & Biol.*, vol. 22, no. 7, pp. 939-948, 1996.

[78] F. Forsberg, W. T. Shi, C. R. B. Merritt, Q. Dai, M. Solcova and B. Goldberg, "On the usefulness of the mechanical index displayed on clinical ultrasound scanners for predicting contrast microbubble destruction," *J Ultrasound Med*, vol. 24, pp. 443-450, 2005.

[79] C. C. Church, "Frequency, pulse length, and the mechanical index," *Acoustical Society of America,* vol. 6, no. 3, pp. 162-168, 2005.

[80] R. S. Reneman, T. Arts and A. P. Hoeks, "Wall shear stress-an important determinant of endothelial cell function and structure-in the arterial system in vivo," *J Vasc Res*, vol. 43, pp. 251-269, 2006.